Exploration of Room Temperature Leaching Methods of Chalcopyrite-based Copper Concentrates

Charles Kim

Submitted in partial fulfillment of the
requirements for the degree of
Doctor of Philosophy
under the Executive Committee
of the Graduate School of Arts and Sciences

COLUMBIA UNIVERSITY

2025

Abstract

Exploration of Room Temperature Leaching Methods of Chalcopyrite-based Copper Concentrates

Charles Kim

This doctoral thesis focuses on the development of low-energy, high-yield hydrometallurgial processes of extracting copper to meet the increasing demands due to global transition towards carbon-free energy. This thesis investigates two room-temperature leaching methods – vanadium reductive leaching and cerium oxidative leaching – as alternatives to traditional high-temperature oxidative leaching methods of chalcopyrite-based copper concentrates.

For the vanadium reductive leaching method, this study focused on the improvement of leaching kinetics across different mineral compositions and the development of a continuous reactor to evaluate the processing rate. Results reveal rapid reaction kinetics and high copper recovery yields across a range of mineral compositions, with improved performance with the addition of $FeSO_4$ in the leach solution. The processing rate was competitive against the incumbent leaching processes, making vanadium leaching a promising candidate for industrial scale-up, despite requiring H_2S gas treatment.

For the cerium oxidative leaching method, this study focused on the improvement of leaching kinetics and the analysis of the leaching reaction and the solid products to overcome the passivation of the copper concentrates. While more environmentally friendly compared to vanadium leaching process, the kinetics were less favorable, and the process faced limitations due to the high consumption and low solubility of Ce^{4+}.

Second, process flow diagrams, reactor sizing, and energy requirement calculations were developed for both methods. Vanadium leaching required significantly smaller reactors and lower power outputs, confirming its scalability and economic feasibility.

Third, the electrochemical and chemical air oxidation regeneration methods of Ce^{3+} were explored. The results indicate that chemical air oxidation method faces challenges due to the consumption of unrecoverable acids and bases, and the overall intense conditions required for the dissolution of $Ce(OH)_4$ to Ce^{4+}. Although limited by the solubility of Ce^{3+} in sulfate media, the electrochemical regeneration method was found to be more feasible.

In conclusion, this thesis presents a comprehensive comparison of two room-temperature leaching strategies for copper recovery. Vanadium-based reductive leaching emerges as the more practical and scalable option for commercial deployment. Future research should prioritize leachant regeneration, environmental risk mitigation, and pilot-scale validation to accelerate the adoption of these low-temperature hydrometallurgical technologies.

Table of Contents

List of Figures

List of Tables

Acknowledgements

Completing this PhD has been one of the most challenging and rewarding experiences of my life, and it would not have been possible without the support, guidance, and encouragement of many individuals.

First, I would like to express my deepest gratitude to my supervisor, Dr. Alan C. West, for their support, feedback, and patience throughout this journey. Thank you for sharing your ideas and experiences with me, and it has been an honor to work with him. His advice helped me improve as a researcher.

Next, I would like to thank my colleagues within the West research group. Dr. Jon Vardner and Dr. Jeff Fitts were instrumental in introducing me to the work in the lab and assisting me throughout my first project. To Dr. John Bernard, Dr. Kedi Hu, and Dr. Karthik Mayilvahanan, thank you for your general assistance and guiding me during my presentations. Finally, I would like to thank Tongwei Xu, Brian Donovan, Curtis Sirkoch, Zeyu Wang, Yu Chen, and all other group members who have worked together with me.

I would like to thank my collaborators, Dr. Scott Banta, Dr. Raymond Farinato and Dr. D.R. Nagaraj, for offering me important advice during my project and aiding me in instrument usage and paper writing.

Finally, to my family, thank you for your love, understanding, and support in me. To my parents, who have taught me and encouraged me, and my brother and grandparents for always cheering me on, I am forever grateful.

Dedication

This work is dedicated to my parents, brother, and grandparents, who taught me the value of education, perseverance, and humility, and have always loved me and never given up on me.

Chapter 1:

Introduction to Copper Production Methods

1.1. Copper, and its Increasing Demands

Copper is one of the most widely used metals globally. Due to its conductivity, it is primarily used for wiring and electrical equipment. As a result of increasing population, economic growth, and development of renewable energy source facilities, over the upcoming decades, the demand for copper is expected to increase, from 25 MT/yr in 2020 to 59 MT/yr in 2050 (World Bank, 2023).

This increase in copper coincides with the declining of ore grades, with the analysis of Chilean mines showing that the average of copper grades has decreased by 28.8% over the course of 10 years (Calvo, 2016). This is a major concern because the total amount of energy required to produce copper is heavily related to the ore grade, with the energy requirement sharply increasing with decreasing ore grades. It is estimated that processing 1kg of copper by concentrating and smelting the ore is 131MJ, 249MJ, and 602MJ, respectively for ore grades of 0.5%, 0.25%, and 0.1% (Norgate, 2010). To completely meet the demands of copper in 2050, around 1.0% to 2.4% of total global energy demand must be invested into production of copper, compared to 0.3% today (Elshkaki, 2016).

Figures 1.1 shows the increasing copper demands and the copper supply required to meet those demands. From 2021 to 2050, 2.3 times more copper is expected to be required, with more copper required for both existing uses and EV battery applications. To match those demands, roughly twice the amount of copper will be required from mining applications, and three times the amount of copper will be required from recycling applications from 2021 to 2050 (World Bank, 2023).

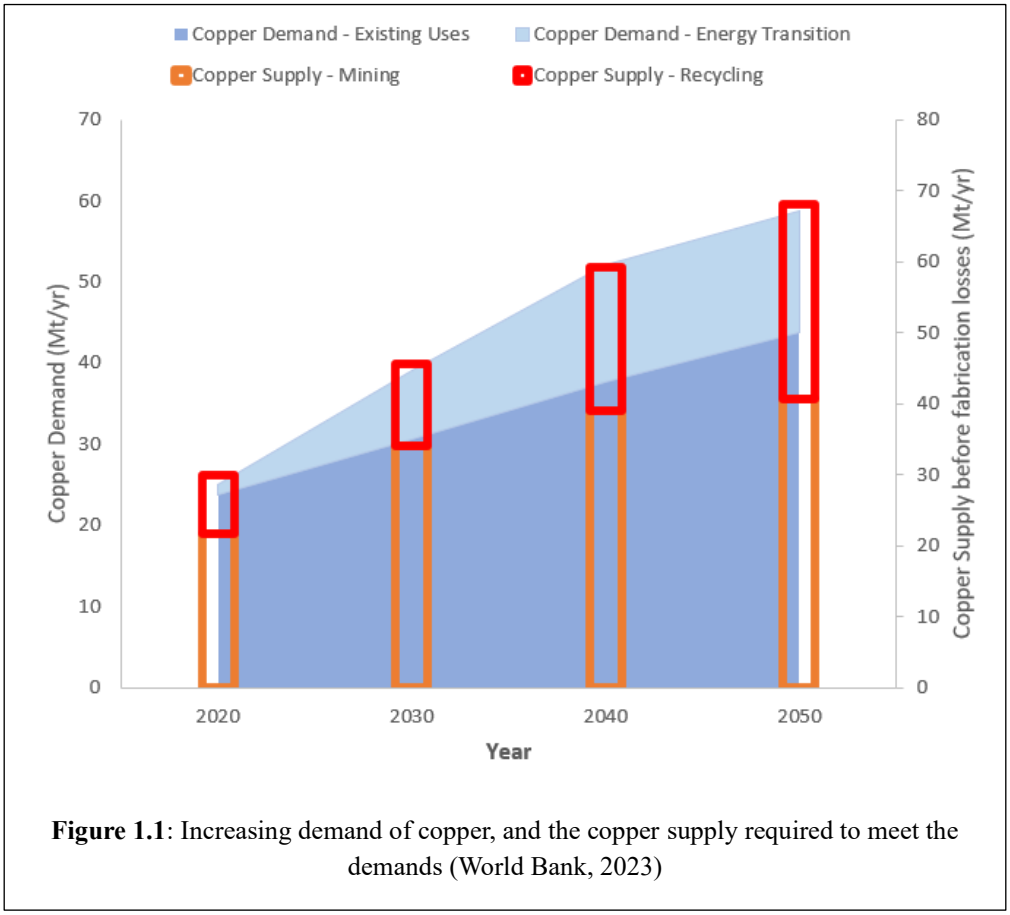

Figure 1.1: Increasing demand of copper, and the copper supply required to meet the demands (World Bank, 2023)

The amount of copper supply produced by simply increasing the number of mines in operation is not enough to meet the demands. As such, a new copper processing method is needed to increase the copper production rates. Currently, there are two main methods of processing copper: pyrometallurgy and hydrometallurgy.

1.2. Pyrometallurgical processing

As described in Figure 1.2, in the pyrometallurgical route, the ores are crushed and concentrated by flotation to obtain a product containing around 20% copper. These copper concentrates are then fed into a smelter at around 1200°C, separating the liquid copper matte

from the gangue. A minimum copper grade of 20% is required for the smelter due to the high temperature, as additional gangue that enters the smelter consumes energy, resulting in decreased energy efficiency (Forsen, 2017). The liquid copper matte is processed further to produce cathode copper, consisting of 99.99% copper. Pyrometallurgical methods account for 80% of the global copper production (Kulczycka, 2015).

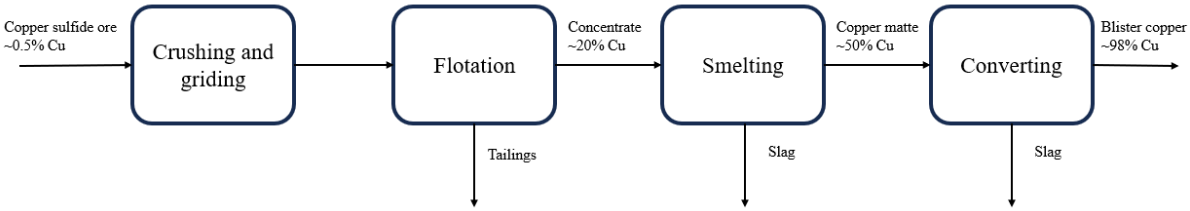

Figure 1.2: Pyrometallurgical processing of copper flowsheet (Hawker, 2017)

1.3. Hydrometallurgical processing

As described in Figure 1.3, in the hydrometallurgical route, the copper ores are first placed in a solution containing oxidizing agents such as ferric ions or oxygen, leaching the copper into the solution. At lower temperatures, the sulfide oxidizes to elemental sulfur, as shown in chemical reaction 1.1 below. At higher temperatures, the elemental sulfur is oxidized further to produce sulfate, shown in reaction 1.2 below.

$$CuFeS_2 + \frac{5}{4}O_2 + 5H^+ \rightarrow Cu^{2+} + Fe^{3+} + 2S^0 + \frac{5}{2}H_2O \quad 1.1$$

$$CuFeS_2 + \frac{17}{4}O_2 + H^+ \rightarrow Cu^{2+} + Fe^{3+} + 2SO_4^{2-} + \frac{1}{2}H_2O \quad 1.2$$

For the leaching of chalcopyrite-pyrite ores, iron is also leached into the solution, as well as other elements such as Al, Mn, Zn, Mg, and Ca. In the solvent extraction step, the pregnant

leach solution is then mixed with an organic solvent containing a Cu-specific extractant, separating the copper in the organic phase from other leached metals in the aqueous phase. The remaining aqueous phase, called raffinate, is recycled back to the leaching step. The Cu-containing organic phase is then mixed with a strong acid to transfer the copper back into the aqueous phase in a process called stripping. The aqueous copper in the acid can be recovered in an electrowinning process as copper cathode, while the remaining strong acid with the copper depleted is reused to strip additional amounts of copper from the organic phase.

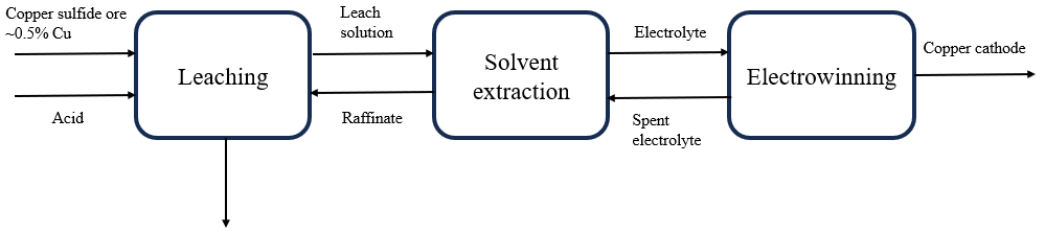

Figure 1.3: Hydrometallurgical processing of copper flowsheet (Hawker, 2017)

1.4. Comparison of two processes

The comparison of the two types of processes is shown in Table 1.1 below. Although the pyrometallurgical processing method generally has a high processing rate, energy is needed to sustain the high operating temperature of the smelter and for the mineral processing to produce copper concentrates. Another disadvantage is the environmental hazards released when operating the smelter, such as As and SO_2 (Dimitrijevic, 2009).

Hydrometallurgical processing methods generally have lower environmental concerns and often have milder operating temperatures. However, processing rate is slower due to the development of a passivation layer during leaching. 80 percent of global copper production

originates from copper sulfide ores such as $CuFeS_2$ (Dimitrijevic, 2009). When these copper sulfide ores are oxidized, the sulfur and metal-defiicent sulfide layers accumulate on the surface, slowing down the leaching kinetics (Cordoba, 2008). There are several strategies to counter the development of passivation layers: grinding the ores to finer sizes increase the surface area and increases the leaching rate. Chloride ions in the leach solution weaken the passivation layer, making it more porous. Operating at higher temperatures and pressures can oxidize the sulfur-based passivation layers to sulfate, solubilizing it and removing it from the surface (Dreisinger, 2006) (Mokmeli, 2020). However, each of these strategies increase the capital cost and the operating cost considerably. Pyrometallurgical processing methods are currently dominant, as only 20% of global copper is processed with hydrometallurgical methods.

Overall, the existing methods are effective in quickly converting copper ores into finished copper products. However, the operating costs prevent the utilization of low-grade ores, damaging the overall processing rates. To meet the increasing demands of copper, the new process must produce copper at a competitive rate cheaply. Two such candidates are considered in this work, and each process is analyzed to determine whether it can replace the current copper processing methods.

Table 1.1: Advantages and disadvantages of pyrometallurgical and hydrometallurgical processing methods of copper (Papagianni, 2022)

	Advantages	Disadvantages
Pyrometallurgical	No mechanical pretreatment	High operating temperature
	High recovery efficiency	Using additional materials as collector
	Processing a wide range of materials independently of their composition	Hazardous emission impact on the environment
Hydrometallurgical	High recovery efficiency	High water consumption
	Mild conditions	High water wastes
	Conduction of low-grade materials	
	Better control of co-products	
	Simple stages	

1.5. Vanadium reductive leaching method

The first proposed method is the vanadium reductive leaching method. As shown in Equation 1.3 and 1.4 below, V^{2+} ions act as a reducing agent, reacting with $CuFeS_2$ to form elemental copper, $Cu_{1.94}S$, Fe^{2+} ions, and H_2S as products at room temperature (Vardner, 2021)(Xu, 2024). In studies by Vardner et al., the $CuFeS_2$-FeS concentrates were observed to yield elemental copper after reacting with excess V^{2+} in solution, and a mixture of Cu_2S and elemental copper with limited V^{2+} (Vardner, 2021). In studies by Xu et al., as shown in Figure

1.4, H_2S was found to be critical in reacting with Cu^{2+} ions to form CuS, which would then react with V^{2+} to form Cu_2S and H_2S (Xu, 2024). Since the sulfide is removed in the form of H_2S gas, a passivation layer does not form, and the reaction proceeds quickly. Experimentally, over 90% of the copper could be recovered as elemental copper within an hour (Vardner, 2021).

$$2\ CuFeS_2 + 6H^+ + 2V^{2+} \rightarrow Cu_2S + 2Fe^{2+} + 3H_2S + 2V^{3+} \quad 1.3$$

$$Cu_2S + 2H^+ + 2V^{2+} \rightarrow 2Cu^0 + H_2S + 2V^{3+} \quad 1.4$$

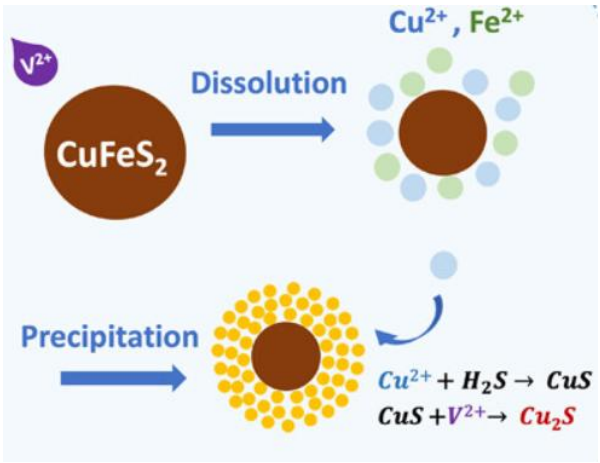

Figure 1.4: Reductive leaching of copper concentrates diagram (Xu, 2024)

Due to the absence of a passivation layer, the particle size does not heavily affect the leaching rate of copper concentrates. The copper and iron are naturally separated during the leaching step, with most of the copper remaining as a solid product and most of the iron in the aqueous phase. The operating costs required for grinding the ores and the capital costs required for the separation of copper and iron are both conserved. However, unlike traditional hydrometallurgical processes, the vanadium reductive leaching method produces H_2S, a safety and environmental hazard. The treatment of H_2S, such as the Claus process, is necessary.

1.6. Cerium oxidative leaching method

The second method is the cerium oxidative leaching method. Ce^{4+} ions act as an oxidizing agent, reacting with $CuFeS_2$ to leach Cu^{2+} and Fe^{3+} into the solution, with the sulfur oxidized to sulfur to form a passivation layer on the surface of the $CuFeS_2$, or oxidized to sulfate and leached into the solution. The chemical reaction is similar to traditional oxidative leaching methods which use oxygen as the leaching agent.

$$CuFeS_2 + 5Ce^{4+} \rightarrow Cu^{2+} + Fe^{3+} + 2S^0 + 5Ce^{3+} \quad 1.5$$

$$CuFeS_2 + 17Ce^{4+} + 8H_2O \rightarrow Cu^{2+} + Fe^{3+} + 2SO_4^{2-} + 16H^+ + 17Ce^{3+} \quad 1.6$$

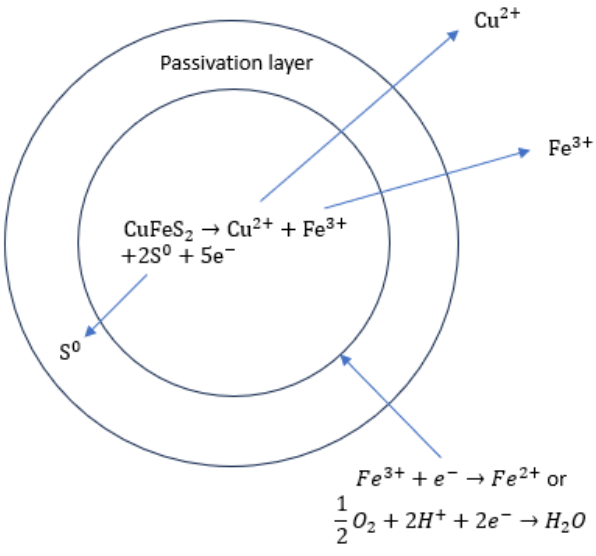

Figure 1.5: Oxidative leaching of copper concentrates diagram (Cordoba, 2008)

The processing rate is slower than the incumbent processes. The solubility of Ce^{4+} at room temperature in 0.1M sulfuric acid is only 0.76M (Paulenova, 2002). The minimum required molar ratio between Ce^{4+} and the $CuFeS_2$ is 5. Therefore, the maximum loading of concentrates that can be leached is limited at approximately 20-30g/L.

The main advantage of the cerium oxidative leaching is its low expected cost. The leaching occurs at room temperature. Cerium is a lower environmental risk than V^{2+}, and the chemical products from leaching are also safer because of the absence of H_2S gas. The separation of cerium from the copper and iron can be done by precipitation to the double salt $NaCe(SO_4)_2$.

1.7. Electrochemical Regeneration

For both the V^{2+} and Ce^{4+} leaching processes, one major weakness is the high chemical cost. Minimizing the losses of chemical reagent during the leaching process is important. One method that shows promise is the recycling of consumed ions by electrochemical regeneration. In the literature, vanadium electrolyzers have been extensively studied for energy storage purposes, with V^{3+} reduced to V^{2+} in sulfuric acid media in the catholyte. This technology has been successfully used to regenerate the V^{2+} leaching solution at laboratory scale for the experiments in this study, with Fe^{2+}, H_2SO_4 solution used as the anolyte.

Although the electrochemical regeneration of vanadium in sulfuric acid is extensively covered in literature, works on cerium regeneration is a bit sparse. This work shows possible schematics of regeneration for cerium, and the necessary catholyte reaction associated with the cerium regeneration. There is also a possibility that cerium can be regenerated chemically, using oxygen at basic conditions, due to the decrease in potential required for oxidation of Ce^{3+} to Ce^{4+} with increasing pH. Although energy required decreases, additional chemicals would be needed to increase the pH for the regeneration, and decrease it to prepare the leaching solution. The performances of the two types of regeneration methods are compared in this work.

1.8. Contributions to the research

Vanadium reductive leaching method was previously developed in the West group. The author designed the continuous reactor for the vanadium reductive leaching. Cerium leaching method was newly developed in the West group. The author analyzed the leach kinetics of the cerium leaching method, and developed the regeneration methods for cerium.

1.9. Summary

With the current processing methods, the copper supply cannot sufficiently meet the demands through 2050. This paper introduces two possible alternative copper processing methods to replace the incumbent processing methods. The criteria list for the viability of the two processes consists of leaching kinetics, costs, separation of ions, regeneration, overall yield, safety, and environment. The two processes shown in this work will be evaluated on these categories.

1.10. References

Calvo, G., Mudd, G., Valero, A., Valero, A. Decreasing Ore Grades in Global Metallic Mining: A Theoretical Issue or Global Reality? *Resources* **2016**, *5*, 36.

Córdoba, E., Muñoz, J., Blázquez, M., González, F., Ballester, A. Leaching of chalcopyrite with ferric ion. Part I: General aspects. *Hydrometallurgy* **2008**, *93* (3–4), 81–87.

Dimitrijević, M., Kostov, A., Tasić, V., Milosević, N. Influence of pyrometallurgical copper production on the environment. *Journal of Hazardous Materials* **2009**, *164*(2-3), 892-899.

Dreisinger, D. Copper leaching from primary sulfides: Options for biological and chemical extraction of copper. *Hydrometallurgy* **2006**, *83* (1–4), 10–20.

Elshkaki, A., Graedel, T.E., Ciacci, L., Reck, B.K. Copper demand, supply, and associated energy use to 2050. *Global Environmental Change* **2016**, *39*, 305-315.

Forsén, O., Aromaa, J., Lundström, M. Primary Copper Smelter and Refinery as a Recycling Plant—A System Integrated Approach to Estimate Secondary Raw Material Tolerance. *Recycling* 2017, *2*(4), 19.

Hawker, W., Vaughan, J., Jak, E., Hayes, P.C. The synergistic copper process concept. *Mineral Processing and Extractive Metallurgy* **2017**, *127*(4), 1-11.

Kulczycka, J., Lelek, Ł., Lewandowska, A., Wirth, H., Bergesen, J.D. Environmental Impacts of Energy-Efficient Pyrometallurgical Copper Smelting Technologies: The Consequences of Technological Changes from 2010 to 2050. *Journal of Industrial Ecology* **2017**, *20*(2), 304-316.

Mokmeli, M. Pre-feasibility study in hydrometallurgical treatment of low-grade chalcopyrite ores from Sarcheshmeh copper mine. *Hydrometallurgy* **2020**, *191,* Article 105215.

Norgate, T., & Jahanshahi, S. Low grade ores – Smelt, leach or concentrate? *Minerals Engineering* **2010**, *23*(2), 65–73.

Papagianni, S., Moschovi, A.M., Sakkas, K.M., Chalaris, M., Yakoumis, I. Preprocessing and Leaching Methods for Extraction of REE from Permanent Magnets: A Scoping Review. *AppliedChem* **2022**, *2*(4), 199-212.

Paulenova, A., Creager, S.E., Navratil, J.D., Wei, Y. Redox potentials and kinetics of the Ce^{3+}/Ce^{4+} redox reaction and solubility of cerium sulfates in sulfuric acid solutions. *Journal of Power Sources* **2002**, *109*(2), 431-438.

Vardner, J. T., Gencer, E., Emerson, M., Farinato, R. S., Nagaraj, D. R., Banta, S., West, A. C. Vanadium(II) sulfate for the reductive leaching of chalcopyrite: Replacing smelting with electrolysis for copper production. *ChemElectroChem* **2022,** *9*(24), e202200920.

World Bank. Commodity markets outlook under the shadow of geopolitical risks. (2023). *World Bank Group.*

Xu, T., Donovan, B., Kim, C., Banta, S., Fitts, J.P., West, A.C. Leaching mechanism for chalcopyrite in electrochemically regenerated vanadium(II). *ACS Sustainable Chemistry & Engineering,* **2024**, *12*(43), 15913-15922.

Chapter 2:

Vanadium(II) Reductive Upgrading of Copper Sulfide Concentrates via Iron Leaching to Facilitate Stagewise Oxidative Copper Leaching at Room Temperature[a]

[a] This chapter has been published: Kim, C., Donovan, B., Fitts, J.P., Farinato, R.S., Nagaraj, D.R., Banta, S., West, A.C. Vanadium(II) reductive upgrading of copper sulfide concentrates via Iron leaching to facilitate stagewise oxidative copper leaching at room temperature. *Hydrometallurgy* **2025**, *236*, 106509. https://doi.org/10.1016/j.hydromet.2025.106509

Abstract

Over this coming decade, copper demand in the United States is projected to increase significantly because of the energy transition to carbon-free sources. Compared to traditional hydrometallurgical processes involving oxidation, reductive leaching of copper mineral concentrates has been shown to yield significant advantages. For example, reductive leaching of chalcopyrite can be performed at ambient temperatures without intensive grinding. This could achieve high yields, reduced processing costs, all while minimizing environmental impacts.

This work explores vanadium reductive leaching of other copper mineral concentrates by measuring leaching kinetics and yields. Over 90% of the copper was successfully extracted from copper concentrates obtained from three active mines, each with different mineral compositions, after reacting in VSO_4, H_2SO_4 solution at room temperature for 60 minutes. It was shown that the addition of $FeSO_4$ enhanced the leaching yields of copper from chalcocite (Cu_2S), from 55.1% to 100% in concentrates having moderate iron concentrations and from 62.7% to 82.2% in low-iron concentrates. The copper recovery in low-iron concentrates could be increased to 99% after leaching a second time, suggesting a staged operation may be favored. Results show that similar yields may be achieved when leaching occurs in a continuous flow reactor with residence times between 10 and 20 minutes. For example, 85.2% - 100% of iron was leached from Source 2 concentrates, and 87.7% - 95.3% of iron was leached from Source 3 concentrates in continuous flow leaching. The processing rate using the continuous flow reactor was 87 g L^{-1} h^{-1}, a rate competitive with existing processing methods.

2.1. Introduction

Without significant technological innovations, a global copper deficit is expected to occur in the upcoming decades due to the increased demand for copper from green industries and the increasing costs of mining and processing copper ores (Rötzer et al., 2020). With an acceleration of decarbonization goals, large amounts of copper are necessary to build and expand the penetration of solar and wind energy for power production and to support the manufacture of electric vehicles. These renewable energy source facilities require approximately five times more copper than traditional energy sources, with wind turbines requiring between 1000-5000 t/GW, and solar panels requiring approximately 4.6 t/MW (Carrara et al., 2020). Between 2023 and 2050, nearly 1.4 billion tonnes of copper will be required to reach net-zero-emission energy production, which is twice the total amount of copper produced over all human history (Schipper et al., 2018, IEA, 2022).

Traditional pyrometallurgical processes to produce copper are expected to face critical issues in the coming decade. The first issue is the declining grade of ores available from mines (Calvo et al., 2016). Pyrometallurgical processes often have stringent requirements on the copper content of the concentrate; approximately 20% of the concentrate weight must consist of copper (Forsén et al., 2017). According to Norgate et al. (2010), the minimum economic ore grade is approximately 0.5% since the energy required to produce copper increases with declining ore grade. It is estimated that 72, 131, 249, and 602 MJ of energy will be required to mine, grind to 75 μm, concentrate, and smelt the ore to produce 1 kg of copper from 1.0%, 0.5%, 0.25%, and 0.1% grade ores, respectively (Norgate and Jahanshahi, 2010).

The second issue is that pyrometallurgical processes can be environmentally harmful due to the release of sulfur dioxide and airborne arsenic compounds. An example was seen in one of

the copper smelters in Serbia, where the SO_2 and arsenic levels surrounding the smelter have consistently exceeded the daily limit suggested by the WHO. The maximum daily SO_2 concentration of 2125 $\mu g/m^3$ was more than 100 times greater compared to the WHO AQG (Serbula et al., 2021). In the United States there is a shortage of smelters. According to Bridge, the decreased profitability of copper production can be traced back to the 1970s, an era when the grade of the copper ore declined, yet the mines neglected to invest in innovations necessary to reduce the production costs, instead postponing the effects of declining ore grades (Bridge, 2000). With the added pressure from environmental regulations in the 1980s, profitability decreased, resulting in a shortage of smelters in the United States. This makes it necessary to export copper concentrates to smelters in Europe and China, further increasing the processing costs and time (Chapman, 1991, Chen et al., 2016).

As such, it may be economically and environmentally appealing to transition away from pyrometallurgical methods to hydrometallurgical alternatives. In current hydrometallurgical processes, copper concentrates must be oxidized before they can be processed in an aqueous medium to leach Cu^{2+} ions (Schlesinger et al., 2011a). However, although copper oxide ores are commercially processed through hydrometallurgy, approximately 80% of the global copper production originates from copper sulfides, most of which consist of chalcopyrite (Dimitrijević et al., 2009). Copper sulfides, such as chalcopyrite ($CuFeS_2$), chalcocite (Cu_2S), and bornite (Cu_5FeS_4), are highly refractory to leaching, as the sulfur layers and the metal-deficient layers accumulate on the surface of the copper ore particles, slowing the leaching kinetics (Córdoba et al., 2008). Some notable methods to counter the slow kinetics and accelerate the leach reaction include the Albion process, in which the ores are finely ground to increase the surface area-to-volume ratio, the Total Pressure Oxidation process, in which high temperatures and high

pressures are used to oxidize and remove the sulfur passivation layers, the Anglo American Corp./ University of British Columbia process, in which surfactants are utilized to disperse the molten sulfur, and silver ion catalysis, in which silver cation adsorbs to the chalcopyrite surface to form Ag_2S (Dreisinger, 2006, Mokmeli, 2020, Ghahremaninezhad et al., 2015).

While oxidative leaching methods have been commercialized, the reductive leaching pathway is relatively unknown outside of the laboratory. Some of the methods investigated to leach chalcopyrite reductively include utilizing solid iron (Dreisinger and Abed, 2002), solid aluminum (Doyle and Lapidus, 2006), SO_2 gas (Sohn and Wadsworth, 1980), or an electrolytic cell (Martínez-Gómez et al., 2018). According to Fuentes-Aceituno et al. (2008), the reduction of chalcopyrite has been shown to produce chalcocite (Cu_2S) and djurleite ($Cu_{1.96}S$), leading to the release of Fe^{2+} ions into the solution. Biegler and Swift (1976) observed small amounts of elemental copper following a reductive leach. Unlike the oxidative leach process in which sulfide oxidation leads to the formation of passivation layers, sulfur in the reductive leach process remains in the mineral as elemental sulfur or evolves as H_2S gas. Although reductive leaching has been shown to prevent the formation of passivation layers, the limited research into reductive leaching has shown few disadvantages. For example, a large excess of reducing agents is required, and the solution temperature must be brought close to the boiling point (Fuentes-Aceituno et al., 2008). These constraints have limited the concentration of chalcopyrite processed to 10 g/L, rendering the process uneconomical (Martínez-Gómez et al., 2018).

However, Vardner *et al*. (2022) used V^{2+} ions as the reducing agent to demonstrate a rapid two-step leaching of copper concentrates, converting chalcopyrite into Cu_2S, which was further reduced to Cu^0, according to chemical reactions in Eq. 2.1 and Eq. 2.2:

$$2\,CuFeS_2 + 6H^+ + 2V^{2+} \rightarrow Cu_2S + 2Fe^{2+} + 3H_2S + 2V^{3+} [\Delta G^0 = -4.50\ kJ] \qquad 2.1$$

$$Cu_2S + 2H^+ + 2V^{2+} \rightarrow 2Cu^0 + H_2S + 2V^{3+} \; [\Delta G^0 = +3.93\ kJ] \quad 2.2$$

Standard Gibbs' free energy data have been obtained from the literature (Dean, 1979, Robie et al., 1985, Milazzo et al., 1978). Unlike comparable oxidation methods, the reaction between V^{2+} and $CuFeS_2$ is relatively fast, even at room temperature and pressure, with the reductive leaching of chalcopyrite producing copper metal within 60 minutes. Additionally, this rapid reductive leaching was demonstrated on chalcopyrite particles with a P_{80} value of 75 microns. This way, copper concentrates would not require grinding beyond current smelter requirements (Schlesinger et al., 2011b). In contrast, traditional oxidative methods often require P_{80} values around 10 microns so that surface passivation does not significantly hinder the reaction rate (Schlesinger et al., 2011a, Dreisinger, 2006).

Furthermore, reductive leaching uses sulfuric acid to control pH, facilitating integration into existing processes. Due to environmental regulations, many smelters operate by converting their SO_2 gas into sulfuric acid, with each tonne of copper producing three tonnes of sulfuric acid as a byproduct (Ayres et al., 2003, Habashi, 2007). The mineral processing operations are obligated to find a market for sulfuric acid. Therefore, incorporating the reductive leaching method into a large-scale continuous process is intriguing, as it might mean that the copper concentrates can be processed at a significantly lower operational cost.

This paper addresses two factors necessary for the determination of the viability of this reductive leaching method in a large industrial setting. The first factor is the requirement to process copper concentrates from various mines. The compositions of copper concentrates produced from different mines are expected to be different. Koizhanova et al. (2023) examined the different concentrate compositions obtained from four mines in Kazakhstan, and concluded that the composition directly affected the leaching rate and the consumption of acid required for

each concentrate. Similarly, various mineral components might assist or hinder the reaction between the copper concentrate and V^{2+}. For example, the presence of pyrite is known to improve the leaching rate in a redox potential window between 410 and 440 mV vs Ag/AgCl due to the galvanic interaction with chalcopyrite (Koleini et al., 2011). In this paper, copper concentrates from three different mines were obtained and tested to analyze the effectiveness of the V^{2+} reductive leaching method based on the copper concentrate composition.

The second factor investigated is the kinetics of this leaching reaction in continuous or semi-batch reactors. Previous experiments by Vardner et al. (2022) were done in a batch experimental reactor . In the current study, a tubular flow reactor was built to determine the copper recovered from concentrates as a function of the amount of concentrate processed and the residence time inside the reactor.

To process copper concentrates from mines, which are often a mixture of copper-containing minerals, the V^{2+} leaching technology must be versatile. This paper aims to achieve five main objectives: (i) to show that V^{2+} is effective in leaching $CuFeS_2$ and other copper sulfides such as Cu_5FeS_4 and Cu_2S, (ii) to extend the scope of the reductive V^{2+} leaching technology in preparation for scale-up to a larger-scale process, (iii) to show that the V^{2+} leaching technology can achieve high copper recoveries while maintaining high processing rates, (iv) to compile the performances of conventional leaching methods and compare them with the results of the V^{2+} leaching technology produced in this work, (v) to show that V^{2+} leaching technology outperform conventional leaching methods.

2.2. Experimental Methods

2.2.1. *Electrochemical generation of V(II)*

Vanadyl sulfate hydrate (Alfa Aesar or Spectrum Chemical) was dissolved in 1 M H_2SO_4 to achieve a concentration of 1 M VO^{2+}. A flow electrolysis cell consisting of copper current collectors, graphite electrodes, and a Nafion 117 membrane (MTI Corporation) was used to reduce VO^{2+} to V^{2+}. This setup is like the one used for a V4RB (Vanadium (IV) redox flow battery), which utilizes V(IV) ions as the sole parent species (Ding et al., 2013). Either a 1 M Fe^{2+} solution or a 1 M VO^{2+} solution was prepared as the anolyte. Oxidation of either Fe^{2+} to Fe^{3+} or VO^{2+} to VO_2^+ occurred at the anode. The reactions for the reduction of VO^{2+}, the oxidation of Fe^{2+}, and the oxidation of VO^{2+} are shown below.

$$VO^{2+} + 2H^+ + 2e^- \rightarrow V^{2+} + H_2O \quad (2.3)$$

$$Fe^{2+} \rightarrow Fe^{3+} + e^- \quad (2.4)$$

$$VO^{2+} + H_2O \rightarrow VO_2^+ + 2H^+ + e^- \quad (2.5)$$

The $VOSO_4$ solution and the anolyte were pumped through the electrolysis cell using Cole-Parmer Masterflex L/S peristaltic pumps. Current was applied to the electrodes using a Ivium-n-Stat potentiostat at cell voltage of 1.6 V until the current density leveled off at approximately 8 mA/cm^2, which signified the nearly complete conversion of VO^{2+} to V^{2+}. The conversion to V^{2+} was confirmed periodically by coulometric titration (Geiser et al., 2019).

2.2.2. Preparation of copper concentrate and characterization

Concentrates were provided from three different mining operations. The mineral composition of the concentrates from each source was determined by the Advance Mineral Identification and Characterization System (AMICS). This technique uses SEM and X-ray energy spectral analysis of the backscattered electrons from epoxy-mounted thin sections of each mineral concentrate to

produce mineralogical maps of individual ore particles (Lou et al., 2020). The images are used to identify mineral composition, element distribution, mineral size, and mineral phase associations. The AMICS analysis was conducted once for each source at Eagle Engineering by Dr. Paul Miranda. Table 2.1 shows the mineral compositions as weight % of the copper concentrates from each source. Table 2.2 summarizes the distribution of copper content assigned to each mineral in the copper concentrates, based on the results of the AMICS analysis.

Table 2.1: Mineral composition of the concentrates from each source via AMICS analysis

Mineral	**Source 1 (% w/w)**	**Source 2 (% w/w)**	**Source 3 (% w/w)**
$CuFeS_2$	83.8	56.5	5.4
Cu_2S	-	4.7	56.9
Cu_5FeS_4	-	4.9	13.9
$Cu_2CO_3(OH)_2$	-	1.8	-
FeS_2	7.7	10.9	-
SiO_2	1.5	2.1	4.2
$KAlSi_3O_8$	1.9	4.1	6.5
Misc.	5.1	15.1	13.1

Table 2.2: Copper assignment of the concentrates from each source via AMICS analysis

Mineral	**Source 1 (%w/w)**	**Source 2 (%w/w)**	**Source 3 (%w/w)**
$CuFeS_2$	100	71.3	3.3
Cu_2S	-	13.7	81.0
Cu_5FeS_4	-	11.3	15.7

$Cu_2CO_3(OH)_2$	-	3.8	-

The main sources of copper and iron are chalcopyrite, chalcocite, bornite, and pyrite minerals. The iron and copper contents were determined by digesting the three samples of copper concentrates from each source in aqua regia and measuring the iron and copper concentrations using iCE 3000 Atomic Absorption Spectroscopy. Table 2.3 summarizes the metal composition determined in each copper concentrate.

Table 2.3: Average metal composition of the concentrates and the standard deviation from each source

Metal	**Source 1 (%w/w)**	**Source 2 (%w/w)**	**Source 3 (%w/w)**
Copper – Mean	27.1	20.0	50.0
Copper – Std. Deviation	2.7	1.0	4.2
Iron – Mean	29.8	16.2	3.0
Iron – Std. Deviation	3.3	1.3	0.5

The XRD spectra shown in Figure 2.1 and the AMICS report indicate that the main source of copper in Source 1 and Source 2 concentrates is from $CuFeS_2$, and Cu_5FeS_4 and Cu_2S in Source 3. Hence, this paper refers to Source 1 concentrates as "high-chalcopyrite" concentrates, Source 2 as "low-chalcopyrite" concentrates, and Source 3 as "low-iron high-bornite" concentrates. The XRD results from this study for Source 1 and Source 2 are consistent with the AMICS report. Although the XRD does not clearly detect chalcocite in Source 3 concentrates, it is highly likely that chalcocite is abundantly present, as shown in the AMICS report, considering the high copper content of Source 3 concentrates (50.0% Cu, 3.0% Fe). The particle size of the concentrates varied, with a P_{80} value of 75 µm (Source 1, 2), and P_{30} value of 106 µm (Source 3).

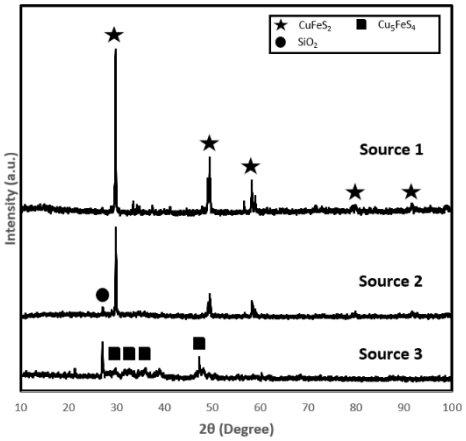

Figure 2.1: XRD analysis of raw copper concentrates from each source

2.2.3. Batch experiments

Figure 2.2 shows the experimental procedure for reacting copper concentrates in a 1 M VSO_4 solution. Copper concentrates (1 - 6 grams) were added into a 25 mL solution composed of 1 M VSO_4 and 1 M H_2SO_4. The solution was stirred with a magnetic stirring bar for 60 minutes, with liquid phase samples of 500 µL taken at time intervals of 0, 5, 10, 20, 40, and 60 minutes to measure their Fe^{2+} content in solution at room temperature. After the reaction, the solid products were filtered and dried, then analyzed using Xpert3 Powder XRD from Malvern Panalytical to determine the recoverable copper content and the crystalline mineral phases. Total recoverable Cu was determined by reacting the solid products in 1 M $Fe_2(SO_4)_3$, 1 M H_2SO_4 solution, thereby leaching out the remaining copper according to Equations 2.6 and 2.7. This procedure was demonstrated by Vardner et al. (Vardner et al., 2022).

$$Cu^0 + 2Fe^{3+} \rightarrow Cu^{2+} + 2Fe^{2+} \ [\Delta G^0 = -83.0\ kJ] \quad (2.6)$$

$$Cu_2O + 2H^+ + 2Fe^{3+} \rightarrow Cu^{2+} + 2H_2O + 2Fe^{2+} \ [\Delta G^0 = -411.3\ kJ] \quad (2.7)$$

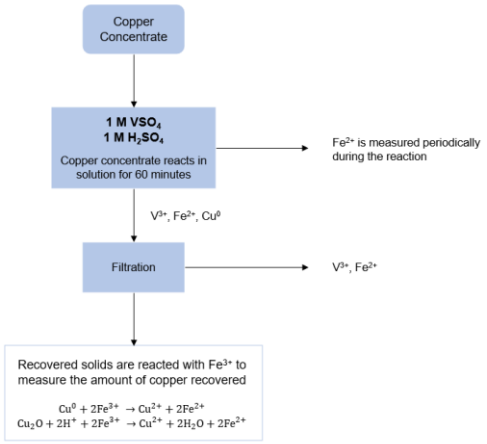

Figure 2.2: Process flow diagram of copper concentrates in 1 M VSO_4 solution in a batch setting.

The complete dissolution of metallic copper in 0.5 M $Fe_2(SO_4)_3$, 1 M H_2SO_4 solution at room temperature has been confirmed using -20+30 µm copper powders obtained from Sigma Aldrich. At a solid liquid ratio of 1.5 g Cu to 50 mL of $Fe_2(SO_4)_3$-H_2SO_4 solution and stirring, 30 minutes were required to leach 100% of the copper from metallic copper.

Vardner *et al.* (2022) previously reported that the copper recovery from source 1 concentrates was less than 5% in a control experiment without the V^{2+} reduction reaction .

2.2.4. *Continuous Reactor Experiments*

(a) (b)

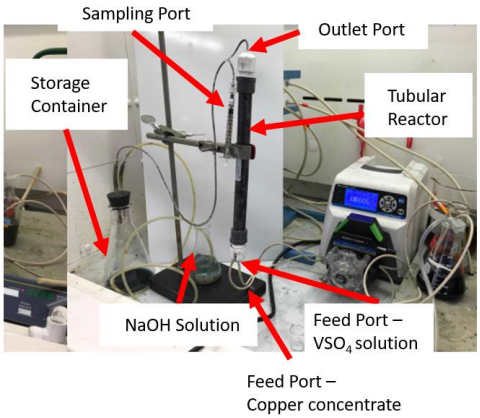

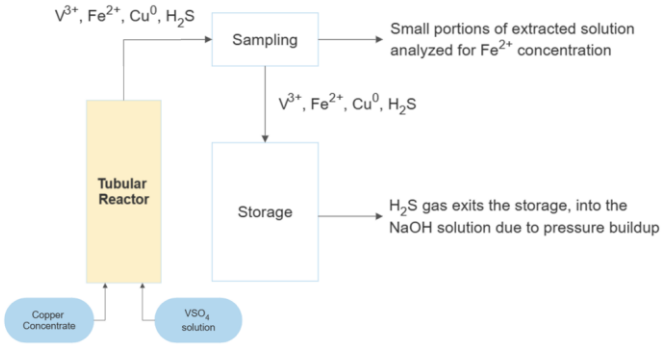

Figure 2.3: (a) Experimental setup of the continuous flow reactor (b) Process flow diagram of the reaction between copper concentrates and V^{2+} in a continuous flow reactor

Figure 2.3a shows the continuous flow reactor – a 60 mL PVC static in-line mixer (Koflo Corp). The two ends of the reactor are sealed with PVC end caps. Two tube adapters were fit through the bottom end cap, and each was connected to Tygon tubing to feed the VSO_4 solution and the copper concentrate slurry (produced by adding copper concentrate to 1 M H_2SO_4 and stirring for 60 minutes) into the reactor. The VSO_4 solution (0.5 M V^{2+}, 1 M H_2SO_4) and the copper concentrate slurry (loadings ranging between 29 – 87 g/L, depending on the experiment) were fed into the reactor at equal volumetric flow rates determined by the desired residence time. One tube adapter was fitted through the top end cap to serve as the outlet for the slurry product. The storage container consisted of a 500-mL Erlenmeyer flask with a rubber stopper at the top, with two glass tubes fitted through the rubber stopper, one for letting in the slurry product and one for letting out the gaseous phase (e.g., H_2S). The gas phase was directed into a 5 M NaOH solution to scrub any H_2S produced.

Figure 2.3b shows the experimental process flow diagram. During the experiment, the V^{2+} solution and the copper concentrate slurry were fed into the reactor simultaneously at the same flow rate. The residence time R_t inside the reactor of the VSO_4 solution and the copper concentrate slurry was adjusted by changing the flow rate of a single channel Q, according to:

$$R_t = \frac{V_{reactor}}{2Q} \tag{2.8}$$

The concentration of the prepared VSO_4 solution was 0.5 M for all experimental conditions. As the VSO_4 and the copper concentrate were fed into the reactor at equal rates, the initial, unreacted V^{2+} concentration inside the reactor was 0.25 M. The amount of copper concentrate used to make the slurry varied between 58 and 87 g/L for Source 2 and between 29 and 58 g/L for

Source 3 concentrates. The copper concentrate loading amount is specified by the amount in the slurry and is reduced by 50% in the reactor given the equal volumetric flow rates of the two feeds.

Once the reactor was filled, the product slurry exited the reactor and into the storage container through one of the glass tubes inserted into the rubber stopper. Due to the fine particle sizes and the decreased density after reaction, approximately 80% of the solids was determined to exit the reactor without settling by measuring the solid content exiting the reactor. The product slurry was maintained in the storage container until the end of the experiment. The resulting H_2S gas exited the storage container through the other glass tube and into a NaOH solution due to the pressurization from the peristaltic pump. The H_2S was neutralized in the NaOH solution. Periodically, a sample of the leach solution was extracted from the sampling port using a 1 mL syringe by fitting it through the Luer lock. This sample was analyzed for its Fe^{2+} concentration, which could be used to determine when the reaction has reached a steady state by noting that the Fe^{2+} concentration between consecutive samples showed minimal deviation.

Since the copper product remained as a solid phase, the measurement of aqueous copper could not be used to determine the amount of $CuFeS_2$ that had reacted with V^{2+}. The measurement of Fe^{2+} ions in the solution was used as an estimate. As shown in Equation 2.1, the Fe^{2+} concentration is a good indicator for the mass of $CuFeS_2$ reduced by V^{2+} ions, as the amount of $CuFeS_2$ reacted directly correlates with the amount of Fe^{2+} ions released into the solution. However, it is not a perfect measurement for the reduction of the copper concentrate due to the presence of other sulfides with differing ratios of Cu:Fe. Nevertheless, the Fe^{2+} concentration was used as an estimate at intermediate reaction times. For the continuous reactor setup, the residence times were below 20 minutes, and the Fe^{2+} concentration was used as a proxy to characterize reaction rates.

2.2.5. *Processing and characterization of solid product and solution analysis for calculation of copper recovery*

After the recovered solids were filtered, the solids were leached in a 1 M $Fe_2(SO_4)_3$, 1 M H_2SO_4 solution for 60 minutes. The Fe^{3+} leaches the solid copper product by oxidation, as shown in Equations 2.6 and 2.7. The concentration of the copper was measured after leaching, and the copper recovery was calculated from the measured Cu^{2+} concentration and volume of solution.

The iron and copper concentrations were measured using iCE 3000 Atomic Absorption Spectroscopy (AAS), obtained from Fisher Scientific. During the experiment, 500 µL samples of the leach solution were taken periodically and diluted to make the iron or copper concentrations between 0 and 4 mg/L. The AAS was calibrated before every measurement using standards ranging between 0 and 4 mg/L to construct linear calibration curves.

A PANalytical Xpert3 Powder XRD system was used for the analysis of product solids. The XRD was operated with filtered Empyrean Cu Kα radiation (k = 0.15418 nm), a tube voltage of 45 kV, and a current of 40 mA. The peak intensities were measured using a PIXcel1D detector in the 2θ range of 5–100° with a step size of 0.026° on a rotating plate with a revolution time of 2.0 s.

2.3. Results and Discussion

2.3.1. Reductive V(II) leaching of concentrates from each source

Adding copper concentrate into a solution of 1 M VSO_4 and 1 M H_2SO_4 resulted in a vigorous, bubbling reaction. Reactions 2.1 and 2.2 for $CuFeS_2$ and Cu_2S, respectively, with Reaction 2.9 below for Cu_5FeS_4, have been postulated as the primary V^{2+} leach reactions.

$$2Cu_5FeS_4 + 2V^{2+} + 6H^+ \rightarrow 5Cu_2S + 2V^{3+} + 2Fe^{2+} + 3H_2S \quad 2.9$$

The Fe^{2+} concentration increased significantly during the reaction due to iron release from $CuFeS_2$ or Cu_5FeS_4. Previous work suggested that pyrite (FeS_2) does not react with V^{2+} (Vardner et al., 2022). Figure 2.4a shows the weight percentage of iron leached out of the copper concentrates according to Reactions 2.1 and 2.9. At various mass loadings, the concentrates from the three sources were reacted in the VSO_4 solution for 60 minutes. The amount of iron leached follows an asymptotic trend for all experimental conditions, as shown in Figures S2.1 and S2.2, with most of the iron content removed during the initial phases of the leaching.

(a) (b)

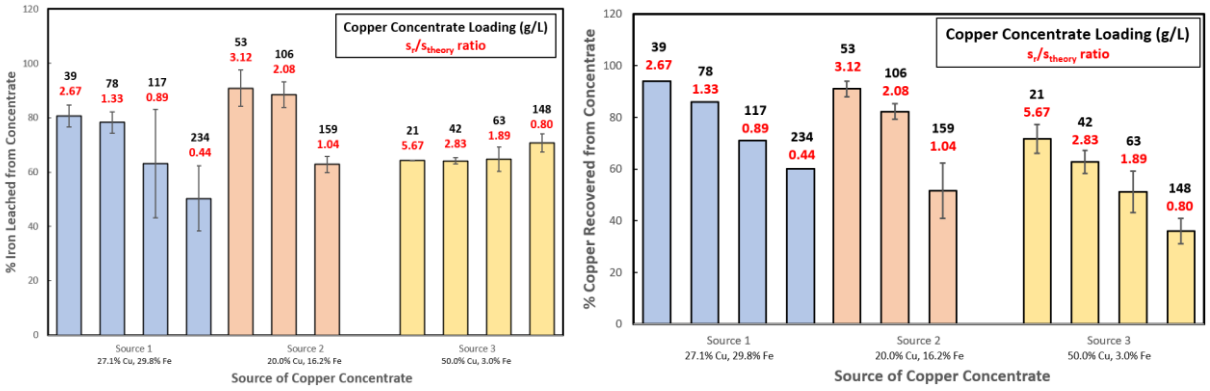

Figure 2.4: (a) Iron leached out from concentrates due to reaction with 1 M VSO_4 and 1 M H_2SO_4 solution in Step 1 in Fig. 3. (b) Copper recovered from copper concentrates after reacting the solid from Step in Fig. 3, with 1 M $Fe_2(SO_4)_3$ and 1 M H_2SO_4 in Fig. 3. The two numbers above each bar represent copper concentrate mass loading g/L (upper scale) and s_r/s_{theory} (lower scale), where S_{theory} is based on Equations 2.6, 2.7 and 2.9 and S_r is based on the concentration of V^{2+}, mass loading of concentrates, and the compositions in each source based on Table 2.3. Other conditions: 60 minutes of reaction time at room temperature.

Similarly, Figure 2.4b shows the weight percentage of copper recoverable after reacting the remaining solid product in $Fe_2(SO_4)_3$ solution for 60 minutes. Increasing the amount of copper concentrate loaded into the 1 M VSO_4 solution generally resulted in a decreased conversion of copper. This trend suggests that when there was a stoichiometric excess of V^{2+} ions

present, lower concentrate mass loadings resulted in a higher content of copper concentrate reduced by V^{2+}. When the excess V^{2+} ions was sufficiently high, large amounts of copper could be recovered from the concentrate after reacting in the VSO_4 solution for 60 minutes.

One possible explanation is that the excess V^{2+} ions greatly aid the reaction thermodynamically, specifically the reduction of Cu_2S to Cu^0 (Equation 2.2). According to the Pourbaix diagrams reported by Garrels et al., the reduction potential of Cu_2S to Cu^0 is -0.25 V vs.SHE, which is similar to the reduction potential of V^{3+} to V^{2+} reported as -0.255 V vs. SHE (Milazzo et al., 1978, Garrels and Christ, 1965). Using the Nernst Equation shown in Equation 2.10, the reduction of Cu_2S to Cu^0 is favorable at ambient conditions and in 1 M sulfuric acid only when V^{2+} consists of over 45% of total vanadium in solution. For the V^{2+} to consist of over 45% of total vanadium in solution until completion of the reaction, the s_r/s_{theory} must exceed 1.82. This calculation does not account for the depletion of H^+ concentration during the reaction and the decreasing reduction potential of Cu_2S with the depletion of H^+. both of which would increase the excess V^{2+} required.

$$E = E^0 - \frac{RT}{nF} \ln \frac{[V^{3+}]}{[V^{2+}][H^+]} \qquad 2.10$$

The amount of iron leached is only slightly affected by excess V^{2+} since the reduction of $CuFeS_2$ occurs at a higher potential, provided that s_r/s_{theory} is greater than 1. However, all concentrates, especially Source 3, contained unleachable iron content due to various types of silicates, which might explain the fluctuations between the maximum of iron that could be leached between each experiment.

A major focus of this work is to confirm the versatility of the V^{2+} reductive leaching method on copper concentrates from three different sources. Since the composition of each concentrate

varies, it is not sufficient to compare the experimental conditions by the mass loading of the concentrates in the V^{2+} solution. A ratio, s_r/s_{theory}, (see definitions below) is developed to compare the experimental conditions of concentrates from different sources.

One mole of V^{2+} is required to reduce either one mole of copper or one mole of iron. The oxidation state of copper in the initial copper concentrates is mostly +1, and the oxidation state of iron is mostly +3 (Klekovkina et al., 2014, Pattrick et al., 2004). According to reaction 2.2, the oxidation state of the final copper product is 0, and according to reactions 2.1 and 2.9, the oxidation state of the final iron product is +2.

The molar concentration of V^{2+} required to reduce all the copper concentrate in the solution, s_{theory}, can be defined as the sum of the molar concentration of copper, c_{Cu}, and the molar concentration of iron, c_{Fe} in the copper concentrate slurry. The ratio between the molar concentration of V^{2+} needed to reduce all the copper and iron in the copper concentrate in the slurry, s_{theory}, and the actual molar concentration of V^{2+}, s_r, is a useful measure of the excess V^{2+} in a reaction. The formula for this ratio is shown below.

$$\frac{s_r}{s_{theory}} = \frac{c_{V^{2+}}}{c_{Cu} + c_{Fe}} \qquad 2.11$$

By comparing the copper recoveries of concentrates from different sources, when the s_r/s_{theory} ratio was similar, it was determined that the copper recovery of low-iron high-bornite concentrates was significantly lower than the copper recovery from the other sources. For the high-iron copper concentrates, it was possible to convert a large amount of its total copper weight into recoverable copper. For example, 94.0% of the copper was recovered when s_r/s_{theory} = 2.67, and 91.0% was recovered when s_r/s_{theory} = 3.12. However, for low-iron high-bornite

concentrates, the copper recovery was only 62.7% when s_r/s_{theory} = 2.83 and 71.7% when s_r/s_{theory} = 5.67.

To investigate the reason for the relatively lower copper recovery obtained from low-iron high-bornite concentrates, XRD analysis was performed on all solid products after the reaction in the VSO_4 solution. The results are shown in Figure 2.5. It was determined that the solid products were mostly Cu_2S, Cu^0, and Cu_2O. It is reasonable to hypothesize that the exposure of Cu^0 to air produce. A similar result was shown by Vardner et al. (2022). They found that the Cu^0 leach product oxidized gradually to $CuSO_4$ in the process of drying and exposure to H_2SO_4 and air. Therefore, the observation of Cu_2O is assumed to originate from metallic copper.

Figure 2.5 illustrates the high copper recovery obtained by reacting 39 g/L of high-chalcopyrite concentrates with 1 M VSO_4, as the copper product is composed mostly of Cu^0, indicating the complete reduction of $CuFeS_2$ to Cu^0. The figure also shows the complete reduction of $CuFeS_2$ in the low-chalcopyrite concentrates by reaction with V^{2+}.

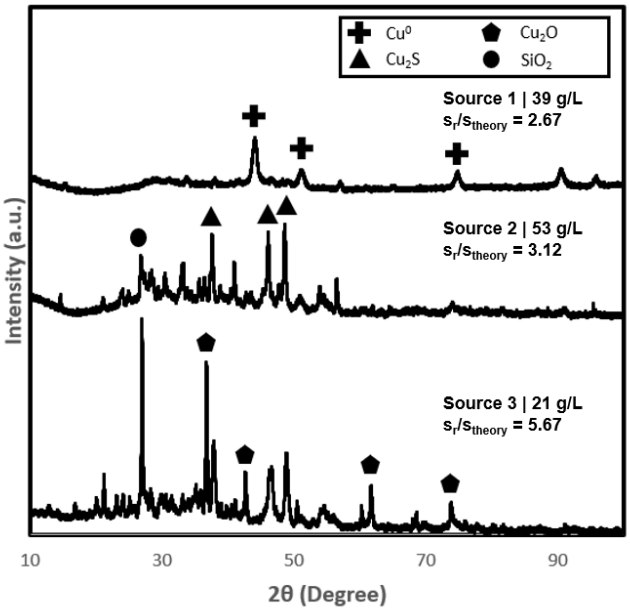

Figure 2.5: XRD analysis of solid products after the copper concentrates are reacted in 1 M VSO_4 solution for 60 minutes at room temperature.

The XRD results for the residual solid samples obtained by reacting 21 g/L of low-iron high-bornite concentrates with 1 M VSO_4 show the presence of both Cu_2O and Cu_2S in the solid product. Despite the theoretical abundance of V^{2+} ions compared to the copper and iron in the concentrate in the slurries, the final product is mainly Cu_2S, not the elemental copper. The incomplete reduction of Cu_2S suggests that there is a factor inhibiting the rate of the reaction. Increasing the low-iron high-bornite concentrate loading in the 1 M VSO_4 solution resulted in an increase in Cu_2S in the solid products.

Overall, the results indicate that the low copper recovery of low-iron high-bornite concentrates is related to the slow reduction rate of Cu_2S since a large amount of Cu_2S remains in the solid product. An example of a slow reduction rate of Cu_2S has also been reported by Yu and Liang (2004) when copper was produced by direct hydrogen reduction of Cu_2S in basic media. As such, more experiments were done by reacting pure Cu_2S with the 1 M VSO_4 solution to understand this reaction better. The results have led to the two hypotheses to explain why the copper recovery of low-iron high-bornite concentrates is lower: (i) the incomplete reduction of concentrates in the VSO_4 solution due to slow chemical kinetics, specifically due to the slow reduction of Cu_2S to Cu^0 in the V^{2+} solution, and (ii) the relatively coarse particle sizes of low-iron high-bornite concentrates.

2.3.2. Effect of Fe^{2+} additives in the reduction rate of Source 3 concentrates

Unexpectedly, the addition of $FeSO_4$ to the solution was found to significantly impact copper yields. This was found to be important for source 3 concentrate rich in Cu_2S, and contains small amounts of iron (Table 2.3). Similar results were found with pure Cu_2S. Figure 2.6 shows the amount of copper recovered for different amounts of Cu_2S loaded into either a 1 M VSO_4

solution or a solution containing 1 M VSO_4 + 0.25 M $FeSO_4$. The additional Fe^{2+} had a significant effect on increasing copper recovery for all tested conditions. The reaction product of Cu_2S in both the 1 M VSO_4 and the 1 M VSO_4 + 0.25 M $FeSO_4$ solutions shows the removal of sulfide from the copper product (Figure S2.5). The transformation of Cu_2S in 1 M VSO_4 + 0.25 M $FeSO_4$ is shown in Equation 2.2, where Cu_2S is reduced to Cu^0, releasing H_2S during the process.

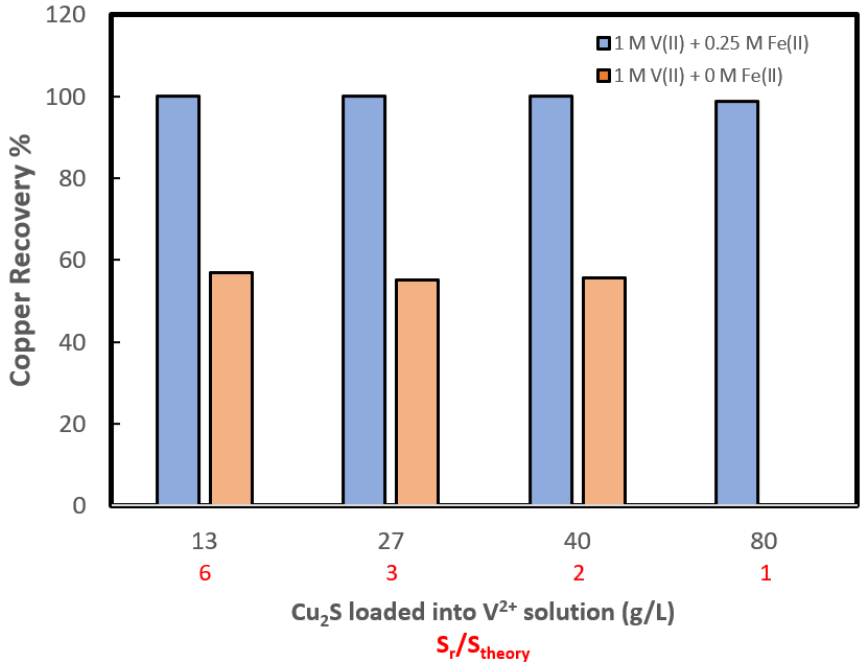

Figure 2.6: Copper recovered from Cu_2S after 60 minutes of reaction time at room temperature. Cu_2S solids were either reacted in 1 M VSO_4 solution, or in 1 M VSO_4 + 0.25 M $FeSO_4$ solution, with the specified mass loading, marked by the x-axis numbers (upper scale) and S_r/S_{theory} (lower scale).

When these solid products are leached in a 1 M $Fe_2(SO_4)_3$ solution, the Cu_2S oxidizes to CuS, and the Cu^0 and Cu_2O solids are consumed. The analysis of solid products matches the observed copper recovery behavior. When the reaction product from Cu_2S in the 1 M VSO_4 is leached in 1 M $Fe_2(SO_4)_3$, solid CuS remains (Figure S2.6). When the reaction product of Cu_2S from the 1 M VSO_4 + 0.25 M $FeSO_4$ solution is leached in 1 M $Fe_2(SO_4)_3$, no solids remain.

This trend can explain why the copper recoveries of concentrates with high iron content were significantly greater. The copper products contained higher content of Cu^0 when reacted in VSO_4 + $FeSO_4$ solution, while the copper products reacted in VSO_4 solution contained higher content of Cu_2S.

The finding that $FeSO_4$ enhances copper recovery was applied to the low-iron, high-bornite copper concentrates. Figure 2.7 shows the copper recovery for the low-iron copper concentrates in 1 M VSO_4 + 0.7 M $FeSO_4$ solution. In all cases, the Cu recovery increased in the presence of $FeSO_4$.

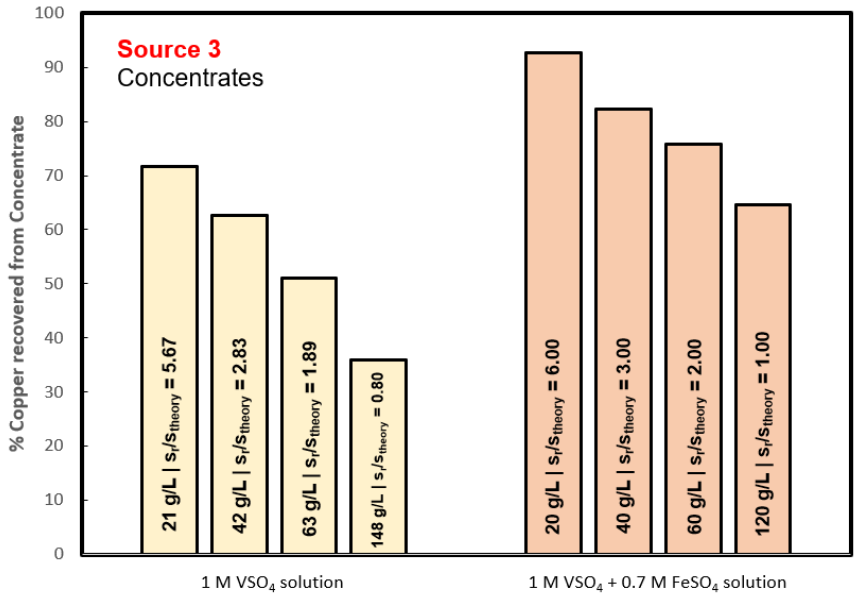

Figure 2.7: Copper recovery from the solid product after 60 minutes of reaction time at room temperature. Low-iron copper concentrates were either reacted in 1 M VSO_4 solution, or in 1 M VSO_4 + 0.7 M $FeSO_4$ solution, with the specified mass loading shown in the figure.

In research reported by Warren et al. (1985), the cathodic reduction current was shown to be significantly higher in the presence of Fe^{2+} in both cathodic potential sweep and in constant

potential regimes. It is possible that Fe^{2+} serves as a catalyst for the reduction of a variety of copper sulfide minerals.

One concern with the vanadium reductive leaching is the production of H_2S, and the possibility that it can corrode the copper product. While Sharma (1980) reports the reaction between Cu_2O and H_2S to produce Cu_2S, and considering the presence of Cu_2O in the reaction product, it is possible the copper product reverts back to Cu_2S (Yu and Liang, 2004). Another concern with the vanadium reductive leaching is the possibility of depleting the H^+ ions required for the leaching process. Starting with a solution of 1 M $VOSO_4$, H^+ is required to reduce VO^{2+} to V^{2+} (Equation 2.1), and also required for the leaching process (Equation 2.9). The depletion of H^+ would likely mean that the reaction product would remain as either $CuFeS_2$ or Cu_2S, since H_2S cannot be produced. Vardner et al. (2022) demonstrated that a H_2SO_4 concentration of 0.5 M was sufficient for 92% copper recovery, but the change in copper sources could have affected the amount of H_2SO_4 needed.

Another issue with depletion of H^+ is the transformation of the V^{2+} ion. According to the Pourbaix diagrams of Zhou et al. (2011), the VSO_4^+ ions are more stable than V^{2+} ions when pH is greater than 1, with a sulfuric acid activity of 1 and vanadium activity of 0.01 at room temperature.

2.3.3. Effect of particle size

Another issue that might affect the reduction of low-iron high-bornite copper concentrates is its coarser particle size distribution compared to the other concentrates. While 80% of the particle mass was found to be below 75 μm for both Source 1 and Source 2 concentrates (P_{80} = 75 μm), only 30% of the particle mass was below 106 μm (P_{30} = 106 μm).

The effects of particle size on the copper recovery were tested by reacting 42 g/L of Source 3 concentrates of specified particle size ranges in either the 1 M VSO_4 solution or the 1 M VSO_4 + 0.7 M $FeSO_4$ solution for 60 minutes. The particle sizes were sieved into the following ranges: [<38 μm, 38-75 μm, 75-150 μm, >150 μm]. Compared to the effect Fe^{2+} has on copper recovery, the effect of particle size on copper recovery was smaller. The copper recovery only changed from 71% to 67% when the particle size was changed from <38 μm to 106-150 μm for the reaction in 1 M VSO_4 solution. The copper recovery was found to range between 68% (resulting from 38-75 μm) to 80% (resulting from >38 μm) for the reaction in 1 M VSO_4 + 0.7 M $FeSO_4$ solution. The difference in copper recovery between the largest particle sizes and the smallest particle sizes was approximately 10%, while the addition of Fe^{2+} into the 1 M VSO_4 solution often increased the copper recovery by approximately 20%.

A reaction time of 60 minutes is likely sufficient for all particle sizes below 150 μm. Increasing the time further would likely contribute to only net minimal gains in copper recovery. In an industrial process, fine grinding may be unnecessary as the copper recovered from coarse particles would not differ significantly from the copper recovered from finer particles.

2.3.4. Continuous reactor

Experiments were also conducted in a continuous reactor as a means of progressing beyond batch processing and to investigate the leaching kinetics of the reaction between copper concentrates and V^{2+} at a steady state. For this purpose, for each experimental run, the copper concentrate slurry and the V^{2+} solution were fed into the reactor until the iron concentration leached held a consistent value over time, which is when the process was deemed to be at steady state.

Figure 2.8 shows the iron percentage leached from the copper concentrate continuously fed into the reactor. The iron concentration of the leach solution exiting the reactor was measured at arbitrary time intervals during the operation. Measurement times on the x-axis are scaled according to the average residence time in Figure 2.8. Each experiment was conducted by feeding either the low-chalcopyrite concentrates slurry (Source 2) or the low-iron high-bornite concentrates slurry (Source 3) into the reactor. The solid weight in the concentrate slurry was varied as 29 g/L, 58 g/L, 87 g/L, while the flow rate was varied to achieve 10 min, 15 min, 20 min residence time. The concentration of V^{2+} in the solution was constant at 0.5 M, with an equal volumetric feed rate compared to the slurry for all conditions. Two repetitions of the experiment were done for Source 2 concentrate slurry at 58 g/L, for residence times of 10 minutes, 15 minutes, and 20 minutes. The other concentrate slurries (Source 3 concentrates, or Source 2 concentrates at 87 g/L) were utilized for each residence time of 10 minutes, 15 minutes, and 20 minutes. Figure 2.8 only shows the results from the Source 2 concentrate slurry at 58 g/L. Each data point represents the average iron content leached from the Source 2 concentrate slurry, after a specified amount of time has passed since the concentrate initially enters the reactor.

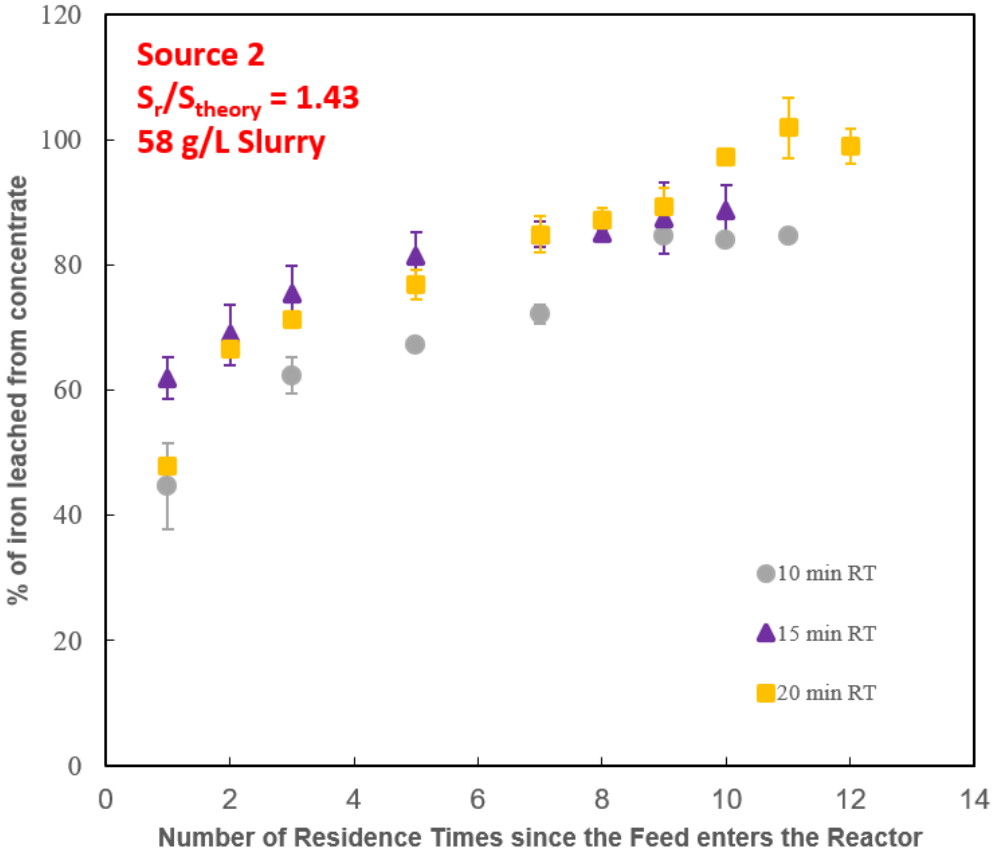

Figure 2.8: The iron content leached from the copper concentrate (relative to the feed rate of iron via copper concentrate) over time during the operation of the continuous reactor at room temperature. 58 g/L of Source 2 concentrates and 0.5 M VSO_4 + 0.1-0.2 M $FeSO_4$ solution were fed into the reactor at equal flow rates, with a residence time of 10 minutes (●), 15 minutes (▲), or 20 minutes (■).

The iron concentration increases during the experiment, until reaching a plateau at approximately 5-10 residence times. The iron concentration at the plateau represents the amount of iron leached at steady state. The iron content leached at a steady state can be estimated from the results of batch experiments. In Figure S2.1, approximately 62% and 83% of the iron were leached from the concentrates when 106 g/L of Source 2 concentrates were reacted in 1 M VSO_4 (s_r/s_{theory} = 2.06), for 10 minutes and 20 minutes, respectively. The reaction rate in the continuous reactor was faster with 85% and 100% of the iron being leached out at 10-minute and 20-minute

residence times, respectively. This increase in reaction rate can be rationalized by the cross-over during the electrochemical regeneration of V^{2+} solution, in which the ferrous ions diffused through the Nafion 117 membrane into the vanadium catholyte as charge carriers during regeneration (the entering ferrous concentration is ~ 10 g/L in the flow experiments but was zero in the batch studies).

Figure 2.9 compiles the data for total weight % of iron leached out of the copper concentrate at steady state after the electrochemical reduction reaction by VSO_4 in the continuous reactor. For both sources of copper concentrates, at least 85% of the iron in the feed stream can be leached, with a short 10-minute residence time. Due to the already high leaching rate, changes in the residence time or the loading affected the amount of iron leached only slightly. Changing the residence time from 10 minutes to 20 minutes changes the iron content leached by less than 15%. Changing the loading resulted in less than a 10% difference in the amount of iron leached. The processing rate is not heavily affected by residence time or concentrate loading amount.

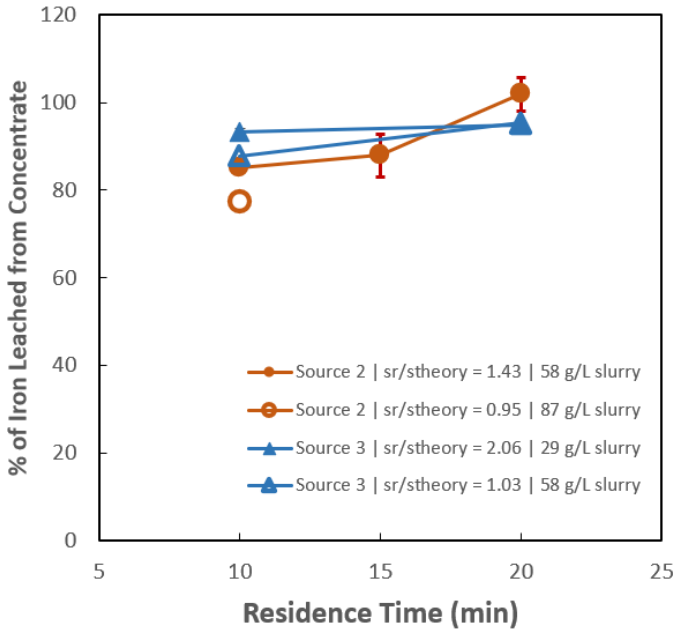

Figure 2.9: The iron content leached from the copper concentrate at steady state at room temperature. Near the end of the experiment, the iron content plateaus after 9-10 residence times, indicating that the process is at steady state.

For low-chalcopyrite concentrates, for $s_r/s_{theory} = 1.43$ and a residence time of 20 minutes, nearly 100% of the iron content was leached. This signifies that the reduction rate of the chalcopyrite fraction entering the reactor was equal to the feed rate. In a large-scale operation, this could increase the processing speed and decrease the reactor volume. Similarly, a high weight % of iron was leached from low-iron high-bornite concentrates, despite the low iron loadings. This is due to the inclusion of ferrous ions at different concentrations between 0.1 and 0.2 M in the injected reducing solution.

2.3.5. Comparison to other leaching methods

Table 2.4 shows the processing rate achieved in this paper to extract 80% of the copper with vanadium reductive leaching. Table 2.5 below shows the processing rates of incumbent leaching processes at pilot or commercial scales.

Table 2.4: Demonstrated experimental processing rates and conditions to extract at least 80% of the copper from the feed concentrates.

Description	Processing Rate [g L^{-1} h^{-1}]	Reactor Size [mL]	Leach Time [h]	Batch/ Continuous	Temperature [ºC]	Particle Size [µm]	Concentrate Composition
1 M V^{2+}	52	25	1.0 (V^{2+}) 0.50 (Fe^{3+})	Batch	25	P_{80} = 75	Source 1 (see table 2.1)
1 M V^{2+}	71	25	1.0 (V^{2+}) 0.50 (Fe^{3+})	Batch	25	P_{80} = 75	Source 2 (see table 2.1)
1 M V^{2+} 0.7 M Fe^{2+}	27	25	1.0 (V^{2+}) 0.50 (Fe^{3+})	Batch	25	P_{30} = 106	Source 3 (see table 2.1)
0.25 M V^{2+} 0.1 M Fe^{2+}	35	60	0.33 (V^{2+}) 0.50 (Fe^{3+})	Continuous	25	P_{80} = 75	Source 2 (see table 2.1)
0.25 M V^{2+} 0.1 M Fe^{2+}	35	60	0.33 (V^{2+}) 0.50 (Fe^{3+})	Continuous	25	P_{30} = 106	Source 3 (see table 2.1)

Table 2.5: Demonstrated processing rate and conditions of incumbent leaching methods at pilot or commercial scales.

Description	Concentrate Processing Rate [g L^{-1} h^{-1}]	Leach Time [h]	Batch/ Continuous	Temperature [ºC]	Pressure [atm]	Particle Size [µm]	Concentrate Composition	Ref.
Albion	15	20	Continuous	85	1	P_{80} = 5 – 10	37% $CuFeS_2$ 44% FeS_2 11% SiO_2	(Dreisinger, 2006) (Hourn et al., 1999)
[a]CESL	128 – 180	1 - 1.25	Continuous	140 – 150	10 – 12	P_{80} = 37	Low Sulfur 28.5% Cu 29.9% Fe 26.4% S High Sulfur 28.5% Cu 29.9% Fe 26.4% S	(Dreisinger, 2006) (Barr and Defreyne, 2005)

AAC-UBC	75	2	Continuous	150	10 – 12	P_{80} = 10 – 15	29% Cu 30% Fe 31% S	(Dreisinger, 2006) (Dempsey and Dreisinger, 2003)
[b]TPOX	128	1	Continuous	200 – 230	30 – 40	P_{80} = 37	28.5% Cu ~95% $CuFeS_2$	(Dreisinger, 2006) (McDonald and Muir, 2007) (Marsden et al., 2003)

[a]Processing rate was estimated assuming 30% solid fraction was approximately 300 g/L

[b]Processing rate was estimated using the copper concentration in pregnant leach solution and the copper grade

The processing rates of vanadium reductive leaching are overall slower than the commercial leaching processes. Compared with the existing processes, vanadium leaching process has unique advantages and weaknesses that affect both the processing rate and cost. Unlike oxidative leaching, the maximum copper concentrate loading is limited by the solubility of the V^{2+} ion in solution. For a copper concentrate with 20% copper grade, the maximum loading is approximately 100 g/L. The production of copper in the solid phase means that the V^{2+} leaching must be a 2-stage process, with the reduction of copper concentrates to produce copper, followed by the oxidation of solid copper products into the solution. The requirement for a 2-stage process lowers the processing rate and increases the capital expenses.

The vanadium leaching process also has unique procedures that are not seen in typical leaching processes. The electrochemical regeneration of vanadium is required to minimize the losses of vanadium. As shown in Figure 2.4, requiring excess V^{2+} in solution would further increase the power requirements for regeneration. The production of H_2S gas is also unique to reductive leaching, and releasing it untreated would be environmentally harmful – it must be carefully handled.

The advantages of the vanadium reductive leaching method are a combination of its low (ambient) operating temperature and its ability to work with moderate particle sizes, which may help minimize the amount of energy required for the process. Its flexibility is also beneficial. In this work, reaction of V^{2+} with copper sulfide minerals has been shown to facilitate the leaching $CuFeS_2$ and Cu_5FeS_4, as well as CuS and Cu_2S. Furthermore, the performance of reductive leaching can be improved by using a staged process. For example, 42 g/L of low-iron high-bornite copper concentrates were first added to a 1 M VSO_4 solution and reacted for 60 minutes. The solid products were subsequently reacted in 1 M Fe^{3+} for 60 minutes. The remaining solids were then reacted in 1 M VSO_4 solution for 60 minutes. All this was done at ambient temperature. This staged process had a positive effect on copper recovery, allowing the **overall copper recovery to approach 99%**.

2.4. Conclusion

Overall, the V^{2+} reductive leach achieved high yields in reaction times of less than an hour from a diversity of feedstocks. Furthermore, the addition of Fe^{2+} ions into the leaching solution can significantly increase the recovery of copper from low-iron copper concentrates. A similar result was seen for the leaching of pure chalcocite. Leaching kinetics in a continuous reactor were consistent with batch results, suggesting a practical operation with a residence time of 10-30 minutes is possible. The overall reaction kinetics are found to be fast relative to other atmospheric-pressure processes documented in the literature. It was also found that a second leach of solid residue improves copper leaching yields to greater than 95%.

2.5. Acknowledgments

We would like to thank Max Dickman for the design and construction of the continuous-flow tubular reactors. We would like to thank Dr. Paul Miranda for the AMICS analysis of copper concentrate samples. The authors gratefully acknowledge funding through ARPA-E grant DE-AR0001340 from the US Department of Energy.

2.6. Chapter 2 Appendix

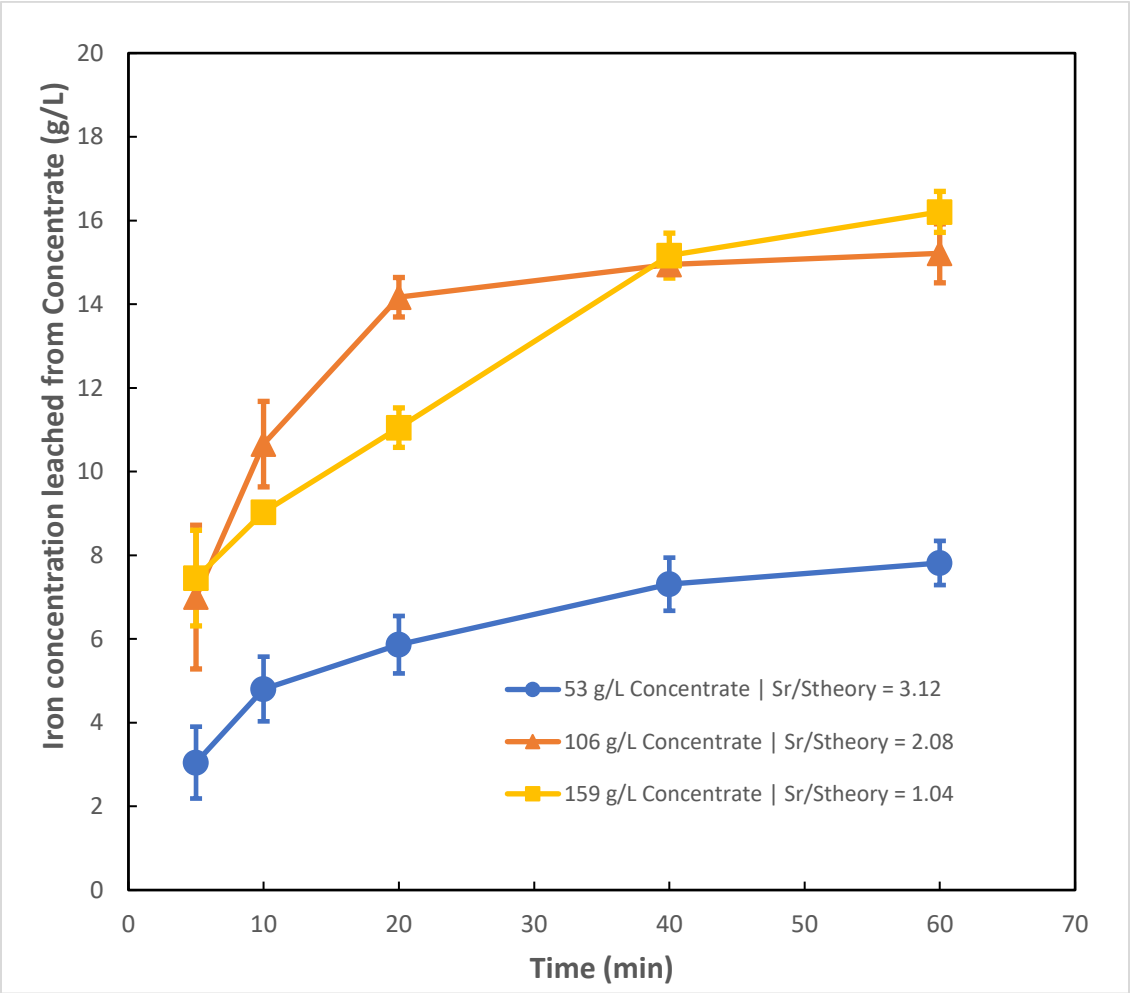

Figure S2.1: Iron concentration of the VSO_4 solution over the course of 60 minutes at room temperature, as Source 2 concentrates are reacted within 1 M VSO_4 solution. The iron concentration plateaus after approximately 40 minutes.

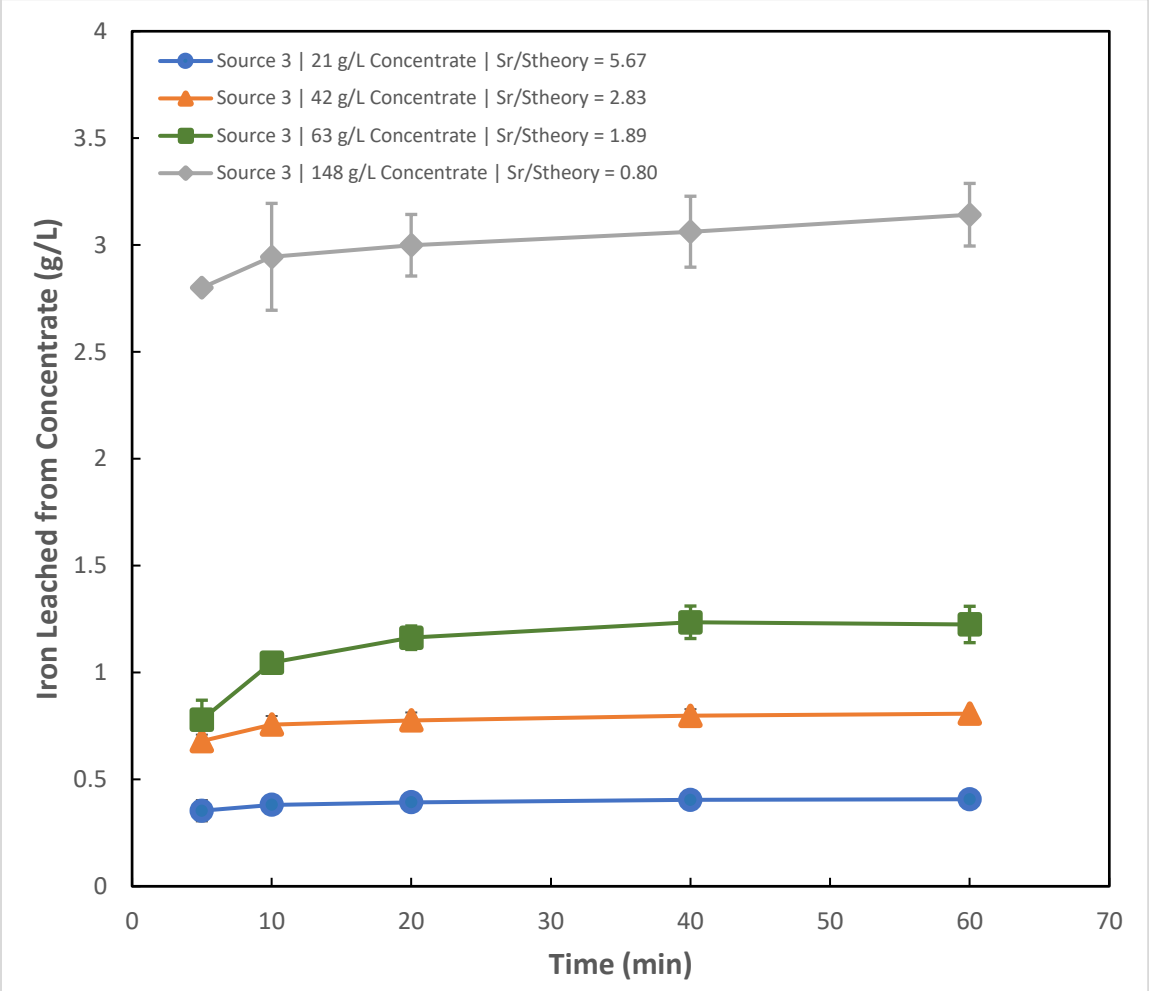

Figure S2.2: Iron concentration of the VSO_4 solution over the course of 60 minutes at room temperature, as Source 3 concentrates are reacted within 1 M VSO_4 solution. The iron concentration plateaus after approximately 20 minutes

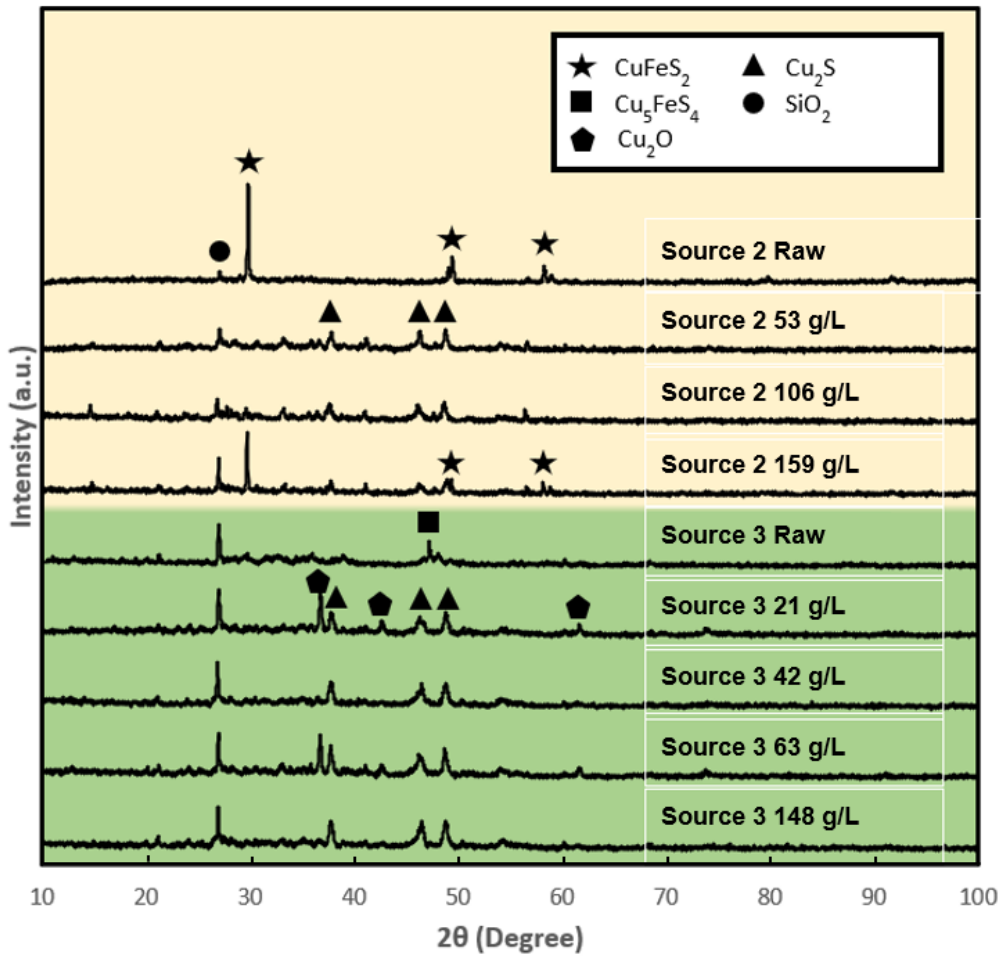

Figure S2.3: XRD analysis of Source 2 and Source 3 concentrates, before and after reaction in 1 M VSO_4 solution at room temperature. Mass loadings of copper concentrates are specified in the figure.

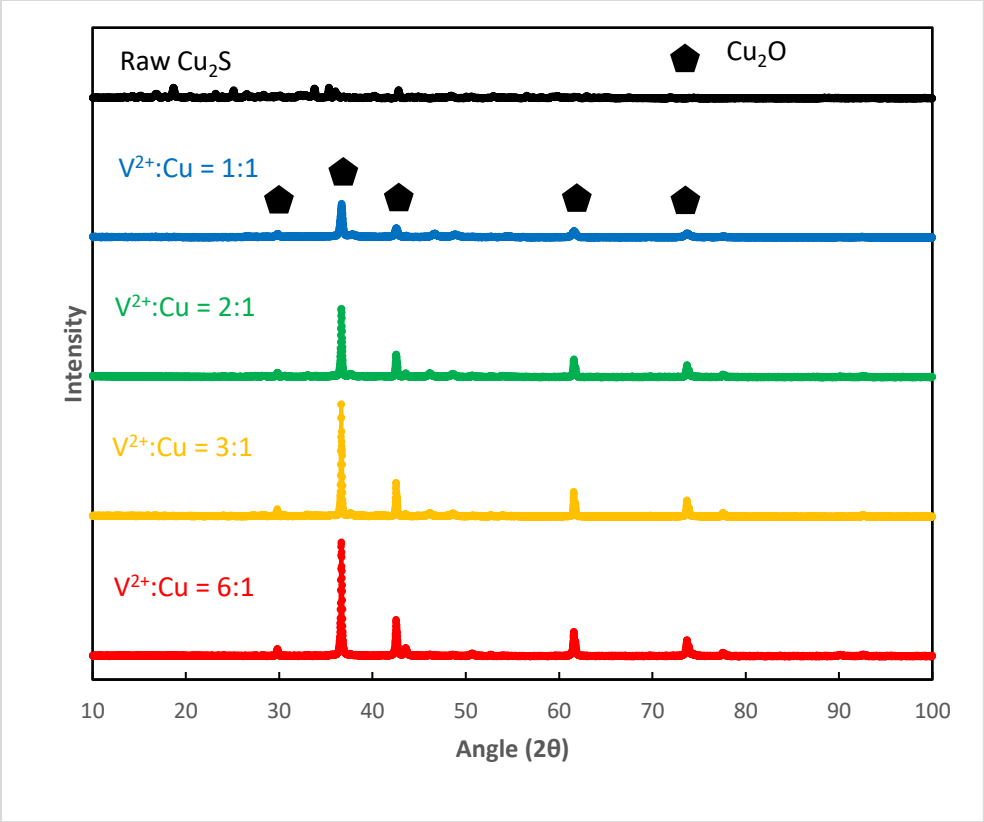

Figure S2.4: XRD analysis of Cu_2S solids, before and after reaction in 1 M VSO_4 + 0.25 M $FeSO_4$ solution at room temperature. Mass loadings of copper concentrates and the s_r/s_{theory} ratio are specified in the figure.

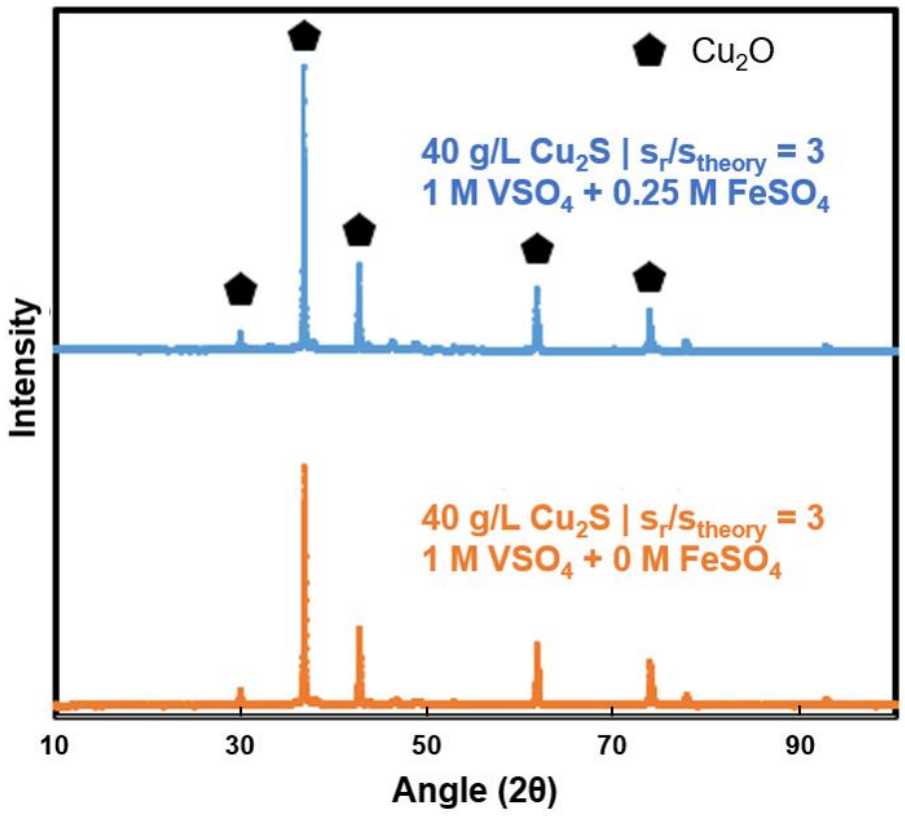

Figure S2.5: XRD analysis of Cu_2S solids, after reacting in either 1 M VSO_4 + 0.25 M $FeSO_4$ solution or 1 M VSO_4 at room temperature. Mass loadings of copper concentrates and the s_r/s_{theory} ratio are specified in the figure.

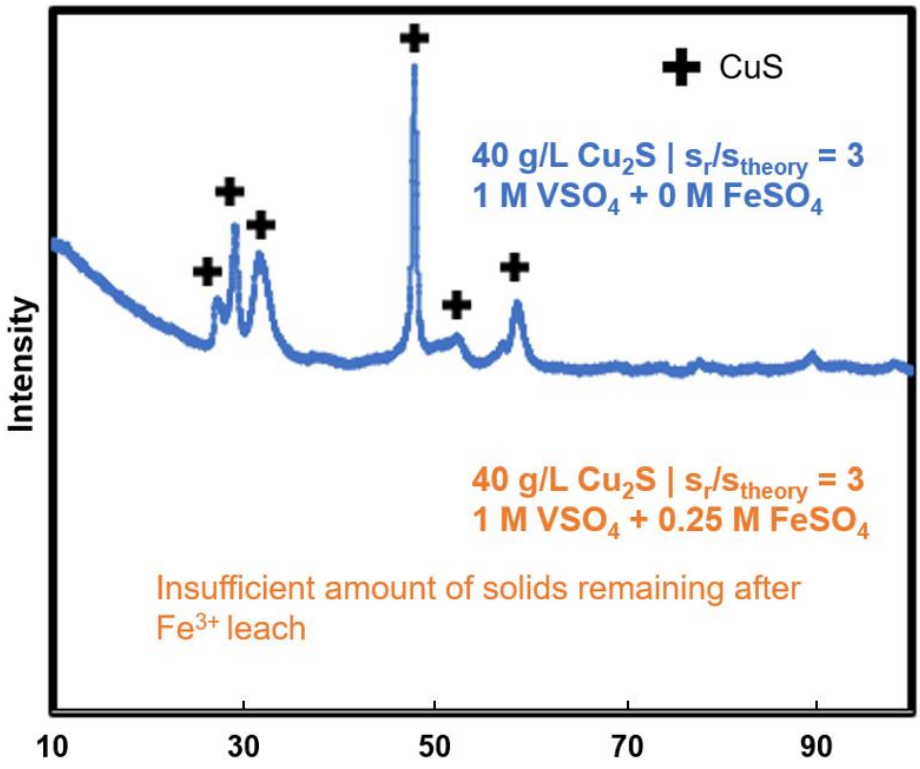

Figure S2.6: XRD analysis of Cu_2S solids, after reacting in either 1 M VSO_4 + 0.25 M $FeSO_4$ solution or 1 M VSO_4 at room temperature, then reacting in 1 M Fe^{3+} solution. Mass loadings of copper concentrates and the s_r/s_{theory} ratio are specified in the figure.

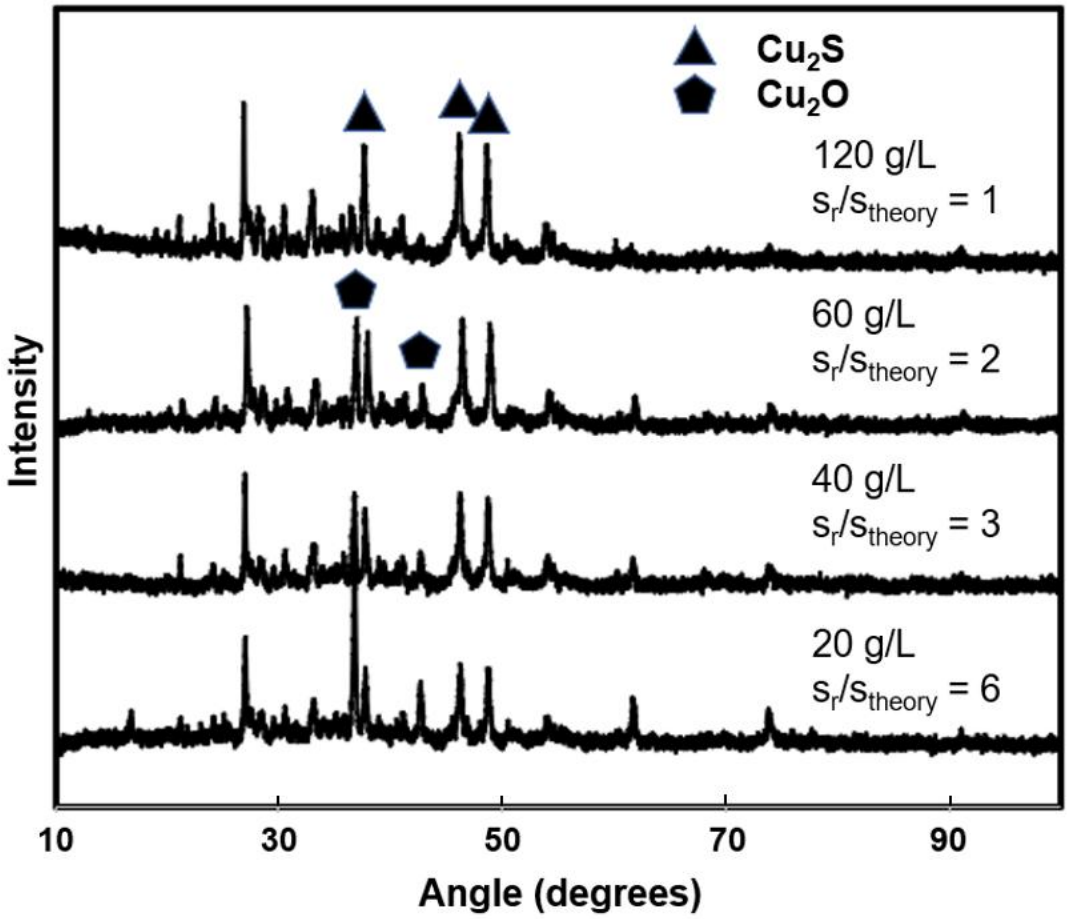

Figure S2.7: XRD analysis of Source 3 concentrates after reaction in 1 M VSO_4 + 0.7 M $FeSO_4$ solution at room temperature. Mass loadings of copper concentrates and the s_r/s_{theory} ratio are specified in the figure.

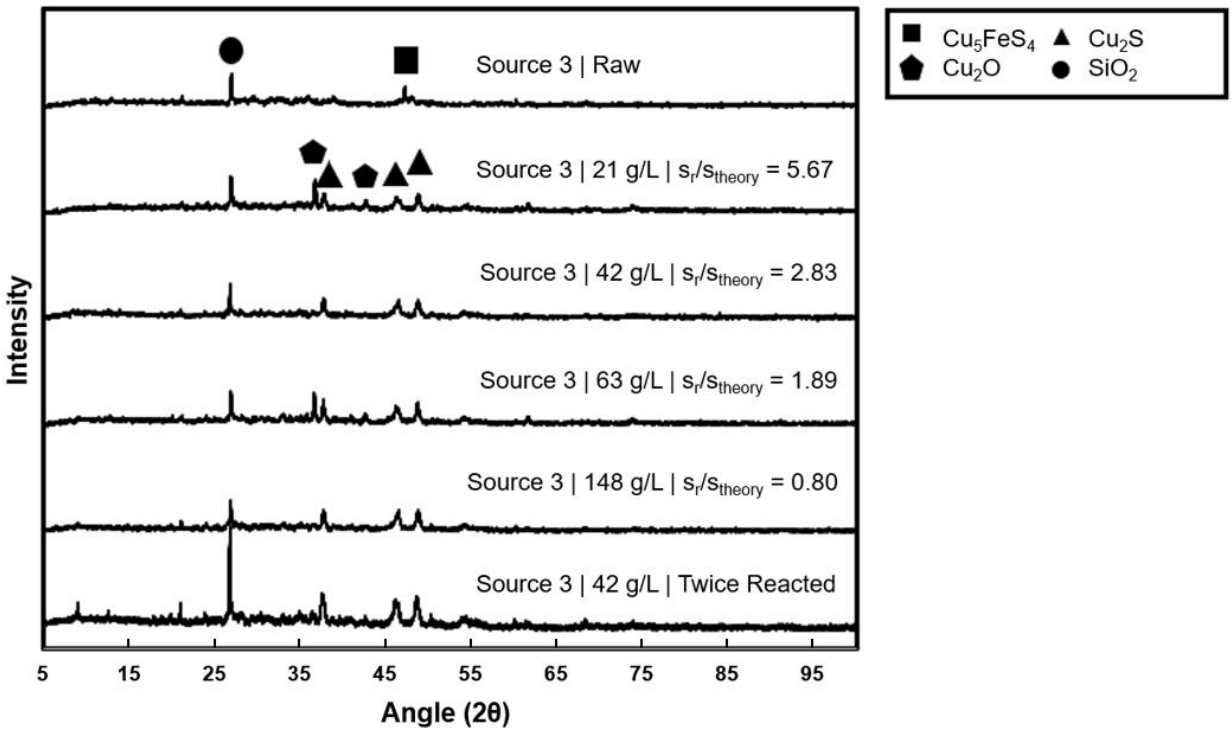

Figure S2.8: XRD analysis of Source 3 concentrates after reaction in 1 M VSO_4 solution at room temperature, followed by reaction in 1 M $Fe_2(SO_4)_3$ solution, followed by reaction in 1 M VSO_4 solution at room temperature. Mass loadings of copper concentrates and the s_r/s_{theory} ratio are specified in the figure.

2.7. References

Ayres, R.U., Ayres, L.W., & Råde, I. Copper: sources and supply. *The Life Cycle of Copper, its Co-products and Byproducts* **2003**, 21-58.

Barr, G., Defreyne, J., Mayhew, K. CESL copper process – an economic alternative to smelting (2005).

Biegler, T., & Swift, D. A. The electrolytic reduction of chalcopyrite in acid solution. *Journal of Applied Electrochemistry* **1976**, *6*(3), 229–235.

Bridge, G. The social regulation of resource access and environmental impact: production, nature and contradiction in the US copper industry. *Geoforum* **2000**, *33(*2), 237-256.

Calvo, G., Mudd, G., Valero, A., Valero, A. Decreasing Ore Grades in Global Metallic Mining: A Theoretical Issue or Global Reality? *Resources* **2016**, *5*, 36.

Carrara, S., Alves Dias, P., Plazzotta, B., Pavel, C., & Others. (2020). Raw materials demand for wind and solar PV technologies in the transition towards a decarbonised energy system. *Doi*, *10*, 160859.

Chapman, D. Environmental Standards and International Trade in Automobiles and Copper: The Case for a Social Tariff. *Natural Resources Journal* **1991**, *31* (3), 449—462.

Chen, W., Wang, M., Li, X. Analysis of copper flows in the United States: 1975-2012. *Resources, Conservation and Recycling* **2016**, *111*, 67-76.

Córdoba, E., Muñoz, J., Blázquez, M., González, F., Ballester, A. Leaching of chalcopyrite with ferric ion. Part I: General aspects. *Hydrometallurgy* **2008**, *93* (3–4), 81–87.

Dean, J.A. Lange's handbook of chemistry, 12th ed. *McGraw-Hill* **1979.**

Dempsey, P., Dreisinger D.B. Acidic redox leaching of copper and other metal values from chalcopyrite, US 6,503,293 (2003).

Dimitrijević, M., Kostov, A., Tasić, V., Milosević, N. Influence of pyrometallurgical copper production on the environment. *Journal of Hazardous Materials* **2009**, *164*(2-3), 892-899.

Ding, C., Zhang, H., Li, X., Liu, T., Xing, F. Vanadium flow battery for energy storage: prospects and challenges. *J. Phys. Chem. Lett.* **2013**, *4*(8), 1281-1294.

Doyle, F., & Lapidus, G. Reductive leaching of chalcopyrite by aluminum. *ECS Transactions* **2006**. 209th ECS Meeting, Denver, Colorado.

Dreisinger, D., & Abed, N. A fundamental study of the reductive leaching of chalcopyrite using metallic iron part I: kinetic analysis. *Hydrometallurgy* **2002**, *66*(1), 37–57.

Dreisinger, D. Copper leaching from primary sulfides: Options for biological and chemical extraction of copper. *Hydrometallurgy* **2006**, *83* (1–4), 10–20.

Forsén, O., Aromaa, J., Lundström, M. Primary Copper Smelter and Refinery as a Recycling Plant—A System Integrated Approach to Estimate Secondary Raw Material Tolerance. *Recycling* 2017, *2*(4), 19.

Fuentes-Aceituno, J. C., Lapidus, G. T., & Doyle, F. M. A kinetic study of the electro-assisted reduction of chalcopyrite. *Hydrometallurgy* **2008**, *92*(1), 26–33.

Garrels, R.M., Christ, C.L. Solutions, minerals, and equilibria. *New York, Harper & Row* **1965,** 213-233.

Geiser, J., Natter, H., Hempelmann, R., Morgenstern, B., Hegetschweiler, K. Photometric determination of the state-of-charge in vanadium redox flow batteries part I: in combination with potentiometric titration. *Z. Phys. Chem.* **2019,** *233* (12), 1683-1694.

Ghahremaninezhad, A., Radzinski, R., Gheorghiu, T., Dixon, D.G., Asselin, E. A model for silver ion catalysis of chalcopyrite ($CuFeS_2$) dissolution. *Hydrometallurgy* **2015**, *155*, 95-104.

Habashi, F. Copper metallurgy at the crossroads. *Journal of Mining and Metallurgy* **2007**, *43*, 1-19.

Hourn, M.M., Turner, D.W., Holzberger, I.R. Atmospheric mineral leaching process, US Patent 5,993,635 (1999).

IEA. The Role of Critical Minerals in Clean Energy Transitions. (2022). *IEA: International Energy Agency.*

Klekovkina, V. V., Gainov, R. R., Vagizov, F. G., Dooglav, A. V., Golovanevskiy, V. A., Pen'kov, I. N. Oxidation and magnetic states of chalcopyrite $CuFeS_2$: A first principles calculation. *Optics and Spectroscopy* **2014,** *116* (6), 885-888.

Koizhanova, A., Kenzhaliyev, B., Magomedov, D., Kamalov, E., Yerdenova, M., Bakrayeva, A., Abdyldayev, N. Study of factors affecting the copper ore leaching process. *ChemEngineering* **2023**, *7*(3), 54.

Koleini, S.M., Aghazadeh, V., Sandström, Å. Acidic sulphate leaching of chalcopyrite concentrates in presence of pyrite. *Minerals Engineering* **2011,** *24*(5), 381-386.

Lou, W., Zhang, D., Bayless, R.C. Review of mineral recognition and its future. *Applied Geochemistry* **2020**, *122*, Article 104727.

Marsden, J.O., Brewer, R.E., Hazen, N. Copper concentrate leaching developments by Phelps Dodge Corporation. In Proceedings of the Hydrometallurgy 2003—Fifth International Conference in Honour of Professor Ian Ritchie, Volume 2: Electrometallurgy and Environmental Hydrometallurgy, Vancouver, BC, Canada, 24–27 August 2003; Young, C.A., Alfantazi, A.M., Anderson, C.G., Dreisinger, D.B., Harris, B., James, A., Eds.; TMS: Warrendale, PA, USA; pp. 1429–1446.

Martínez-Gómez, V. J., Fuentes-Aceituno, J. C., Pérez-Garibay, R., & Lee, J.-C. A study of the electro-assisted reductive leaching of a chalcopyrite concentrate in HCl solutions. Part I: Kinetic behavior and nature of the chalcopyrite reduction. *Hydrometallurgy* **2018**, *181*, 195–205.

McDonald, R.G., Muir, D.M. Pressure oxidation leaching of chalcopyrite. Part I. Comparison of high and low temperature reaction kinetics and products. *Hydrometallurgy* 2007, *86*(3-4), 206-220.

Milazzo, G., Caroli, S., Sharma, V.K. Tables of standard electrode potentials. *International Journal of Physical Chemistry* **1978,** *82*(10), 1114.

Mokmeli, M. Pre-feasibility study in hydrometallurgical treatment of low-grade chalcopyrite ores from Sarcheshmeh copper mine. *Hydrometallurgy* **2020**, *191,* Article 105215.

Norgate, T., & Jahanshahi, S. Low grade ores – Smelt, leach or concentrate? *Minerals Engineering* **2010**, *23*(2), 65–73.

Pattrick, R. A. D., van der Laan, G., Charnock, J. M., Grguric, B. A. Cu L3 X-ray absorption spectroscopy and the electronic structure of minerals: Spectral variations in non-stoichiometric bornites, Cu_5FeS_4. *American Mineralogist* **2004,** *89* (4), 541-546.

Robie, R.A., Wiggins, L.B., Barton, P.B. Jr., Hemingway, B.S. Low-temperature heat capacity and entropy of chalcopyrite ($CuFeS_2$): estimates of the standard molar enthalpy and Gibbs free energy of formation of chalcopyrite and bornite (Cu_5FeS_4). *The Journal of Chemical Thermodynamics* **1985,** *17*(5), 481-488.

Rötzer, N., Schmidt, M. Historical, current, and future energy demand from global copper production and its impact on climate change. *Resources* **2020,** *9*(4), 44.

Schipper, B. W., Lin, H.-C., Meloni, M. A., Wansleeben, K., Heijungs, R., & van der Voet, E. (2018). Estimating global copper demand until 2100 with regression and stock dynamics. *Resources, Conservation and Recycling*, *132*, 28–36.

Schlesinger, M. E., King, M. J., Sole, K. C., Davenport, W. G. Chapter 15 – Hydrometallurgical copper extraction: introduction and leaching. *Extractive Metallurgy of Copper (Fifth Edition)* **2011a**, 281-322.

Schlesinger, M. E., King, M. J., Sole, K. C., Davenport, W. G. Chapter 3 – Production of high copper concentrates – introduction and comminution. *Extractive Metallurgy of Copper (Fifth Edition)* **2011b**, 31-49.

Serbula, S. M., Milosavljevic, J. S., Kalinovic, J. V., Kalinovic, T. S., Radojevic, A. A., Apostolovski Trujic, T. Lj., Tasic, V. M. Arsenic and SO_2 hotspot in south-eastern Europe: an overview of the air quality after the implementation of the flash smelting technology for copper production. *Science of the Total Environment* **2021**, *777*, 145981.

Sharma, S.P. Reaction of copper and copper oxide with H_2S. *J. Electrochem. Soc* **1980,** *127.* 21-26.

Sohn, H.J., & Wadsworth, M. E. Reduction of Chalcopyrite with SO2 in the Presence of Cupric Ions. *JOM Journal of the Minerals Metals and Materials Society* **1980**, *32*(11), 18–22.

Warren, G. W., Sohn, H. J., Wadsworth, M. E., Wang, T. G. The effect of electrolyte composition on the cathodic reduction of $CuFeS_2$. *Hydrometallurgy* **1985,** *14*, 133-149.

Vardner, J. T., Gencer, E., Emerson, M., Farinato, R. S., Nagaraj, D. R., Banta, S., West, A. C. Vanadium(II) sulfate for the reductive leaching of chalcopyrite: Replacing smelting with electrolysis for copper production. *ChemElectroChem* **2022,** *9*(24), e202200920.

Yu, K., Liang, H. Attempt at preparing Cu by direct hydrogen reduction of Cu2S Slurry. *Materials Letters* **2004**, *58*(24), 3045-3048.

Zhou, X., Wei, C., Li, M., Qiu, S., Li, X. Thermodynamics of vanadium-sulfur-water systems at 298K. *Hydrometallurgy* **2011**, *106* (1-2), 104-112.

Chapter 3:

Room Temperature Production of Copper: Cerium(IV) Oxidative Leaching of Chalcopyrite from Concentrates

Abstract

In the upcoming decades, copper demand in the United States is expected to increase due to the transition to carbon-free energy sources, while mining and processing costs increase due to reduced copper grades. Room temperature oxidative leaching method using sulfuric acid is slow with poor yields. Therefore, a room temperature leaching method with faster leaching kinetics would be desirable, if it reduces environmental risks and remains economical

This study investigates cerium-based oxidative leaching of copper mineral concentrates as a potential alternative method of processing copper. Approximately 7.5 moles of Ce^{4+} were required to leach one mole of chalcopyrite ($CuFeS_2$) , with higher Ce^{4+} consumption required for copper concentrates with higher pyrite (FeS_2) content. The analysis of solid products show an absence of elemental sulfur in the initial 24 hours of leaching. In the following 24 hours of leaching, elemental sulfur is observed, and the Ce^{4+} consumption required for one mole of $CuFeS_2$ decreased to 4.7.

Experiments showed that 52% of the copper was leached from the concentrates at room temperature after 24 hours in a $Ce(SO_4)_2$, H_2SO_4 solution. The yield was increased to 82%, by pretreating the copper concentrates in $Fe_2(SO_4)_3$, H_2SO_4 solution for one hour at room temperature, followed by drying at 70ºC for one hour. The low solubility of Ce^{4+} and the amount of Ce^{4+} consumed limits the solid loading allowed in the leaching solution to approximately 20g/L.

3.1. Introduction

With the emergence of green industries due to an acceleration of decarbonization goals, the global copper market is expected to face a significant deficit as the demand for copper outpaces the available supply (Rötzer, 2020). Copper is a key component for the manufacturing of electric vehicles, the building of solar and wind energy facilities, and infrastructure projects in emerging economies. Between 2023 and 2050, nearly 1.4 billion tonnes of copper will be required to reach net-zero-emission energy production, which is twice the total amount of copper produced over all human history (Schipper, 2018)(IEA, 2022).

The copper supply will struggle to meet the demands of copper due to increasing costs of mining and processing of copper ores. One major issue is the limited number of new copper mines, as the discovery of copper deposits have slowed significantly in recent years. This means that existing copper mines are aging, with ore grades declining (Calvo, 2016). The declining ore grades create challenges for pyrometallurgical processes, which are responsible for 80% of global copper production, due to the stringent requirements on copper content (Forsén ,2017)(Kulczycka, 2017). Approximately 20 wt % of the concentrate must be copper (Forsén, 2017), and according to Norgate et al., a minimum economic copper ore grade of approximately 0.5% is necessary (Norgate, 2010). Pyrometallurgical processes have an additional challenge in handling environmental pollutants such as sulfur dioxide and airborne arsenic compounds, further increasing the processing costs (Serbula, 2021).

As such, it may be appealing to transition away from pyrometallurgical methods to hydrometallurgical alternatives, which provide potential advantages such as a lower carbon footprint due to lower operating temperatures, lower ore-grade requirements, and fewer air pollutants such as sulfur dioxide. In a general hydrometallurgical process, copper ores or

concentrates are oxidized in an aqueous medium to leach Cu^{2+} ions (Schlesinger, 2011). Although copper oxides are commercially processed through hydrometallurgy, copper sulfides, which consists of approximately 80% of the global copper production, have difficulties due to passivation. Copper sulfides, such as chalcopyrite ($CuFeS_2$), chalcocite (Cu_2S), and bornite (Cu_5FeS_4), are highly refractory to leaching, as the sulfur layers and the metal-deficient layers accumulate on the surface of the copper ore particles, slowing the leaching kinetics (Córdoba, 2008).

Several strategies have been implemented in commercial processes to overcome the formation of passivation layers. At room temperature, low investment processes such as heap leaching or dump leaching are utilized. A cheap leaching reagent, such as sulfuric acid, is fed into coarse, low-grade ores (Pyper, 2019). Despite the low leaching rate, the large land area allows for a much larger volume of copper ores processed, and the process remains profitable as the extracted copper value exceeds the investment.

At temperatures near 100ºC and at atmospheric pressure, the sulfides in the copper concentrates oxidize to elemental sulfur or remains as metal-deficient sulfide layers on the surface of the concentrates. In the commercial Albion process, the particles are ground to 5-10μm, greatly increasing the surface-to-volume ratio for the oxidation reaction (Hourn, 1999). Chloride ions can also be utilized, as demonstrated by the CESL process, to weaken the passivation layer and increase the leaching rate (Barr, 2005).

At moderate temperatures near 150ºC and moderate pressures near 10 atm, the Anglo-American - University of British Columbia process utilizes surfactants to disperse the molten sulfur, preventing it from passivating the chalcopyrite (Dreisinger, 2006). At high temperatures near 220ºC and high pressures near 35 atm, Phelps-Dodger Placer Dome has shown that the

sulfur-based passivation layers are oxidized further to produce sulfuric acid, weakening the formation of passivation layers (Dreisinger, 2006).

Tank leaching is typically reserved for processes that provide rapid leaching and significant investments. Faster leaching rates result in higher revenue, which justifies adoption of higher operating temperatures, smaller particle sizes, corrosive chloride ions, and higher ore grades. Therefore, a tank leaching process that operates at room temperature without chloride ions, yet operates at a competitive processing rate, is highly desirable, as the expected processing cost would be significantly lower.

This paper aims to examine the potential for Ce^{4+}-based leaching of copper concentrates, specifically $Ce(SO_4)_2$, as a candidate for room temperature tank leaching process. The primary reason why a room temperature Ce^{4+}-based leaching process would be possible is the higher oxidation potential of Ce^{4+}, reported at 1.61V vs. SHE, compared to traditional oxidizing potentials such as Fe^{3+}, 0.771V vs. SHE, and oxygen, at 1.229V vs. SHE at pH 0 (Bard, 1985). A higher potential increases the thermodynamic driving force, and may allow oxidization of the sulfur to higher states $S_2O_3^{2-}$ or SO_4^{2-}, decreasing the formation of passivation layers and increasing the reaction rates (Ghahremaninezhad, 2010).

After oxidation, the Ce^{4+} ions are reduced to Ce^{3+}, which can be regenerated to allow continued use of cerium. One method to separate Ce from the pregnant leach solution, would be to utilize Na^+ and SO_4^{2-} ions to form the double-salt $NaCe(SO_4)_2$, which has poor solubility in aqueous solutions (Lokshin, 2005). The $NaCe(SO_4)_2$ can be converted with OH^- to form $Ce(OH)_3$, which can be dissolved in acidic solutions and oxidized to obtain Ce^{4+} (Um, 2016).

However, Ce^{4+}-based oxidative leaching has disadvantages. First is the general low solubility of Ce^{4+}, reported at 0.8M (Paulenova, 2002). Unlike oxygen-based leaching methods,

the solid loading allowed for leaching is limited by the solubility in ion-based leaching methods, which limits the processing rate. According to Paulenova et al., the solubility of Ce^{4+} decreases with increasing temperature, in sulfuric acid media (Paulenova, 2002). Although increasing the operating temperature in traditional leaching is often viable, for Ce^{4+}-based leaching the advantages gained are minimal due to the limited solid loading allowed. Ce^{4+} also forms complexes with anions, affecting the reduction potential depending on the stability of the complex formed. According to Buchanan et al., the formation of $Ce(SO_4)^{2+}$ is thermodynamically favorable. The Gibbs' free energy of the cerium complexes have been ranked highest to lowest: $Ce(ClO_4)^{3+}$, Ce^{4+}, $Ce(NO_3)^{3+}$, $Ce(SO_4)^{2+}$, and $CeCl^{3+}$ (Buchanan, 2020). The measured potentials decrease accordingly, from 1.70V vs SHE in perchloric acid media, to 1.61V and 1.44V in nitric acid and sulfuric acid media, respectively (Wadsworth, 1957). It is possible that the lower oxidation potential would lower the reaction rate.

To determine whether Ce^{4+}-based leaching method is a viable candidate for room temperature tank leaching, the leach reaction is characterized under a variety of condition. This paper shows that although the leaching rate is higher than incumbent processes at room temperature, Ce^{4+} leaching method is probably too limited by its solid loading to be considered for room temperature tank leaching.

3.2. Experimental Procedure

3.2.1. *Preparation of Ce(IV) sulfate solutions*

Ceric sulfate (GFS Chemicals or 1PlusChem) was dissolved in 0.1M or 1.0M H_2SO_4 (Sigma Aldrich) to achieve a concentration of 0.5M Ce^{4+}. A 0.5M $Ce(SO_4)_2$, 0.1M H_2SO_4 solution is referred to as the control ceric sulfate solution. *Preparation of Ce(IV) nitrate solutions*. Cerium

ammonium nitrate (Sigma Aldrich) was dissolved in 1M HNO_3 (Sigma Aldrich) to achieve a concentration of 1.0M Ce^{4+}. A 1.0M $(NH_4)_2Ce(NO_3)_6$, 1.0M HNO_3 solution is referred to as the control ceric nitrate solution.

3.2.2. Preparation of copper concentrates

Concentrates were provided from two different mining operations. The mineral composition of the concentrates from each source was determined by the Advance Mineral Identification and Characterization System (AMICS). This technique uses SEM and X-ray energy spectral analysis of the backscattered electrons from epoxy-mounted thin sections of each mineral concentrate to produce mineralogical maps of individual ore particles (Lou, 2020). The images are used to identify mineral composition, element distribution, mineral size, and mineral phase associations. The mineral compositions of the copper concentrates from each source are shown as weight % below in Table 3.1.

Table 3.1: Mineral composition (wt %) of the concentrates from each source via AMICS analysis

Mineral	**Source 1**	**Source 2**
$CuFeS_2$	83.8%	56.5%
Cu_2S	-	4.7%
Cu_5FeS_4	-	4.9%
$Cu_2CO_3(OH)_2$	-	1.8%
FeS_2	7.7%	10.9%
SiO_2	1.5%	2.1%
$KAlSi_3O_8$	1.9%	4.1%
Misc.	5.1%	15.1%

The main sources of copper and iron are chalcopyrite, chalcocite, bornite, and pyrite minerals. The iron and copper contents were determined by digesting the three samples of copper concentrates from each source in aqua regia and measuring the iron and copper concentrations using iCE 3000 Atomic Absorption Spectroscopy. Table 3.2 summarizes the metal composition determined in each copper concentrate.

Table 3.2: Average metal composition (wt %) of the concentrates and the standard deviation from each source

Metal	**Source 1**	**Source 2**	**Cu_2S**	**CuS**
Copper – Mean	27.1%	20.2%	79.0%	66.7%
Copper – Std. Deviation	2.7%	1.6%	2.2%	1.8%
Iron – Mean	29.8%	19.1%	N/A	N/A
Iron – Std. Deviation	3.3%	1.4%	N/A	N/A

The leaching of Cu_2S and CuS (Sigma Aldrich) in Ce^{4+} was also tested. The copper contents were determined by digesting the Cu_2S and CuS in aqua regia and measuring the copper concentrations using iCE 3000 Atomic Absorption Spectroscopy, and are also shown in Table 3.2.

3.2.3. Batch experiments

Copper concentrates were added into 25mL leach solution and stirred with a magnetic stirring bar for 24 hours, with liquid phase samples of 100µL taken at time intervals of 1, 4, and 24 hours to measure the Cu^{2+} and Fe^{3+} content in solution.

Prior to Ce^{4+} leaching, the copper concentrates underwent pretreatment dependent on the experiment. Acid pretreatment was utilized by mixing copper concentrates in 1M H_2SO_4 for 1 hour at room temperature, filtering out the solids with a Buchner funnel, drying the solids in an oven at 75°C for 1 hour, and inserting the filtered solids into the Ce^{4+} solution. Ferric

pretreatment was similar, mixing the copper concentrates in 0.5M $Fe_2(SO_4)_3$, 1M H_2SO_4 for 1 hour at room temperature, filtering out the solids with a Buchner funnel, drying the solids in an oven at 75ºC for 1 hour, and inserting the filtered solids into 0.5M Ce^{4+} solution. After the reaction, the solid products were filtered and dried, then analyzed using Xpert3 Powder XRD from Malvern Panalytical to estimate the composition of the remaining solids.

3.2.4. *Titration of concentration of Ce^{4+}*

The concentrations of Ce^{4+} before and after leaching were determined by potentiometric titration. The titrant was prepared by dissolving 1M $FeSO_4$ (Sigma Aldrich) in 0.1M H_2SO_4. After extracting 1mL of the Ce^{4+} leach solution by pipette, 1M $FeSO_4$ was added in 20 microliter increments, with the solution potential measured using an ORP probe (Thermo Scientific). The titration endpoint was determined by the sudden decrease in solution potential from 1100mV vs. Ag/AgCl to 550mV vs. Ag/AgCl, and the Ce^{4+} concentration in the leach solution was calculated accordingly.

3.2.5. *Titration of concentration of SO_4^{2-}*

The concentrations of SO_4^{2-} before and after leaching were determined using a $BaCl_2$ titrant (Sigma Aldrich). After preparing 10mL of 0.1M $BaCl_2$ solution, 1mL of leach solution was added into the $BaCl_2$ solution by pipette, and mixed for 10 minutes prior to sampling 50 microliters of the solution for ICP measurement. The difference in Ba^{2+} concentration before and after the addition of leach solution was used to report the concentration of SO_4^{2-}.

3.2.6. *Measurement of Fe^{2+} and Cu^{2+} concentrations*

The iron and copper concentrations were measured using iCE 3000 Atomic Absorption Spectroscopy (AAS), obtained from Fisher Scientific. During the experiment, 100µL samples of the leach solution were taken periodically and diluted to make the iron or copper concentrations

between 0 and 4 mg/L. The AAS was calibrated before every measurement using standards ranging between 0 and 4 mg/L to construct linear calibration curves.

3.2.7. *X-ray diffraction analysis of product solids*

A PANalytical Xpert3 Powder XRD system was used. The XRD was operated with filtered Empyrean Cu Kα radiation (k = 0.15418 nm), a tube voltage of 45 kV, and a current of 40 mA. The peak intensities were measured using a PIXcel1D detector in the 2θ range of 5–100° with a step size of 0.026° on a rotating plate with a revolution time of 2.0 s.

3.3. Results and Discussion

3.3.1. Possible reaction pathways of oxidation of copper concentrates by Ce^{4+}

The possible oxidation products of $CuFeS_2$ have been compiled by Ghahremaninezahd et al. (Ghahremaninezhad, 2010). As the oxidation potential increased, the sulfur product is shown to oxidize from S_n^{2-}, to S^0, $S_2O_3^{2-}$, and SO_4^{2-} products.

The addition of copper concentrates into the control ceric sulfate solution resulted in aqueous Cu^{2+} and Fe^{3+}. Based on the reactions proposed by Ghahremaninezhad et al., three primary oxidative reactions have been postulated as the primary Ce^{4+} leach reactions (Ghahremaninezhad, 2010).

$$CuFeS_2 + 5Ce^{4+} \rightarrow Cu^{2+} + Fe^{3+} + 2S^0 + 5Ce^{3+} \quad 3.1$$

$$CuFeS_2 + 9Ce^{4+} + 3H_2O \rightarrow Cu^{2+} + Fe^{3+} + {S_2O_3}^{2-} + 6H^+ + 9Ce^{3+} \quad 3.2$$

$$CuFeS_2 + 17Ce^{4+} + 8H_2O \rightarrow Cu^{2+} + Fe^{3+} + 2SO_4^{2-} + 16H^+ + 17Ce^{3+} \quad 3.3$$

The standard reduction potential of Ce^{4+} in SO_4^{2-} media is sufficient for the formations of S^0, $S_2O_3^{2-}$, and SO_4^{2-} . Although the solution conditions support the formation of SO_4^{2-}, XRD measurements have confirmed the presence of elemental sulfur after leaching the copper

concentrates with Ce^{4+}. Controls in which elemental sulfur is leached by Ce^{4+} in sulfate or nitrate media, showed very minimal leaching, suggesting that the less-oxidized sulfur intermediate is relatively stable.

Although Ghahremaninezhad et al. reports production of $S_2O_3^{2-}$ electrochemically, most literature reports that sulfur exists as S^0 (Dutrizac, 2013), S_2^{2-} (Yin, 1995), S_n^{2-} (Hackl, 1995), SO_4^{2-} ions (Harmer, 2006), or jarosite phases (Parker, 2003)(Li, 2013). It is also unlikely $S_2O_3^{2-}$ remains in the presence of Ce^{4+}, as the oxidation potential of Ce^{4+} is greater than both $S_2O_3^{2-}$ and SO_4^{2-}, making the accumulation of $S_2O_3^{2-}$ unlikely as it would quickly oxidize to SO_4^{2-}.

The ratio between the Ce^{4+} consumed and the $CuFeS_2$ leached is an indicator of the relative importance of reactions 3.1-3.3 (i.e, if S^0 and SO_4^{2-} is the leach product). In this paper, this ratio has been identified s_{Ce}, which is the ratio between the molarity of Ce^{4+} consumed (difference between the initial Ce^{4+} concentration, $[Ce^{4+}]_i$, and final Ce^{4+} concentration, $[Ce^{4+}]_f$) and the average molarity of Cu^{2+} leached ($[Cu^{2+}]$) and Fe^{3+} leached ($[Fe^{3+}]$) and has been defined in Equation 3.4. If the copper concentrates were to be leached completely according to Equation 3.1, the s_{Ce} value would be 5.

$$s_{Ce} = \frac{[Ce^{4+}]_i - [Ce^{4+}]_f}{\frac{[Cu^{2+}] + [Fe^{3+}]}{2}} \qquad 3.4$$

Table 3.3 shows the experimental results after leaching the two copper concentrates in the control ceric sulfate solution.

Table 3.3: s_{Ce} of copper concentrates leached in control ceric sulfate solutions

Time leached	Loading	Cu leached	Fe leached	Ce consumed	s_{Ce}

1h	16g/L	0.015M (S1) 0.016M (S2)	0.034M (S1) 0.022M (S2)	0.30M (S1) 0.16M (S2)	**12.3 (S1)** **8.6 (S2)**
4h	16g/L	0.017±0.001M (S1) 0.018±0 M (S2)	0.033±0.006M (S1) 0.023±0.003 M (S2)	0.29±0.04M (S1) 0.16±0.02 M (S2)	**11.6±0.1 (S1)** **7.9±0.3 (S2)**
	32g/L	0.047M (S2)	0.056M (S2)	0.40M (S2)	**7.8 (S2)**
24h	16g/L	0.023±0.001M (S1) 0.023M (S2)	0.041±0.002M (S1) 0.033M (S2)	0.35±0.01M (S1) 0.21M (S2)	**10.8±0.1 (S1)** **7.5 (S2)**

The s_{Ce} was determined for all experimental runs. For source 1, $CuFeS_2$ is the predominant copper-bearing mineral, and we see that s_{ce} is 12.3 after one hour of leaching. This suggests that 39% of the oxidation of the sulfide results in elemental sulfur according to reaction 3.1 and 61% to sulfate according to reaction 3.3. For longer times, the s_{Ce} declines, and possible explanations are discussed below.

The source-2 concentrate also contains significant amounts of chalcocite and bornite (*c.f.* Table 3.1). The s_{Ce} is initially found to be 8.6, lower than source 1. This can be explained by Source 2 concentrates – s_{Ce} value is 4.0 when leaching Cu_2S by producing S^0, and 4.3 when leaching Cu_5FeS_4, according to Reactions 3.5 and 3.7, compared to 5.0 moles when leaching $CuFeS_2$. The s_{Ce} value is 10 when leaching Cu_2S by producing SO_4^{2-}, and 12.3 when leaching Cu_5FeS_4, according to Reactions 3.6 and 3.8, compared to 17 necessary when leaching $CuFeS_2$.

$$Cu_2S + 4Ce^{4+} \rightarrow 2Cu^{2+} + S^0 + 4Ce^{3+} \quad 3.5$$

$$Cu_2S + 10Ce^{4+} + 4H_2O \rightarrow 2Cu^{2+} + {SO_4}^{2-} + 8H^+ + 10Ce^{3+} \quad 3.6$$

$$Cu_5FeS_4 + 13Ce^{4+} \rightarrow 5Cu^{2+} + Fe^{3+} + 4S^0 + 13Ce^{3+} \quad 3.7$$

$$Cu_5FeS_4 + 37Ce^{4+} + 16H_2O \rightarrow 5Cu^{2+} + Fe^{3+} + 4SO_4^{2-} + 32H^+ + 37Ce^{3+} \quad 3.8$$

The presence of pyrite also affects s_{Ce} values for both concentrates. We have shown pyrite leaches quickly in Ce^{4+} at room temperature. As shown in Figure 3.1, the XRD results of Source 2 concentrates (16g/L) leached in 1M H_2SO_4 for 1 hour, or in 0.25M $Fe_2(SO_4)_3$, 0.1M H_2SO_4 for 1 hour, indicates the presence of remaining FeS_2 after leach. In contrast, the results after leach in control ceric sulfate for 15 minutes show a significantly reduced FeS_2 peak.

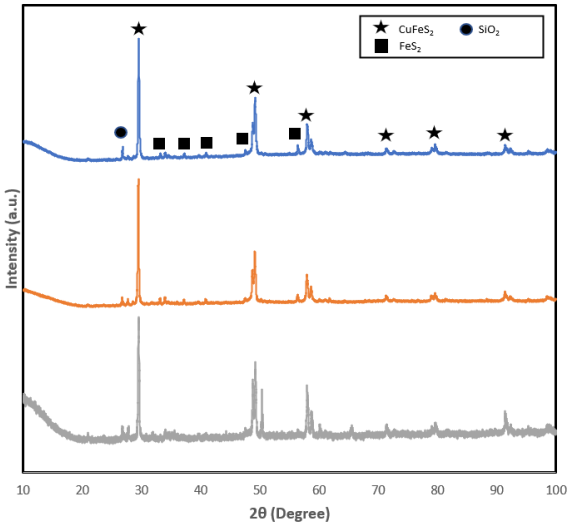

Figure 3.1: XRD of Source 2 concentrates (16g/L) after being leached in 1M H_2SO_4 for 1 hour (top), 0.25M $Fe_2(SO_4)_3$, 0.1M H_2SO_4 for 1 hour (middle), 0.5M $Ce(SO_4)_2$, 0.1M H_2SO_4 for 15 minutes (bottom)

In the literature, the FeS_2 is generally shown to react according to Equation 3.9, where S_2^{2-} ions oxidize to SO_4^{2-} (Antonijević, 1997). This reaction is reported to be far from equilibrium with essentially no reverse rate.

$$FeS_2 + 15Ce^{4+} + 8H_2O \rightarrow Fe^{3+} + 2SO_4^{2-} + 16H^+ + 15Ce^{3+} \quad 3.9$$

However, although the leaching of FeS_2 follows the shrinking sphere model closely in the initial stages of leaching, Long et al. claims that the buildup of elemental S^0 passivation layer causes the experimental results to deviate from the shrinking sphere model in the later stages of leaching when leaching FeS_2 in sulfuric acid with O_2 feed at elevated temperatures (Long, 2004). The following reactions are proposed to explain this buildup of elemental S^0 passivation layer, in which S_2^{2-} is instead oxidized to $S_2O_3^{2-}$, which decays into S^0.

$$FeS_2 + 7Ce^{4+} + 3H_2O \rightarrow Fe^{3+} + S_2O_3^{2-} + 6H^+ + 7Ce^{3+} \quad 3.10$$

$$S_2O_3^{2-} \rightarrow S^0 + SO_3^{2-} \quad 3.11$$

$$SO_3^{2-} + 2Ce^{4+} + H_2O \rightarrow SO_4^{2-} + 2Ce^{3+} + 2H^+ \quad 3.12$$

The production of elemental S^0 as the only sulfur product according to Equation 3.13 has also been considered as a possibility. However, the oxidation potential required for elemental S^0 from FeS_2 is significantly lower than the potential required for $CuFeS_2$. Chandra et al. reports that Fe^{3+} reacts with FeS_2 to form Fe^{2+} and SO_4^{2-}, and that S^0 is formed if leached at low Eh between 250-300 mV vs. SHE (Chandra, 2010).

$$FeS_2 + 3Ce^{4+} \rightarrow Fe^{3+} + 2S^0 + 3Ce^{3+} \quad 3.13$$

The following analysis assumes that all the FeS_2 has been leached from the concentrates in the first hour of leaching in the control ceric solution, with 7 moles of Ce^{4+} required to leach out one mole of FeS_2 (s_{Ce} = 14). Table 3.4 shows the s_{Ce} values, assuming all FeS_2 has been removed from the concentrates prior to leaching.

The overall s_{Ce} values are lower than the values shown in Table 3.3, which is reasonable since the s_{Ce} required for FeS_2 leaching is higher than $CuFeS_2$ leaching. Overall, with the assumptions made, the presence of FeS_2 increases the amount of Ce^{4+} required to leach the copper and iron by 10-20% across all conditions.

Table 3.4: s_{Ce} of copper concentrates leached in control ceric sulfate solutions, assuming that FeS_2 consumes 7 Ce/Fe.

Time leached	Loading	Cu leached	Fe leached	Ce consumed	s_{Ce}
1h	16g/L	0.015M (S1) 0.016M (S2)	0.008M (S1) 0.014M (S2)	0.12M (S1) 0.10M (S2)	**10.4 (S1)** **6.7 (S2)**
4h	16g/L	0.017M (S1) 0.018M (S2)	0.007M (S1) 0.015M (S2)	0.11M (S1) 0.10M (S2)	**9.2 (S1)** **6.1 (S2)**
	32g/L	0.047M (S2)	0.039M (S2)	0.28M (S2)	**6.5 (S2)**
24h	16g/L	0.023M (S1) 0.023M (S2)	0.015M (S1) 0.025M (S2)	0.17M (S1) 0.15M (S2)	**8.9 (S1)** **6.3 (S2)**

The s_{Ce} was also measured by mixing copper concentrates in control ceric nitrate solution and are shown below in Table 3.5. Overall, a higher amount of Ce^{4+} was required for leaching. A higher oxidation potential of Ce^{4+} in NO_3^- medium is expected to increase the amount of SO_4^{2-} products, increasing the amount of Ce^{4+} consumed. However, the accumulation of free SO_4^{2-} ions was *not detected* when the leach solution was mixed with a 0.1M $BaCl_2$ solution. One possible reason might be the formation of insoluble SO_4^{2-} products such as jarosites, with one such reaction shown in Table 3.3 occurring at 1340 mV vs. SHE.

Table 3.5: s_{Ce} of copper concentrates leached in control ceric nitrate solutions

Time leached	Loading	Cu leached	Fe leached	Ce consumed	s_{Ce}	**s_{Ce}, FeS_2 adjusted**
1h	32g/L	0.016M (S1)	0.054M(S1)	0.58M (S1)	**16.6 (S1)**	**24 (S1)**

		0.028M (S2)	0.038M(S2)	0.32M (S2)	**9.8 (S2)**	**8.3 (S2)**
24h	32g/L	0.024M (S1) 0.036M (S2)	0.063M (S1) 0.050M (S2)	0.66M (S1) 0.39M (S2)	**15.1 (S1)** **9.1 (S2)**	**16.9 (S1)** **7.9 (S2)**

*s_{Ce}, FeS_2 adjusted assumes that all FeS_2 was removed from concentrates prior to leach, assuming that FeS_2 consumes 7 Ce/Fe

Although an overall higher ratio of Ce^{4+} was expected, as the Ce^{4+} in nitrate is a stronger oxidizing agent than Ce^{4+} in sulfate media, the overall leaching rate was slower in Ce^{4+} nitrate than in Ce^{4+} sulfate. The higher consumption of Ce^{4+} did not translate into a higher amount of copper leached. The XRD in Figure 3.2 further support the observations made in above. The copper concentrate contents have been measured after 24 hours of leaching either 16g/L of concentrates in control ceric sulfate or 32g/L of concentrates in control ceric nitrate solution. The slower leaching rates in the Ce^{4+} nitrate solution resulted in higher $CuFeS_2$ content remaining in the solid after leaching. The absence of elemental sulfur in the solid content most likely means that the sulfur exists as $S_2O_3^{2-}$, SO_4^{2-}, or surface layers.

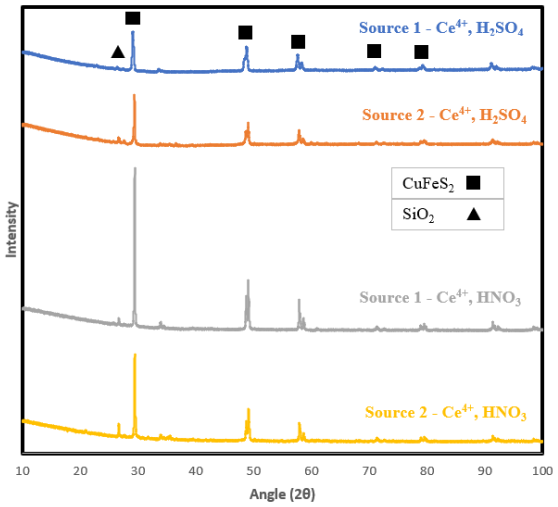

Figure 3.2: XRD of copper concentrates after leaching in either 0.5M $Ce(SO_4)_2$, 0.1M H_2SO_4 or in 1.0M $(NH_4)_2Ce(NO_3)_6$, 1.0M HNO_3 for 24 hours, for Source 1 or Source 2 concentrates.

Compiling the data for the Ce^{4+} consumption at each time interval, the overall trend shows that the s_{Ce} value generally decreased as the leaching duration increased (Figure 3.3). This trend was studied by comparing the solid residue after leaching in control ceric sulfate for 24 hours, against results in 2-stage leach, where the concentrates were leached in control ceric sulfate for 24 hours, recovered, and leached again in a fresh batch of control ceric sulfate for an additional 24 hours.

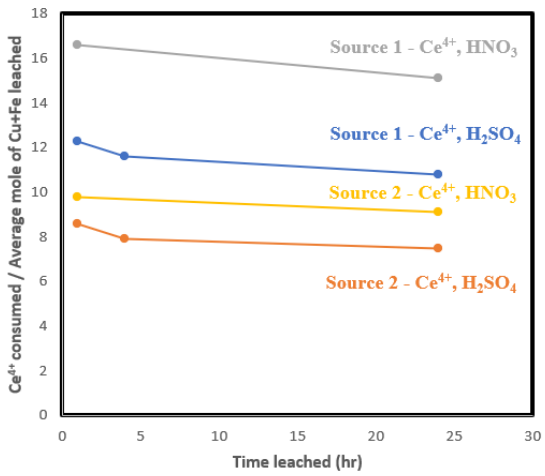

Figure 3.3: Compilation of data in Tables 3.3 and 3.5, showing the decreasing s_{Ce}, as the leaching duration increases

Table 3.6: s_{Ce} of copper concentrates leached in control ceric sulfate solutions, Source 2 concentrates

Time leached	Loading	Cu leached	Fe leached	Ce consumed	s_{Ce}
Ce^{4+} (One stage leach) + Source 2 concentrates					
24h	16g/L	0.023M	0.033M	0.21M	7.5
Ce^{4+} (Two stage leach) + Source 2 concentrates					
24h + 4h	16g/L	0.012M	0.009M	0.05M	4.7
24h + 24h	16g/L	0.018M	0.014M	0.07M	4.3

*Data from two-stage leach lists the data obtained from the second leach solution only

The decreased Ce^{4+} demand suggests a higher production of elemental sulfur in the later stages of leaching. The XRD measurements have shown that the elemental sulfur content was significantly higher after 48 hours of cumulative leaching.

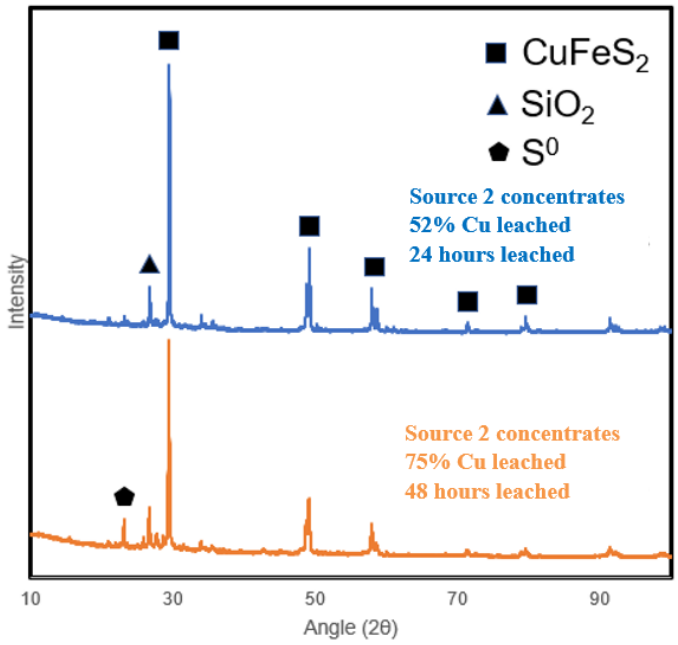

Figure 3.4: XRD of Source 2 copper concentrates after 24 hours of leaching in 0.5M $Ce(SO_4)_2$, 0.1M H_2SO_4 (top) and Source 2 copper concentrates after leaching in 0.5M $Ce(SO_4)_2$, 0.1M H_2SO_4 for 48 hours, in two consecutive batches of 24 hours (bottom)

As shown previously, FeS_2 also contributes in the decreasing s_{Ce} values over time. Although the presence of FeS_2 partially explains the difference in Ce requirements between the initial 24-hour leach and the second stage of 24-hour leach, there is still a considerable difference, with 6.3 moles of Ce^{4+} required per average mole of copper and iron leached, assuming that FeS_2 was excluded in the initial 24-hour leach, compared to 4.3 moles required in the second stage of 24-hour leach. The explanation that elemental sulfur production increases in the later stages of leaching remains as a possibility.

In summary, a possible explanation for the experimental results is that the leaching of copper concentrates in Ce^{4+} sulfate oxidizes the sulfide to SO_4^{2-} during the initial stages of leaching. Increasing the leach duration favors the formation of elemental sulfur, decreasing the Ce^{4+} required.

The leaching of copper concentrates in Ce^{4+} nitrate also oxidizes most of the sulfur to SO_4^{2-} during the initial stages of leaching. While the SO_4^{2-} formation is likely due to the higher oxidation

potential, the absence of detectable sulfate ions in $BaCl_2$ titration supports the conclusion that aqueous SO_4^{2-} is not a significant product under these conditions.

3.3.2. Reaction pathways of oxidation of Cu_2S and CuS

To investigate the behavior of intermediate copper sulfide species and to help reconcile difference between the two concentrate, additional experiments were conducted on Cu_2S and CuS. According to Silvester et al., the leaching of $CuFeS_2$ with Cu(II) at low pH yielded CuS, and the leaching of $CuFeS_2$ with Fe(III) at low pH yielded a product similar to CuS_2 (Silvester, 1994). In this study, the amount of Ce^{4+} consumed to leach Cu_2S and CuS was measured. The results are shown below in Table 3.7.

Table 3.7: Molar ratio of Ce consumed to average moles of copper and iron leached, Cu_2S and CuS

Time leached	Loading	Cu leached	Ce consumed	s_{Ce}
1h	8g/L (Cu_2S)	0.049±0.001M	0.11±0M	**4.2±0.2**
4h	8g/L (Cu_2S)	0.050±0.001M	0.11±0M	**4.2±0.2**
4h	16g/L (CuS)	0.069M	0.15M	**4.4**
24h	8g/L (Both)	0.054±0.001M (Cu_2S) 0.049±0.002M (CuS)	0.12±0M (Cu_2S) 0.10±0M (CuS)	**4.2±0.2 (Cu_2S)** **4.6±0.2 (CuS)**
24h	16g/L (CuS)	0.072M	0.22M	**6.0**

The results indicate that the primary product is elemental sulfur, as approximately two moles of Ce^{4+} are consumed for each mole of Cu^{2+} leached according to Equations 3.14 and 3.15 below. The XRD results also indicate the formation of elemental sulfur for both Cu_2S and CuS leach products.

$$Cu_2S + 2Ce^{4+} \rightarrow Cu^{2+} + CuS + 2Ce^{3+} \quad 3.14$$

$$CuS + 2Ce^{4+} \rightarrow Cu^{2+} + S0 + 2Ce^{3+} \quad 3.15$$

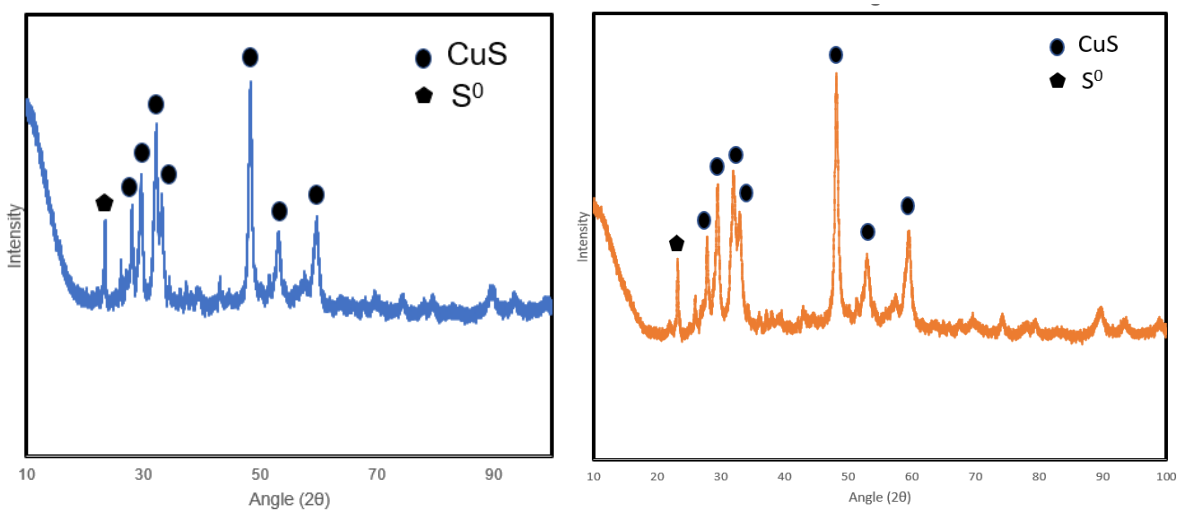

Figure 3.5: XRD of Cu_2S leached in 0.5M $Ce(SO_4)_2$, 0.1M H_2SO_4 for 24 hours (left) and CuS leached in 0.5M $Ce(SO_4)_2$, 0.1M H_2SO_4

It is possible that another sulfur-based product exists as the passivation layer. For both leaching of Cu_2S and CuS, the leaching rates plateaued quickly compared to the leaching of $CuFeS_2$. In the case of Cu_2S, leaching in Ce^{4+} yielded a solid product with only CuS and S^0, indicating that Cu_2S is completely oxidized.

According to these results, the leaching of $CuFeS_2$ in the later stages is similar to the leaching of CuS in which both produce elemental sulfur. However, although it is possible that CuS

or CuS_2 exists as a thin layer, these experiments cannot be used to determine whether CuS or CuS_2 is formed in the leaching process of $CuFeS_2$.

3.3.3. Reaction rates of oxidation of copper concentrates

Figure 3.6 shows the extent of copper leached from the copper concentrates over time. The leaching rate in Ce^{4+} was higher than in Fe^{3+}. However, the leaching rate in the control ceric nitrate solution was consistently lower than the leaching rate in the control ceric sulfate solution. The passivation of concentrates by jarosites is a possibility according to literature that explains the lower leaching rate in Ce nitrate. Despite the lack of alkali metals, some studies suggest that Ce^{3+} can replace the alkali metals for the production of jarosites under certain conditions (Desborough, 2010)(Lazareva, 2015).

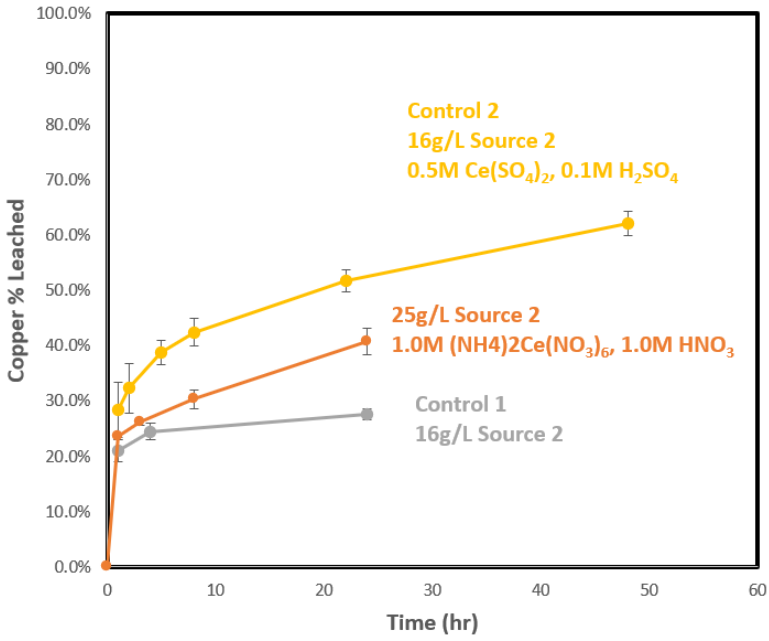

Figure 3.6: Leaching rates of control experiments. Source 2 concentrates were leached in Fe^{3+} solution (Control 1), Ce^{4+} sulfate solution (Control 2), and Ce^{4+} nitrate solution

Based on the results of Table 3.3, assuming an s_{Ce} value of 7.5 to leach $CuFeS_2$, the maximum loading of 100% $CuFeS_2$ allowed to be leached in 0.5M Ce^{4+} without depletion of Ce^{4+}

is 12.2g/L. To achieve practical processing rates, the target residence time to leach out the copper concentrates is approximately one hour. The results in Figure 3.6 indicates that the leaching rates are significantly slower than the requirement.

It was found that drying the solid residue between oxidative leaching cycles substantially increases the leaching rate. As shown in Figures 3.7, extending the duration of the drying process from 0 to 60 minutes led to an increase in leaching rates for copper concentrates. The 16g/L Source 2 concentrates were pretreated in ferric solution, oven dried at 70°C, then leached in the control ceric sulfate solution.

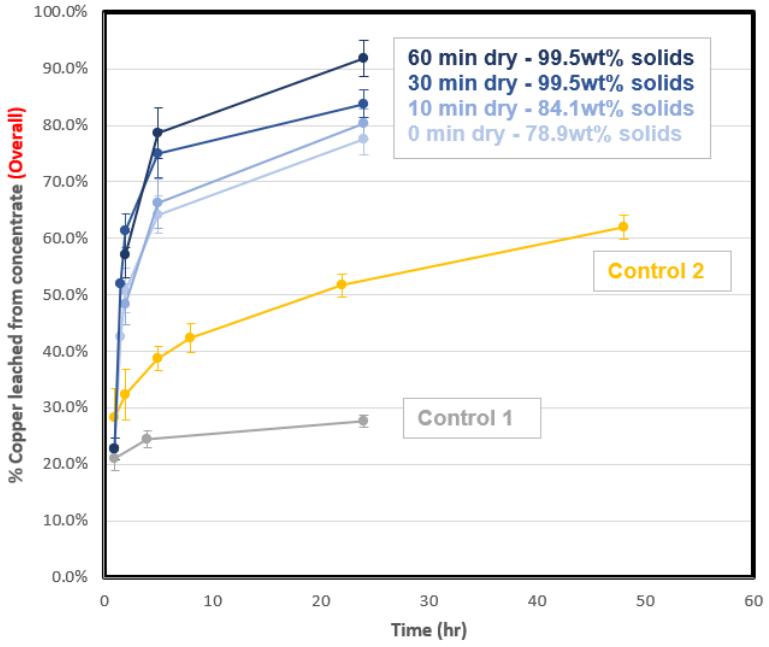

Figure 3.7: Leaching rates of Source 2 concentrates compared for various drying durations. 16g/L Source 2 concentrates were Fe^{3+}-treated, oven dried at 70°C, and leached in 0.5M $Ce(SO_4)_2$, 0.1M H_2SO_4 (24hr)

3.3.4. Comparison against leaching of copper concentrates in H_2O_2, H_2SO_4 systems

It is noteworthy that H_2O_2, H_2SO_4 leaching of copper concentrates is similar to the leaching of copper concentrates in control ceric sulfate solution in that both rely on high oxidation potential, theoretically high enough to oxidize the sulfur to sulfate, to leach out the copper concentrates at room temperature. However, according to the studies by Adebayo et al., the copper concentration

of the leach solution increased linearly with time even after 80% of the copper was leached from the concentrates (Adebayo, 2003)n contrast, the leaching rates in Ce^{4+} leaching plateau.

One key difference between the two methods was that increasing the concentration of sulfuric acid in H_2O_2, H_2SO_4 leaching greatly improved the leaching rates, whereas the acid concentration did not affect the Ce^{4+} leaching rates significantly. According to Baba et al., H^+ ion concentration increases the elemental sulfur production rate (Equation 3.16), which increases the overall leaching rate since H_2O_2 oxidizes elemental sulfur to sulfate (Baba, 2012). Oxidation rate of elemental sulfur in Ce^{4+} at room temperature was slow in a 24-hour timeframe, and it's possible Ce^{4+} is not removing the passivation layer as effectively as H_2O_2.

$$CuFeS_2 + 2H_2SO_4 + O_2 \rightarrow CuSO_4 + FeSO_4 + 2S^0 + 2H_2O \quad 3.16$$

$$S^0 + 1.5O_2 + H_2O \rightarrow 2H^+ + SO_4^{2-} \quad 3.17$$

3.4. Conclusion

Overall, the leaching rates of copper concentrates in Ce^{4+} sulfate media is insufficient to be considered for commercial scale, despite the efforts to increase the leaching rates by ferric pretreatment of concentrates and oven drying. The leaching extent of reaction plateaus, which suggest the buildup of a passivation layer, despite the Ce^{4+} having a theoretically high enough oxidation potential to oxidize sulfur to sulfate. Approximately 7.5 moles of Ce^{4+} were required to leach out one mole of $CuFeS_2$ in 24 hours, suggesting that the production of elemental sulfur was favored over the production of sulfate.

3.5. Acknowledgements

We would like to thank Dr. Paul Miranda for the AMICS analysis of copper concentrate samples. The authors gratefully acknowledge funding through ARPA-E grant DE-AR0001340 from the US Department of Energy.

3.6. Chapter 3 Appendix

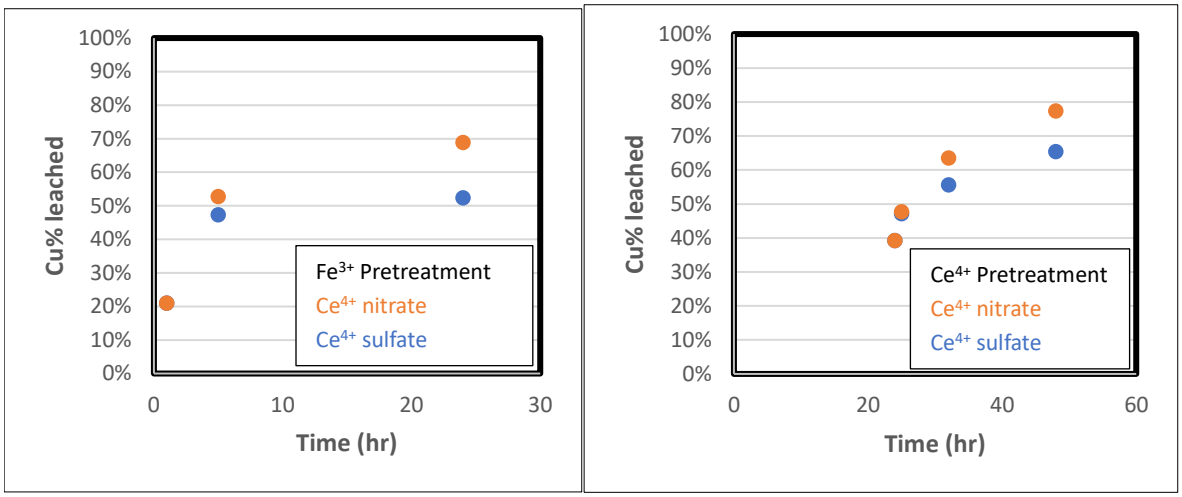

Figure S3.1: 16g/L of Source 2 concentrates reacted in 1.0M Fe^{3+}, 0.1M H_2SO_4 solution for 1 hour prior to reacting in 0.5M Ce^{4+}, 0.1M H_2SO_4 solution or 0.5M $(NH_4)_2Ce(NO_3)_6$, 1.0M HNO_3 for 24 hours (left) 16g/L of Source 2 concentrates reacted in 0.5M Ce^{4+}, 0.1M H_2SO_4 solution for 24 hours prior to reacting in 0.5M Ce^{4+}, 0.1M H_2SO_4 solution or 0.5M $(NH_4)_2Ce(NO_3)_6$, 1.0M HNO_3 for 24 hours (right)

3.7. References

Rötzer, N., Schmidt, M. Historical, current, and future energy demand from global copper production and its impact on climate change. *Resources* **2020,** *9*(4), 44.

Schipper, B. W., Lin, H.-C., Meloni, M. A., Wansleeben, K., Heijungs, R., & van der Voet, E. (2018). Estimating global copper demand until 2100 with regression and stock dynamics. *Resources, Conservation and Recycling*, *132*, 28–36.

The Role of Critical Minerals in Clean Energy Transitions. (2022). *IEA: International Energy Agency.* IEA.

Calvo, G., Mudd, G., Valero, A., Valero, A. Decreasing Ore Grades in Global Metallic Mining: A Theoretical Issue or Global Reality? *Resources* **2016**, *5*, 36.

Forsén, O., Aromaa, J., Lundström, M. Primary Copper Smelter and Refinery as a Recycling Plant—A System Integrated Approach to Estimate Secondary Raw Material Tolerance. *Recycling* **2017**, *2*(4), 19.

Kulczycka, J., Lelek, Ł., Lewandowska, A., Wirth, H., Bergesen, J.D. Environmental Impacts of Energy-Efficient Pyrometallurgical Copper Smelting Technologies: The Consequences of Technological Changes from 2010 to 2050. *Journal of Industrial Ecology* **2017**, *20*(2), 304-316.

Norgate, T., & Jahanshahi, S. Low grade ores – Smelt, leach or concentrate? *Minerals Engineering* **2010**, *23*(2), 65–73.

Serbula, S. M., Milosavljevic, J. S., Kalinovic, J. V., Kalinovic, T. S., Radojevic, A. A., Apostolovski Trujic, T. Lj., Tasic, V. M. Arsenic and SO_2 hotspot in south-eastern Europe: an overview of the air quality after the implementation of the flash smelting technology for copper production. *Science of the Total Environment* **2021**, *777*, 145981.

Schlesinger, M. E., King, M. J., Sole, K. C., Davenport, W. G. Chapter 15 – Hydrometallurgical copper extraction: introduction and leaching. *Extractive Metallurgy of Copper (Fifth Edition)* **2011**, 281-322.

Córdoba, E., Muñoz, J., Blázquez, M., González, F., Ballester, A. Leaching of chalcopyrite with ferric ion. Part I: General aspects. *Hydrometallurgy* **2008**, *93* (3–4), 81–87.

Pyper, R., Cassiday &. Associates, Seal, T., Uhrie, J.L., Miller, G.C. Dump and heap leaching. *SME Mineral Processing and Extractive Metallurgy Handbook* **2019**, 31-48.

Hourn, M.M., Turner, D.W., Holzberger, I.R. Atmospheric mineral leaching process, US Patent 5,993,635 (1999).

Barr, G., Defreyne, J., Mayhew, K. CESL copper process – an economic alternative to smelting (2005).

Dreisinger, D. Copper leaching from primary sulfides: Options for biological and chemical extraction of copper. *Hydrometallurgy* **2006**, *83* (1–4), 10–20.

Bard, J.A. Standard potentials in aqueous solution, 1st ed. *Routledge* **1985.**

Ghahremaninezhad, A., Asselin, E., Dixon, D.G. Electrochemical evaluation of the surface of chalcopyrite during dissolution in sulfuric acid solution. *Electrochimica Acta* **2010**, *55*(18), 5041-5046.

Lokshin, E.P., Tareeva, O.A., Ivlev, K.G., Kashulina, T.G. Solubility of double alkali metal (Na,K) rare-earth (La, Ce) sulfates in sulfuric-phosphoric acid solutions at 20ºC. *Russian Journal of Applied Chemistry*, **2005**, *78*, 1058-1063.

Um, N., Hirato, T. A hydrometallurgical method of energy saving type for separation of rare earth elements from rare earth polishing powder wastes with middle fraction of ceria. *Journal of Rare Earths* **2016**, *34*(5), 536-542.

Paulenova, A., Creager, S.E., Navratil, J.D., Wei, Y. Redox potentials and kinetics of the Ce^{3+}/Ce^{4+} redox reaction and solubility of cerium sulfates in sulfuric acid solutions. *Journal of Power Sources* **2002**, *109*(2), 431-438.

Buchanan, C.A., Ko, E., Cira, S., Balasubramanian, M., Goldsmith, B.R., Singh, N. Structures and free energies of cerium ions in acidic electrolytes. *Inorganic Chemistry* **2020**, *59*, 12552-12563.

Wadsworth, E., Duke, F.R., Goetz, C.A. Present status of Cerium(IV)-Cerium(III) potentials. *Analytical Chemistry* **1957**, *29*(12), 1824-1825.

Lou, W., Zhang, D., Bayless, R.C. Review of mineral recognition and its future. *Applied Geochemistry* **2020**, *122*, Article 104727.

Dutrizac, J.E. Elemental sulphur formation during the ferric sulfate leaching of chalcopyrite. *Chemical Extractive Metallurgy* **2013**, *28*(4), 337-344.

Yin, Q., Kelsall, G.H., Vaughan, D.J., England, K.E.R. Atmospheric and electrochemical oxidation of the surface of chalcopyrite (CuFeS2). *Geochim Cosmochim Acta* **1995**, *59*(6), 1091-1100.

Hackl, R.P., Dreisinger, D.B., Peters, E., King, J.A. Passivation of chalcopyrite during oxidative leaching in sulfate media. *Hydrometallurgy* **1995**, *39*, 25-48.

Harmer, S.L., Thomas, J.E., Fornasiero, D., Gerson, A.R. The evolution of surface layers formed during chalcopyrite leaching. *Geochim Cosmochim Acta* **2006**, *70*, 4392-4402.

Parker, A., Klauber, C., Kougianos, A., Watling, H.R., van Bronswijk, W. An X-ray photoelectron spectroscopy study of the mechanism of oxidative dissolution of chalcopyrite. *Hydrometallurgy* **2003**, *71*, 265-276.

Li, Y., Kawashima, N., Li, J., Chandra, A.P., Gerson, A.R. A review of the structure, and fundamental mechanisms and kinetics of the leaching of chalcopyrite. *Advances in Colloid and Interface Science* **2013**, *197-198*, 1-32.

Antonijević, M.M., Dimitrijević, M., Janković, Z. Leaching of pyrite with hydrogen peroxide in sulphuric acid. *Hydrometallurgy* **1997**, *46*(1-2), 71-83.

Chandra, A.P., Gerson, A.R. The mechanisms of pyrite oxidation and leaching: A fundamental perspective. *Surface Science Reports* **2010**, *65*(9), 293-315.

Long, H., Dixon, D.G. Pressure oxidation of pyrite in sulfuric acid media: a kinetic study. *Hydrometallurgy* **2004**, *73*, 335-349.

Silvester, E., Grieser, F., Healy, T.W., Meisel, D., Sullivan, J.C. Thermodynamics and kinetics of the reaction of copper(II) and iron(III) with ultra-small colloidal chalcopyrite ($CuFeS_2$). *J. Chem. Soc.* **1994**, *90*, 3301-3307.

Desborough, G.A., Smith, K.S., Lowers, H.A., Swayze, G.A., Hammarstrom, J.M., Diehl, S.F., Leinz, R.W., Driscoll, R.L. Mineralogical and chemical characteristics of some natural jarosites. *Geochimica at Cosmochimica Acta* **2010**, *74*(3), 1041-1056.

Lazareva, E.V., Zhmodik, S.M., Dobretsov, N.L., Tolstov, A.V., Shcherbov, B.L., Karmanov, N.S., Gerasimov, E.Yu., Bryanskaya, A.V. Main minerals of abnormally high-grade ores of the Tomtor deposit (Arctic Siberia). *Russian Geology and Geophysics* **2015**, *56*, 844-873.

Adebayo, A.O., Ipinmoroti, K.O., Ajayi, O.O. Dissolution kinetics of chalcopyrite with hydrogen peroxide in sulfuric acid medium. *Chem. Biochem. Eng. Q.* **2003**, *17*(3), 213-218.

Baba, A.A., Ayinla, K.I., Adekola, F.A., Ghosh, M.K., Ayanda, O.S., Bale, R.B., Sheik, A.R., Pradhan, S.R. A review on novel techniques for chalcopyrite ore processing. *International Journal of Mining Engineering and Mineral Processing*. **2012**, *1*(1), 1-16.

Chapter 4:

Process Flowsheets and Economic Analysis of Room Temperature Leaching Methods

Abstract

Although both V^{2+} and Ce^{4+} room temperature leaching of copper concentrates have potential, there are still many concerns with the overall post-leach process that are not seen in incumbent processes. Due to the costs of the raw vanadium and cerium, the ions must be recycled, so the V^{3+} and Ce^{3+} ions in the post-leach solution must be regenerated to V^{2+} or Ce^{4+} ions. The V^{2+} and Ce^{4+} ions must also be separated from the copper product and the iron by-product, adding additional separation processes.

This chapter explores the overall process and develops a simplified flowsheet necessary for each process. Based on the experimental results obtained, the reactor sizes were calculated, and the energy costs associated with each process were estimated. Assuming processing of 10 tonnes concentrate/day, the reactor sizes and electrical power necessary for vanadium leaching were smaller due to the higher processing rates, at $2.8m^3$ and 0.13MW compared to $600m^3$ and 0.67MW for the cerium leaching process. Despite the additional investments required for the vanadium leaching process for the treatment of H_2S, the vanadium leaching process is more likely to be the feasible option when comparing the two leaching processes as candidates for scale-up.

4.1. Introduction

Although both the V^{2+} and Ce^{4+} leaching methods are candidates for scale-up due to the relatively fast leaching rates at room temperature, there are still many factors that must be considered, such as the overall processing of the leach products after the leaching. Both V^{2+}-reductive leaching and Ce^{4+}-oxidative leaching have unique procedures that are not seen in typical leaching processes, namely the regeneration of consumed ions after leaching. Although the process occurs at room temperature, the additional operation and energy required can significantly increase the costs.

This chapter presents possible (simplified) flowsheets for each leaching method and the expected reactor sizes and energy costs associated with each method. The overall leaching method is divided into three major operations – leaching, regeneration of ions, and separation.

The electrochemical regeneration of ions requires an electrolyzer, which has many similarities with flow batteries, which have been developed at large scales over the past several decades. The vanadium flow battery, which has been researched extensively for the purposes of energy storage due to its resistance against cross-over, which results in a higher lifecycle (Parasuraman, 2013). Although a typical flow battery utilizes a separator to prevent the cross-over between two solutions, vanadium flow batteries typically utilize vanadium ions in both the catholyte and the anolyte, due to the existence of vanadium ions across many oxidation states (V^{2+}, V^{3+}, VO^{2+}, VO_2^{+}). A typical charge reaction in the anolyte and the catholyte of the vanadium flow battery are shown in Reactions 4.1 and 4.2 below (Rychcik, 1988). The leach solution that contains V^{3+} is expected to be regenerated to V^{2+} following the catholyte charge reaction.

$$V^{3+} + e^{-} \rightarrow V^{2+} \qquad 4.1$$

$$VO^{2+} + H_2O \rightarrow VO_2^+ + 2H^+ + e^- \quad 4.2$$

A cerium flow battery, specifically the Ce-Zn flow battery, also has seen used due to the high potential, which leads to higher energy density. For instance, Ce-Zn flow battery achieved 2.4V at full charge and 35 Wh/L (Wang, 2019). The typical charge reactions in the anolyte and catholyte of the Ce-Zn flow battery are shown below in Reactions 4.3 and 4.4. The Ce^{3+} in the leach solution is regenerated to Ce^{4+} following Reaction 4.4.

$$Zn^{2+} + 2e^- \rightarrow Zn^0 \quad 4.3$$

$$Ce^{3+} \rightarrow Ce^{4+} + e^- \quad 4.4$$

However, the solubility of Ce^{3+} in sulfuric acid is reportedly too low to be used for practical energy applications (<0.3M) (Leung, 2015). Although the solubility can be increased to 0.8M utilizing methanesulfonic acid media, such an option is not suitable for the mining applications, which constantly accumulates sulfate ions from the leached concentrates and have other economical constraints.

An air oxidative regeneration method of cerium was also investigated as a possible alternative to the electrochemical regeneration method due to the limited solubilities of Ce^{3+}. Air oxidation in energy storage applications are typically used in metal-air batteries, where the metal is oxidized to metal hydroxides during charge at the anode (Reaction 4.5) and oxygen is reduced to provide hydroxide ions at the cathode (Reaction 4.6) (Liu, 2020).

$$M + nOH^- \rightarrow M(OH)_n + ne^- \quad 4.5$$

$$\frac{n}{4}O_2 + ne^- \rightarrow \frac{n}{2}H_2O + nOH^- \quad 4.6$$

However, the air oxidation of cerium is a chemical process that occurs with the oxygen reacting directly with the cerium hydroxide solids, as shown below in Reaction 4.7. Since the reaction occurs without the need to dissolve the cerium prior to oxidation, the air oxidative regeneration process was investigated as a possible alternative to electrochemical regeneration process.

$$2Ce(OH)_3 + H_2O + \frac{1}{2}O_2 \rightarrow 2Ce(OH)_4 \qquad 4.7$$

The separation processes for ions in the leach solution are different, depending on Ce or V leach steps. The most common method to separate copper and iron in the leach solution is by solvent extraction, which is a mixing of the leach solution with an organic solvent to selectively remove copper from the leach solution (Rotuska, 2008). Although the incumbent solvent extraction method is expected to be suitable for the V^{2+} leaching solution, the Ce^{4+} leaching solution includes Ce^{3+} ions in the leach solution that must be separated from the Cu^{2+} and Fe^{3+}.

The method described in this chapter separates cerium by the $NaCe(SO_4)_2$ precipitation method proposed by Lokshin et al. (Lokshin, 2005). Due to the low solubilities of Ce^{3+} in the simultaneous presence of Na^+ and SO_4^{2-} ions, it was experimentally observed that Ce^{3+} can be removed completely from the Cu^{2+} and Fe^{3+} ions in solution, even at very low pH values. This $NaCe(SO_4)_2$ can be readily converted to $Ce(OH)_3$, which can be dissolved in acid to form Ce^{3+} for electrochemical regeneration, or converted to $Ce(OH)_4$ by air oxidation.

This chapter reviews the economics of the proposed leaching processes, which include unique procedures not commonly seen in the incumbent leaching procedures. The reactor sizes and the operating costs required to process 10 tons/day of 20% copper-grade $CuFeS_2$-based copper concentrates are calculated for each process. The V^{2+} leaching procedure is expected to

be more economical than the Ce^{4+} leaching process – the residence time in the leaching reactor and the concentrate loading greatly favored the processing rates of the V^{2+} leaching process.

4.2. Experimental Procedure

The following assumptions have been made based on the experimental results of leaching and regeneration.

4.2.1. Target Processing Rate

All calculations were made assuming that 10 tons/day of 20.0% Cu-grade copper concentrates will be processed. The copper source is assumed to be from $CuFeS_2$. Therefore, 57.8% of the copper concentrate mass is comprised of $CuFeS_2$.

4.2.2. Chemical Composition

The initial leach solution for vanadium leaching is assumed to consist of 1M VSO_4, 1M H_2SO_4 solution. The initial leach solution for cerium leaching is assumed to consist of 0.5M $Ce(SO_4)_2$, 1M H_2SO_4 solution.

4.2.3. Leach Reaction

The vanadium leach reaction is assumed to proceed according to Reaction 4.8, shown below. Two moles of V^{2+} are assumed to be required for each mole of $CuFeS_2$.

$$2V^{2+} + CuFeS_2 + 4H^+ \rightarrow 2V^{3+} + Cu^0 + Fe^{2+} + H_2S \quad 4.8$$

The cerium leach reaction is assumed to proceed as a mixture of the two reactions, Reactions 4.9 and 4.10, shown below. Due to experimental results, nine moles of Ce^{4+} are assumed to be required for each mole of $CuFeS_2$. Therefore, 67% of the reaction occurs according to Reaction 4.9, and 33% according to Reaction 4.10.

$$5Ce^{4+} + CuFeS_2 \rightarrow 5Ce^{3+} + Cu^{2+} + Fe^{3+} + 2S^0 \quad 4.9$$

$$17Ce^{4+} + CuFeS_2 + 8H_2O \rightarrow 17Ce^{3+} + Cu^{2+} + Fe^{3+} + 2SO_4^{2-} + 16H^+ \quad 4.10$$

4.2.4. Concentrate Loaded

The concentrate loading has been calculated according to Equation 4.11 shown below. According to this equation, the expected copper concentrate loading in V^{2+} leach solution is 159g/L. The expected copper concentrate loading in Ce^{4+} leach solution is 17.6g/L.

$$\text{Concentrate Loaded} = \frac{\text{Ion concentration}}{\text{Ratio of ion required per } CuFeS_2 * \%\text{wt } CuFeS_2 \text{ in concentrate}} \quad 4.11$$

4.2.5. *Residence Times*

Based on experimental data in chapters 3 and 5, the following residence times have been selected for each operation based on experimental results.

Table 4.1: Residence Times of each reactor in each leach process

Process	Reactor	Residence Time
V^{2+} leach process	V^{2+} leach reactor	1 hour
	Fe^{3+} leach reactor	1 hour
Ce^{4+} leach process	Ce^{4+} leach reactor	24 hours
	Ce^{4+} separator	1 hour
	Ce^{4+} air oxidation	8 hours
	$Ce(OH)_4$ acid dissolution	24 hours

4.2.6. Electrochemical Regenerator Current Density

The current density used in the vanadium electrolyzer has been obtained from Skyllas-Kazacos et al., who reports a maximum current density of 130mA/cm^2, 1.6V OCP in a general all-vanadium redox flow battery system (Skyllas-Kazacos, 2011). In this paper, an OCP of 1.8V

will be used since the oxidation of VO^{2+} to VO_2^+ is unnecessary – H_2O will be oxidized to O_2 instead in the anolyte. The current density for the cerium electrolyzer has been experimentally determined to be 40mA/cm^2 operating at approximately 2V.

4.2.7. Electrochemical Regenerator Reactions

The reactions in the catholyte of the V^{2+}-electrolyzer are shown below in Reactions 4.12. The electrolyzer was designed to reduce all V^{3+} to V^{2+} The reaction in the anolyte is shown in Reaction 4.13.

$$V^{3+} + e^- \rightarrow V^{2+} \quad 4.12$$

$$H_2O \rightarrow \frac{1}{2}O_2 + 2H^+ + 2e^- \quad 4.13$$

The reactions in the catholyte of the Ce^{4+}-electrolyzer are shown below in Reactions 4.14, 4.15, and 4.16. Reduction of Fe^{3+} takes precedence over the reduction of Cu^{2+}, and the reduction of Cu^{2+} takes priority over reduction of H^+. Therefore, reaction 4.14 proceeds until Fe^{3+} is completely consumed before reaction 4.18 takes place. The reaction in the anolyte of the Ce^{4+}-electrolyzer is shown in Reaction 4.20. The efficiency is assumed to be 100% with no cross-over.

$$Fe^{3+} + e^- \rightarrow Fe^{2+} \quad 4.14$$

$$Cu^{2+} + 2e^- \rightarrow Cu^0 \quad 4.15$$

$$H^+ + e^- \rightarrow \frac{1}{2}H_2 \quad 4.16$$

$$Ce^{3+} \rightarrow Ce^{4+} + e^- \quad 4.17$$

4.2.8. Air Oxidation of $Ce(OH)_3$

Mixing 119g/L of $NaCe(SO_4)_2$ in 2M NaOH with air feed for 8 hours produces $Ce(OH)_4$, shown in Reaction 4.7.

4.2.9. Acid Dissolution of $Ce(OH)_4$

Mixing 1M of $Ce(OH)_4$ in 2.5M H_2SO_4 at 65°C for 24 hours completely dissolves $Ce(OH)_4$ to Ce^{4+}, shown in Reaction 4.18.

$$Ce(OH)_4 + 4HNO_3 \rightarrow Ce^{4+} + 4NO_3^- + 4H_2O \qquad 4.18$$

4.2.10. Extent of Reaction

The following criteria have been defined as the extent of reaction in all reactors of each process, in Table 4.2.

Table 4.2: Extent of reaction of each reactor in each leach process

Process	**Reactor**	**Criteria**
V^{2+} leach process	V^{2+} leach reactor	All V^{2+} consumed
	V^{2+} electrolyzer	All V^{3+} converted to V^{2+}
Ce^{4+} leach process	Ce^{4+} leach reactor	All Ce^{4+} consumed
	Ce^{4+} electrolyzer	All Ce^{3+} converted to Ce^{4+}
	Ce^{4+} separator	All Ce^{3+} converted to $NaCe(SO_4)_2$
	Ce^{4+} air oxidation	All $Ce(OH)_3$ converted to $Ce(OH)_4$
	$Ce(OH)_4$ acid dissolution	All $Ce(OH)_4$ dissolved to Ce^{4+}

With these assumptions, the chemical compositions in each stream of the overall process were calculated. Excel Solver has been used to calculate the compositions in each stream and converge the overall process.

4.3. Results and Discussion

4.3.1. Vanadium, Reduction Process

The overall flowsheet of the vanadium leaching process has been proposed by Xu et al., and is shown in Figure 4.1. (Xu, 2024).

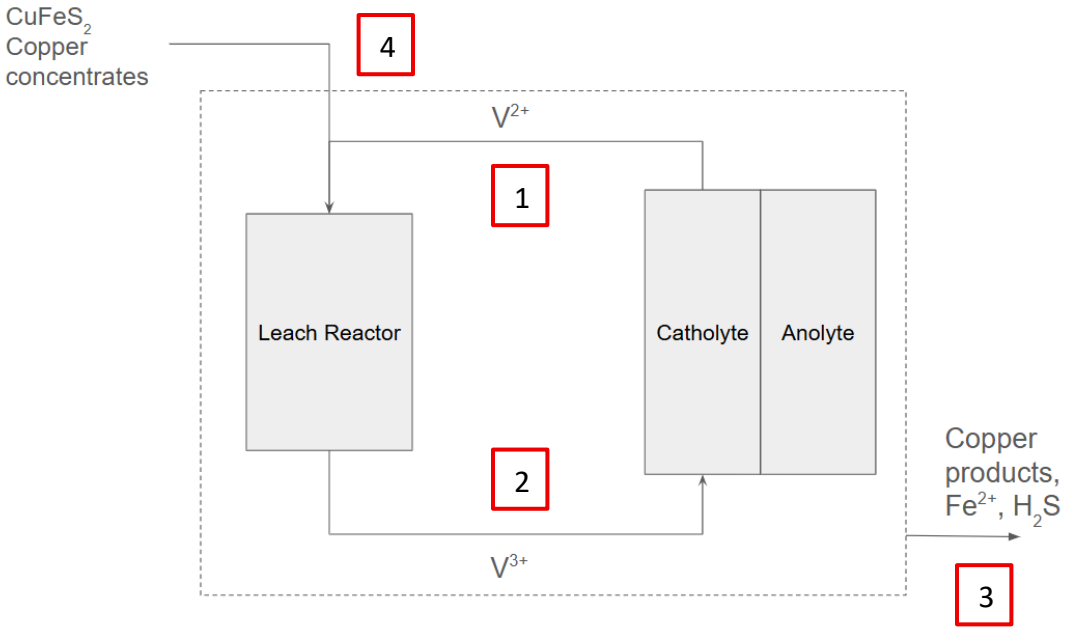

Figure 4.1: Overall schematics of vanadium leaching process of copper concentrates

The flowsheet shows the V^{2+} leach solution (Stream 1) and copper concentrates (Stream 4) enter the leach reactor continuously. The pregnant leach solution (Stream 2) exits the leach reactor and is separated into liquid, solid, and gaseous phases. The gas phase containing H_2S and the solid phase containing the copper product are removed from the system (Stream 3). The solid copper products are reacted in a 1M Fe^{3+}, 1.0M H_2SO_4 solution to leach the copper prior to

recovery of copper. Some iron is also released from the system to control the accumulation of iron in the leach solution. The liquid phase containing V^{3+} and Fe^{2+} is sent to the vanadium electrolyzer as the catholyte to reduce the V^{3+} back to V^{2+}. Replenishment of H_2SO_4 to Stream 1 is necessary due to the consumption of H_2SO_4 in the leach reactor The regenerated vanadium solution (Stream 1) enters the leach reactor to complete the cycle. Table 4.3 summarizes the compositions in each stream.

Table 4.3: Compositions in each stream of the vanadium reductive leaching process

Stream	V^{2+}	H^+	SO_4^{2-}	V^{3+}	Fe^{2+}	Cu^0
1	1.0M	2.0M	6.0M	-	1.0M	-
2	-	-	6.0M	1.0M	2.0M	0.5M
3	-	-	1.0M	-	1.0M	0.5M
4	159g/L copper concentrates (92g/L $CuFeS_2$)					

Based on the composition shown in Table 4.3, the leach reactor required to process 10 tons/day of 20.0% Cu-grade copper concentrates was calculated to be 2.8m^3. The Fe^{3+}-leach reactor was calculated to be 1.3m^3, assuming that Fe^{3+} reacts with Cu^0 at 2:1 molar ratio, divided by the 30-minute residence time. With the operation of the electrolyzer at 130mA/cm^2, the required current to reduce the pregnant leach solution of 1.0M V^{3+} at 2.8m^3/hr is 75,000A. The area required for the electrolyzer is 58m^2, assuming 100% efficiency.

When operated at 1.8V, the power requirement would be 0.13MW. Additional operating costs would be expected due to the treatment of H_2S, recovery of Fe^{3+} ions after Cu^0 leach, the loss of vanadium through the process, and the recovery of copper product by solvent extraction and electrowinning.

4.3.2. Cerium Oxidation Process with Electrochemical Regeneration

The overall flowsheet of the cerium leaching process with electrochemical regeneration is shown in Figure 4.2.

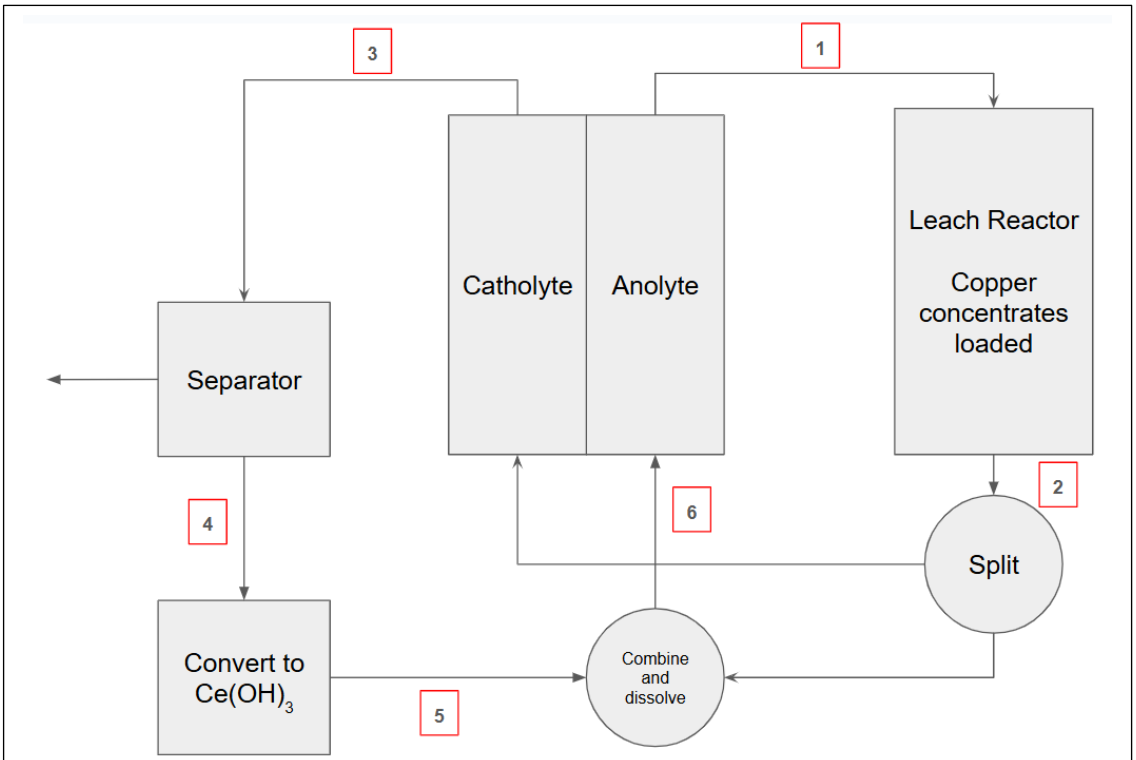

Figure 4.2: Overall schematics of cerium leaching process of copper concentrates

The flowsheet shows the Ce^{4+} leach solution (Stream 1) enter the leach reactor pre-loaded with copper concentrates. The pregnant leach solution (Stream 2) exits the leach reactor and is separated into two streams, with one stream entering as the anolyte and the other as the catholyte, both streams having the same composition. The stream exiting the catholyte (Stream 3) is reacted with Na^{+} and SO_4^{2-} to precipitate out the Ce^{3+} as $NaCe(SO_4)_2$, separating the Ce^{3+} from Fe^{2+} in the leach solution. The $NaCe(SO_4)_2$ stream (Stream 4) reacts with NaOH to produce a $Ce(OH)_3$ stream (Stream 5) and is combined with the leach solution intended for the anolyte. The H^{+} in the leach solution dissolves the $Ce(OH)_3$ to form Ce^{3+} prior to entering the anolyte stream. The

recycled leach solution exiting the anolyte (Stream 1) enters the leach reactor, completing the cycle. Table 4.4 summarizes the composition in each stream. The data converged when the anolyte to catholyte volume ratio was 0.75:0.25.

Table 4.4: Compositions in each stream of the cerium oxidative leaching process with electrochemical regeneration

Stream	Ce^{4+}	H^+	SO_4^{2-}	Ce^{3+}	Fe^{3+}	Cu^{2+}
1	0.50M	1.2M	1.2M	-	0.17M	0.17M
2	-	1.3M	1.2M	0.50M	0.22M	0.22M
3	-	-	1.2M	0.50M	0.22M $Fe2^+$	-
4	0.5M $NaCe(SO_4)_2$ solids					
5	0.5M $Ce(OH)_3$ solids					
6	-	1.2M	1.2M	0.50M	0.17M	0.17M

Based on the composition shown in Table 4.4, the leach reactor required to process 10 tons/day of 20.0% Cu-grade copper concentrates was calculated to be 600m^3. To regenerate the pregnant leach solution of 0.50M Ce^{3+} at 25m^3/hr, with a current density of 40mA/cm^2, 335,000A is required at 100% Coulombic efficiency. The required electrolyzer area is 840m^2. The separator for the precipitation of $NaCe(SO_4)_2$ and the $Ce(OH)_3$ conversion reactor were both calculated to be 6.3m^3 by dividing the volumetric flow rate into the catholyte by the residence time of 1 hour.

The electrical requirements in the electrolyzer was calculated to be 335,000A, assuming 100% Coulombic efficiency. When operated at 2.0V, the power requirement would be 0.67MW. Additional operating costs would be expected due to the recovery of Fe^{2+} ions after separation, the

feed of Na^+, SO_4^{2-}, OH^-, and H^+ required for the conversion of Ce^{3+} to $Ce(OH)_3$, then back to Ce^{3+}, the loss of cerium through the process, and the purification of copper product from the cathode.

The difference in the volume of the leaching reactor between the vanadium and cerium leaching processes is mostly from the difference in residence time (1 hour vs. 24 hours). The differences in the ion concentration (1M vs. 0.5M) and the molar ratio of ions required per $CuFeS_2$ (2 vs. 9) also contributes to the difference. The difference in electrical requirements is mostly due to the difference in the molar ratio of ions required per $CuFeS_2$, as more electrons are required for the oxidation of $CuFeS_2$ compared to the reduction reaction.

Even after accounting for the additional investments needed for the vanadium leaching process, the difference in reactor sizing and energy requirements is significant enough for the vanadium leaching process to be preferable over the cerium leaching process.

4.3.3. Cerium Oxidation Process with Chemical Regeneration

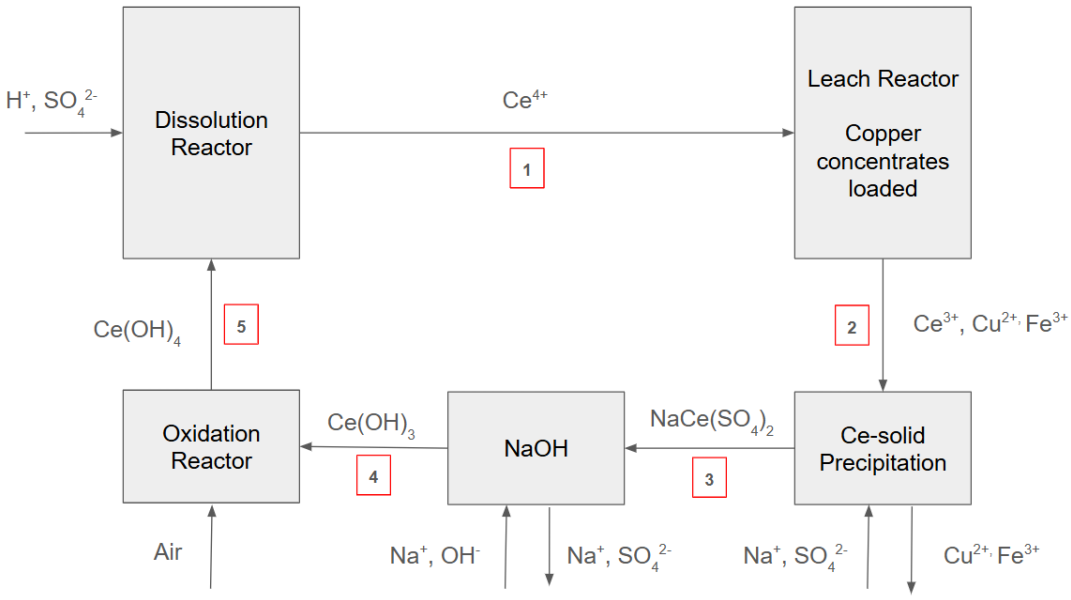

Figure 4.3: Overall schematics of cerium leaching process of copper concentrates, with air oxidation regeneration

The overall flowsheet of the cerium leaching process with chemical regeneration is shown in Figure 4.3.

The flowsheet shows the Ce^{4+} leach solution (Stream 1) enter the leach reactor pre-loaded with copper concentrates. The pregnant leach solution (Stream 2) exits the leach reactor and is reacted with Na^{+} and SO_4^{2-} to precipitate out the Ce^{3+} as $NaCe(SO_4)_2$, separating the Ce^{3+} from Fe^{3+} and Cu^{2+} in the leach solution. The $NaCe(SO_4)_2$ stream (Stream 3) reacts with NaOH to produce a $Ce(OH)_3$ stream (Stream 4). The $Ce(OH)_3$ oxidizes to $Ce(OH)_4$ (Stream 5) in the oxidation chamber, which is then dissolved to form Ce^{4+}, which can be recycled back (Stream 1) to enter the leach reactor. Table 4.5 summarizes the composition in each stream.

Table 4.5: Compositions in each stream of the cerium oxidative leaching process with air oxidation

Stream	Ce^{4+}	H^{+}	SO_4^{2-}	Ce^{3+}	Fe^{3+}	Cu^{2+}
1	0.50M	3.0M	3.5M	-	-	-
2	-	3.2M	3.6M	0.50M	0.055M	0.055M
3	0.5M $NaCe(SO_4)_2$ solids					
4	0.5M $Ce(OH)_3$ solids					
5	0.5M $Ce(OH)_4$ solids					

Based on the composition shown in Table 4.5, the leach reactor required to process 10 tons/day of 20.0% Cu-grade copper concentrates was calculated to be 600m³. Based on the flowsheet shown, the volumetric flow rates are equal across all reactors shown. The $NaCe(SO_4)_2$ precipitation reactor, $Ce(OH)_3$ conversion reactor, $Ce(OH)_4$ air oxidation reactor, and the acid dissolution reactor had residence times of 1 hour, 1 hour, 8 hours, and 24 hours respectively, and the reactor volumes were calculated to be $25m^3$, $25m^3$, $200m^3$, and $600m^3$, respectively.

There are no electrical requirements due to the absence of the electrolyzer. Additional operating costs are from the separation of Cu^{2+} and Fe^{3+} after the removal of Ce^{3+} ions, the feed of Na^{+}, SO_4^{2-}, OH^{-}, and H^{+} required for the conversion of Ce^{3+} to $Ce(OH)_4$, then back to Ce^{4+}, and the increased operating temperature (>65°C) required for the acid dissolution reactor.

Although the electrical requirements have been removed, some of the same weaknesses remain from the cerium leaching process with electrochemical regeneration, such as the large reactor size requirements and the need for acid-base swings to convert the cerium ions to cerium hydroxides, then back to soluble cerium ions. Additionally, the acid dissolution process is likely to be a major concern, requiring a significantly higher temperature and residence time compared to the other reactors. Overall, the cerium leaching process with chemical regeneration introduces new issues that the removal of electrical requirements cannot justify.

4.4. Conclusion

Overall, the vanadium leaching process is preferable over the cerium leaching process. One major reason is the difference in the volume of the leaching reactor between the vanadium and cerium leaching processes, which were calculated to be $2.8m^3$ and $600m^3$, respectively. This difference was due to the differences in residence time, ion concentrations, and the molar ratio of ions required per $CuFeS_2$. The electrical power requirements were also more favorable for vanadium regeneration, requiring 0.13MW for operation compared to 0.67MW for the operation of cerium regeneration.

For comparison, one example of an incumbent leach reactor is the Phelps Dodge reactor in Bagdad, which operates by total pressure and oxidation process. With an operating temperature of 210-220^{o}C, the reactor was capable of processing 136 t/d of copper concentrates with a reactor size of 110m^{3} (Wang, 2005)(Adams, 2004). The leaching reactor for the vanadium leaching process would be capable of a similar processing rate at such scale. It is likely that the vanadium leaching process would be competitive compared to incumbent leaching processes due to its low operating temperature.

4.5. References

Parasuraman, A., Lim, T.M., Menictas, C., Skyllas-Kazacos, M. Review of material research and development for redox flow battery application. *Electrochimica Acta* **2013**, *101*, 27-40.

Rychcik, M., Skyllas-Kazacos, M. Characteristics of a new all-vanadium redox flow battery. *Journal of Power Sources* **1988**, *22*(1), 59-67.

Wang, Q., Daoud, W.A. Reaction kinetics of cerium on glassy carbon with in situ electrochemical treatment for cerium-based flow battery. *Electrochimica Acta*, **2019**, *315*, 1-8.

Leung, P.K., Mohamed, M.R., Shah, A.A., Xu, Q., Conde-Duran, M.B. A mixed acid based vanadium-cerium redox flow battery with a zero-gap serpentine architecture. *Journal of Power Sources*, **2015**, *274*, 651-658.

Liu, Q., Pan, Z., Wang, E., An, L., Sun, G. Aqueous metal-air batteries: Fundamentals and applications. *Energy Storage Materials*, **2020**, *27*, 478-505.

Rotuska, K., Chmielewski, T. Growing role of solvent extraction in copper ore processing. *Physicochemical Problems of Mineral Processing*, **2008**, *42*, 29-36.

Lokshin, E.P., Tareeva, O.A., Ivlev, K.G., Kashulina, T.G. Solubility of double alkali metal (Na,K) rare-earth (La, Ce) sulfates in sulfuric-phosphoric acid solutions at 20ºC. *Russian Journal of Applied Chemistry*, **2005**, *78*, 1058-1063.

Wang, S. Copper leaching from chalcopyrite concentrates. *JOM*, **2005**, *57*, 48-51.

Adams, M.D., van der Meulen, D.R., Lunt, D.J., Anderson, P. Selection of piloting parameters in pressure hydrometallurgy. *Australasian Institute of Mining and Metallurgy Publication Series*, **2004**, 543-555.

Xu, T., Donovan, B., Kim, C., Banta, S., Fitts, J.P., West, A.C. Leaching mechanism for chalcopyrite in electrochemically regenerated vanadium(II). *ACS Sustainable Chemistry & Engineering,* **2024**, *12*(43), 15913-15922.

Skyllas-Kazacos, M., Chakrabarti, M.H., Hajimolana, S.A., Mjalli, F.S., Saleem, M. Progress in flow battery research and development. *Journal of Electrochemical Society* -**2011**, *158*(8), 55-7

Chapter 5:

Regeneration Methods of Ce^{4+}: Comparisons between electrochemical and air oxidation routes

Abstract

The oxidation of Ce^{3+} to Ce^{4+} is a necessary step in developing a cerium leaching process. This chapter discusses two regeneration methods: an electrochemical process and a chemical process involving air oxidation at high pH in the presence of $Ce(OH)_3$ solids. Although the electrochemical process is well-established, its performance is limited by the solubility of Ce^{3+}, which limits the processing rate. As a result, the chemical process was considered as an alternative.

The chemical air oxidation process presents problems due to the substantial amounts of acid and base required to convert the Ce^{3+} to $Ce(OH)_3$ and $Ce(OH)_4$ back to Ce^{4+}. Moreover, the dissolution of $Ce(OH)_4$ to Ce^{4+} demands high acid concentrations and high operating temperatures. Overall, the electrochemical process is most likely preferred when scaling up the cerium leaching process.

5.1 Introduction

In the leaching of copper concentrates using redox-active species such as V^{2+} or Ce^{4+}, the regeneration of these ions is crucial to ensure process sustainability and economic viability. One effective method is through electrochemical regeneration. In the case of V^{2+} regeneration, vanadium redox flow battery technology can be implemented to reduce the V^{3+} in the leach solution back to V^{2+} after separation of iron, as shown previously in Figure 4.1. As reviewed by Cunha et al., one incumbent vanadium redox flow battery setup utilizes 2M V^{3+} in the catholyte with 2M V^{4+} in the anolyte, dissolved in sulfuric acid, to yield between 60-80% energy efficiency at a current density of 20-80 mA/cm^2 at room temperature (Cunha, 2015).

Although a similar technology exists to oxidize Ce^{3+} ions to Ce^{4+}, it is less developed due to some disadvantages compared to the vanadium redox flow battery, mainly due to the lower solubility of cerium, which limits the energy density, and slower kinetics, resulting in lower maximum current densities. One of the most advanced cerium-based electrolyzer is a Ce-Zn RFB, which is utilized for its high standard cell potential of 2.48V, uses MSA solutions to increase the cerium concentrations (Arenas, 2016). However, with the presence of sulfate ions in the leach solution, the electrochemical regeneration becomes more limited. In the work by Kocyigit et al., oxidizing 0.2M Ce(III), 4.0M H_2SO_4, with 0.2M Cr(III), 4.0M H_2SO_4 in the catholyte, yielded an energy efficiency of 58.6% at a current density of only 0.8 mA/cm^2 at room temperature (Kocyigit, 2021).

Due to the difficulties with electrochemical regeneration of cerium, the chemical regeneration process was also investigated. Figure 5.1 shows the overall flow diagram of the chemical regeneration process. $NaCe(SO_4)_2$ is precipitated by adding Na^+ and SO_4^{2-} ions into a pregnant leach solution containing Ce^{3+}. Due to the low solubility of $NaCe(SO_4)_2$ in acidic media

as reported by Lokshin et al. (Lokshin, 2005), cerium was nearly completely precipitated from the leach solution as a solid. $NaCe(SO_4)_2$ can be subsequently introduced into NaOH in solution to form $Ce(OH)_3$. Although the equilibrium potential required for Ce^{3+} to oxidize to Ce^{4+} is 1.61V vs. SHE at a pH of ~ 0, this potential decreases in basic media (Dean, 1979), enabling air oxidation of $Ce(OH)_3$ to $Ce(OH)_4$ at room temperature. The dissolution of $Ce(OH)_4$ in sulfuric acidic media completed the formation of aqueous Ce^{4+}.

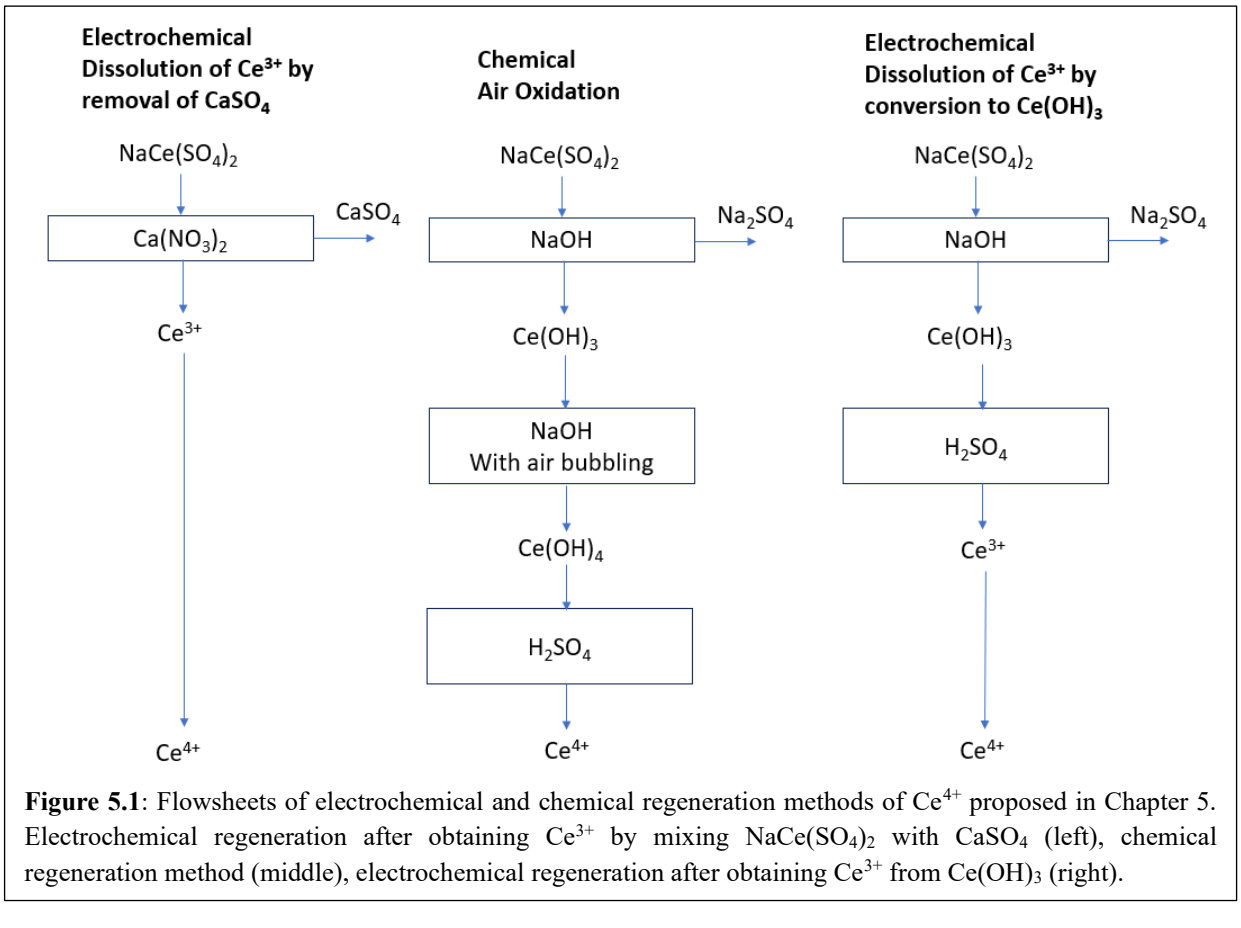

Figure 5.1: Flowsheets of electrochemical and chemical regeneration methods of Ce^{4+} proposed in Chapter 5. Electrochemical regeneration after obtaining Ce^{3+} by mixing $NaCe(SO_4)_2$ with $CaSO_4$ (left), chemical regeneration method (middle), electrochemical regeneration after obtaining Ce^{3+} from $Ce(OH)_3$ (right).

This chapter reports experimental results of both electrochemical and chemical regeneration of Ce^{3+} to Ce^{4+}. The advantages and disadvantages of both processes were investigated, and the conclusion is that the electrochemical regeneration method is most likely economically preferable over the chemical regeneration method.

5.2. Experimental Methods

5.2.1. Precipitation of $NaCe(SO_4)_2$

The initial Ce^{3+} solution was prepared by mixing 250ml of 1M $Ce(NO_3)_3$ (Sigma-Aldrich) in 1.0M HNO_3 solution (Sigma-Aldrich). Na^+ and SO_4^{2-} ions were inserted into the solution as $NaNO_3$ (Sigma-Aldrich) or H_2SO_4 (Sigma-Aldrich), respectively. The solutions were stirred with a magnetic stirring bar for 24 hours, either at room temperature or at 65°C. The solids were recovered by filtration in a Buchner filtration setup, utilizing an 11µm pore filter paper (Cole Parmer). The solid content was analyzed with XRD.

5.2.2. $Ce(OH)_3$ production

Two experimental setups were used. In the first setup, 119g/L, 238g/L, or 357g/L of $NaCe(SO_4)_2$ precipitates were loaded into a 100ml 2M NaOH (Sigma-Aldrich) solution and mixed for 2 hours with a magnetic stirring bar at room temperature. In the second setup, 119g/L, 238g/L, or 357g/L of $NaCe(SO_4)_2$ were loaded into a 100ml 2M NaOH solution, in a 250ml glass aspiration vessel (Eisco). Air was fed into the bottom port of the glass vessel while the solution was stirred with a magnetic stirring bar at room temperature for 5 minutes. The solids were recovered by filtration in a Buchner filtration setup, utilizing an 11 µm pore filter paper (Cole Parmer). The cerium content in the solids were analyzed with XRF.

5.2.3. $Ce(OH)_4$ production

Two experimental setups were used. In the first experimental setup, $NaCe(SO_4)_2$ was converted directly to $Ce(OH)_4$ by loading 119g/L of $NaCe(SO_4)_2$ precipitates into a 100ml 2M NaOH solution, in a 250ml glass aspiration vessel (Eisco). Air was fed into the bottom port while stirring the solution with a magnetic stirring bar at room temperature for 8 hours. In the second experimental setup, after the production of $Ce(OH)_3$, 85% of the NaOH solution was decanted

out and replenished with a fresh 1M NaOH solution, removing most of the Na^+ and SO_4^{2-} ions extracted from the $NaCe(SO_4)_2$ during the conversion to $Ce(OH)_3$. The solution was then mixed with a magnetic stirring bar at room temperature with air feed for 8 hours. The solids were recovered by filtration in a Buchner filtration setup, utilizing an 11µm pore filter paper (Cole Parmer).

5.2.4. Dissolution of $Ce(OH)_3$ with acid

100ml 119g/L of $NaCe(SO_4)_2$ was mixed in 2M NaOH for 5 minutes to produce $Ce(OH)_3$. 85% of the NaOH solution was decanted out and replenished with either 4M HNO_3 or 4M H_2SO_4 and mixed for 1 minute at room temperature. This process was used instead of filtration to minimize the time $Ce(OH)_3$ exposed to air and to prevent conversion to $Ce(OH)_4$.

5.2.5. Dissolution of $Ce(OH)_4$ with acid

Filtered $Ce(OH)_4$ solids were placed in 100mL 2.5M or 5M HNO_3 solutions and mixed for 24 hours. The solution was mixed at either room temperature or at 65ºC. HNO_3 was chosen for this step because of the limited solubility of Ce^{4+} in higher sulfuric acid concentrations at higher temperatures.

5.2.6. Dissolution of $NaCe(SO_4)_2$ in the presence of Ca^{2+}

$NaCe(SO_4)_2$ solids were mixed into a 100mL solution containing $Ca(OH)_2$ (Sigma-Aldrich) and HNO_3 at room temperature for 24 hours. $Ca(OH)_2$ and HNO_3 were mixed so that the H^+ concentration in the solution would be 1M for all trials. $NaCe(SO_4)_2$ and $Ca(OH)_2$ were mixed so that the Ca^{2+}:Ce^{3+} ratio would be either 2:1 or 6:1.

5.2.7. *Electrochemical regeneration setup*

Figure 5.2 shows the experimental setup - all tests were conducted in an H-cell with 100ml of 2M H_2SO_4 at the catholyte and 100ml of solution in the anolyte. The current was applied using Ivium-n-Stat instrument (Ivium Technologies) with a current density of 40mA/cm^2, with a stainless steel cathode (Analytical Scientific), lead anode (Analytical Scientific), and a Nafion-117 separator (MTI Corporation), at room temperature. The anolyte was composed of 0.1M $Ce_2(SO4)_3$, at different H_2SO_4 concentrations.

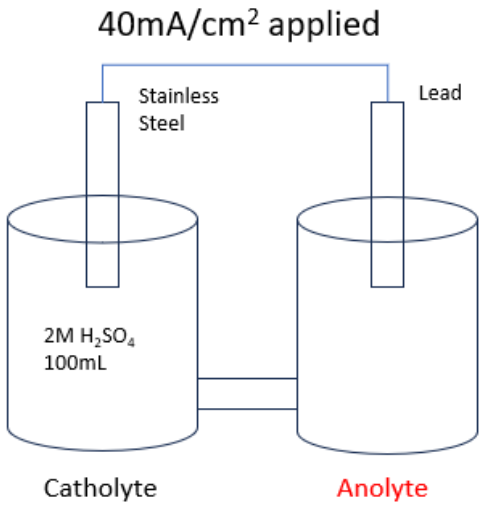

Figure 5.2: Experimental setup for electrochemical regeneration of Ce^{3+} solution to Ce^{4+} solution

5.2.8. *Measurement of Ce^{4+} concentration*

The concentrations of Ce^{4+} were determined by potentiometric titration. The titrant was prepared by dissolving 1M $FeSO_4$ (Sigma Aldrich) in 0.1M H_2SO_4. After extracting 1mL of the Ce^{4+} solution by pipette, 1M $FeSO_4$ was added in 20 microliter increments, with the solution potential measured using an ORP probe (Thermo Scientific). The titration endpoint was determined by the sudden decrease in solution potential from 1100mV vs. Ag/AgCl to 550mV vs. Ag/AgCl for solutions without NO_3^- present, and the sudden decrease to 800mV vs. Ag/AgCl for solutions with NO_3^- present. The Ce^{4+} concentration in the leach solution was calculated accordingly.

5.2.9. Measurement of Ce^{3+} concentration in solution

The concentration of Ce^{3+} was determined to be the difference between the total cerium concentration determined by ICP and the Ce^{4+} concentration measured by titration.

5.2.10. ICP analysis

Iron, copper, and cerium concentrations were measured using iCE 3000 Atomic Absorption Spectroscopy (AAS), obtained from Fisher Scientific. 100µL samples of solution were diluted in 50ml of 2% HNO_3 solution prior to measurement.

5.2.11. XRF analysis

A EDX-7200 instrument (Shimadzu) was used for energy dispersive X-ray fluorescence spectroscopy. Powder samples were loaded into sample holders with polyethylene membrane and measured with a collimator diameter of 3mm.

5.2.12. XRD analysis

A PANalytical Xpert3 Powder XRD system was used for the analysis of product solids. The XRD was operated with filtered Empyrean Cu Kα radiation (k = 0.15418 nm), a tube voltage of 45 kV, and a current of 40 mA. The peak intensities were measured using a PIXcel1D detector in the 2θ range of 5–100° with a step size of 0.026° on a rotating plate with a revolution time of 2.0 s.

5.3. Results and Discussion

5.3.1. $NaCe(SO_4)_2$ precipitation

The precipitation of $NaCe(SO_4)_2$ was used for all regeneration methods due to its effectiveness in separating the Ce^{3+} ions from the Cu^{2+} and Fe^{3+} ions mixed in the solution. Although the solubility of Ce^{3+} in 0.1M H_2SO_4 at room temperature is 0.207M according to Paulenova et al., the solubility decreases as low as 0.0024M at sufficiently high Na^+ and SO_4^{2-} concentrations (Lokshin, 2005)(Paulenova, 2002). The experimental results demonstrating the precipitation process is shown below in Figure 5.3, where a specified amount of $NaNO_3$ and H_2SO_4 were added into a solution of 1.0M $Ce(NO_3)_3$, 1.0M HNO_3 solution, and mixed at room temperature or at 65°C. The chemical reaction of this process is shown in Reaction 5.1.

$$Na^+ + Ce^{3+} + 2SO_4^{2-} \rightarrow NaCe(SO_4)_2 \qquad 5.1$$

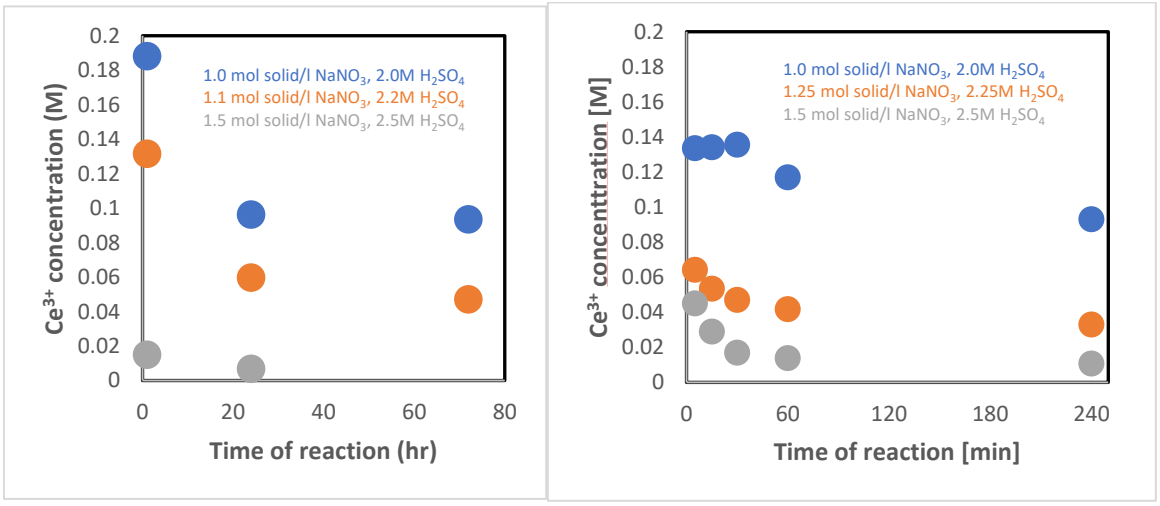

Figure 5.3: Precipitation of $NaCe(SO_4)_2$ by addition of $NaNO_3$ and H_2SO_4 into 1.0M $Ce(NO_3)_3$, 1.0M HNO_3 solution at room temperature (left) and at 65°C (right).

The results show a faster precipitation rate and a lower Ce^{3+} concentration with higher concentrations of Na^+ and SO_4^{2-} added. This trend is expected as $NaCe(SO_4)_2$ follows the principles of solubility equilibrium, reported by Lokshin et al. (2005). Table 5.1 below shows the expected Ce^{3+} concentrations with the additions of Na^+ and SO_4^{2-} in 1.0M Ce^{3+} solution, utilizing the solubility constant of $0.426*10^{-8}$ (g-equiv l^{-1})^4 reported by Lokshin et al (2005).

Table 5.1: Expected Ce^{3+} concentration after additions of Na^+ and SO_4^{2-} in 1.00M Ce^{3+} solution

Na^+ concentration	SO_4^{2-} concentration	Final Ce^{3+} concentration
1.00M	2.00M	0.105M
1.25M	2.25M	0.008M
1.50M	2.50M	0.001M

The results also show that a higher temperature increases the precipitation rate during the initial stages – approximately one hour of reaction time was required at 65°C for the concentration of Ce^{3+} to reach the minimum value. At room temperature, one hour was insufficient at lower excess concentrations of Na^+ and SO_4^{2-}, as the concentration measured after 24 hours of precipitation is significantly different from the concentration after 1 hour.

Nevertheless, increasing the Na^+ and SO_4^{2-} concentration during precipitation also decreased the reaction time needed, with 99% of cerium precipitated after one hour of reaction at room temperature, after adding 1.5 mol solid/l $NaNO_3$ and 2.5M H_2SO_4. The advantages gained from increasing the precipitation rate by increasing the operating temperature may not justify the energy investments for a large-scale process.

The separation of Ce^{3+} from Fe^{3+} in the solution was confirmed by adding incremental amounts of NaOH into a solution containing 0.25M $Ce_2(SO_4)_3$, 0.25M $Fe_2(SO_4)_3$, and 0.5M

H_2SO_4, and tracking the concentrations of Ce^{3+} and Fe^{3+} at different pH values after 24 hours of reaction, shown in Figure 5.4. After adding 0.5M NaOH (solution pH = 0.55), Ce^{3+} concentration declined, indicating all the Ce^{3+} in the solution was precipitated to $NaCe(SO_4)_2$. The solid product also was found to be $NaCe(SO_4)_2$ in the XRD measurements containing no iron. The separation of cerium from iron is shown to be possible in acidic conditions at pH < 1.

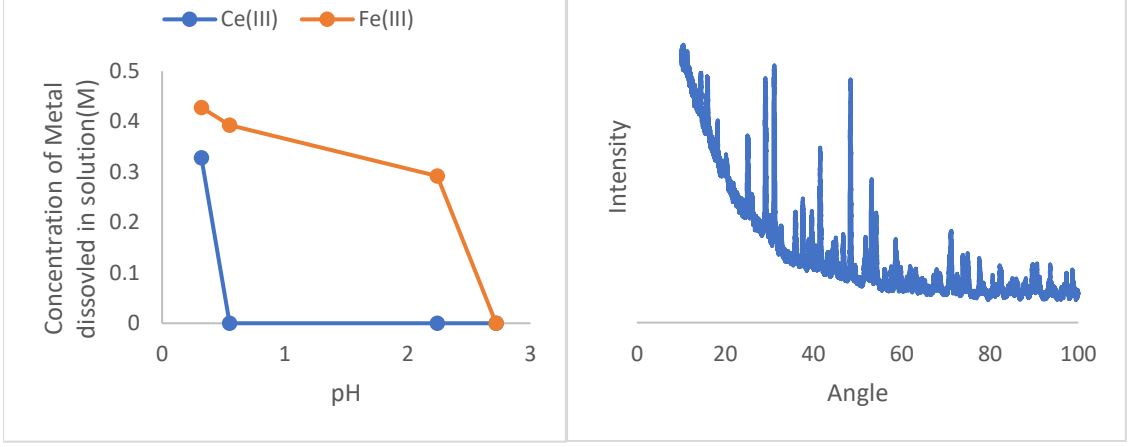

Figure 5.4: Concentration of Ce^{3+} and Fe^{3+} after addition of NaOH to precipitate out $NaCe(SO_4)_2$ (left). XRD analysis of solids after precipitation reveals pure $NaCe(SO_4)_2$ (right).

5.3.2 Chemical regeneration – $Ce(OH)_4$ formation

The basis for the air oxidation of $Ce(OH)_3$ is the lower potential required for oxidation of $Ce(OH)_3$ to $Ce(OH)_4$ in basic media compared to the potential required for Ce^{3+} to oxidize to Ce^{4+}, reported by Yu et al. (2005). Zou et al. demonstrated experimentally that at pH values above 10, Ce precipitate as solid $Ce(OH)_3$, and that air oxidation is a thermodynamically possible reaction (Zou, 2014). Although the air oxidation of Ce^{3+} to Ce^{4+} is thermodynamically possible at pH of 6 according to Yu et al., it was not experimentally observed. The conversion of Ce^{3+} to solid $Ce(OH)_3$ was deemed necessary to the formation of $Ce(OH)_4$. The chemical reaction for the

conversion of Ce^{3+} to $Ce(OH)_3$, and from $Ce(OH)_3$ to $Ce(OH)_4$, is shown below in Reactions 5.2 and 5.3, respectively.

$$NaCe(SO_4)_2 + 3OH^- \rightarrow Ce(OH)_3 + Na^+ + 2SO_4^{2-} \quad 5.2$$

$$2Ce(OH)_3 + H_2O + \frac{1}{2}O_2 \rightarrow 2Ce(OH)_4 \quad 5.3$$

Reacting the 119g/L $NaCe(SO_4)_2$ in 2M NaOH solids for 90 minutes at room temperature yielded a sulfur content of 2.5%, with the initial sulfur content measured at 18%. This reaction was observed to accelerate significantly in the presence of air feed – only 5 minutes were required to yield a solid with a sulfur content of 0.3%, indicating near complete conversion of $Ce(OH)_3$.

Although $Ce(OH)_3$ can be oxidized in dry air, the oxidation rate is slow and inconsistent, as only the surface layer exposed to air was oxidized. Therefore, a wet air oxidation method was used to oxidize $Ce(OH)_3$ to $Ce(OH)_4$.

Table 5.2 below shows the experimental parameters used – after reacting $NaCe(SO_4)_2$ in 2M NaOH to produce $Ce(OH)_3$, the NaOH solution was either decanted to be replaced with a fresh 1M NaOH solution or left untouched. Air was bubbled afterwards for 8 hours to produce $Ce(OH)_4$. The amount of $Ce(OH)_4$ produced for each setup is shown in Figure 5.4.

Table 5.2: Experimental parameters for conversion of $NaCe(SO_4)_2$ to $Ce(OH)_4$

Experiment #	$NaCe(SO_4)_2$ loading	NaOH solution concentration	NaOH decanted after production of $Ce(OH)_3$
1	119g/L	2M	No
2	119g/L	2M	Yes
3	238g/L	2M	Yes

4	357g/L	2M	Yes

At 2M NaOH, the theoretical maximum loading of $NaCe(SO_4)_2$ allowed the oxidation of all $NaCe(SO_4)_2$ to $Ce(OH)_4$ was calculated to be 238g/L, due to requiring a OH^-:Ce^{3+} ratio of 3:1, utilizing Reactions 5.2 and 5.3. The experimental results are consistent, as the $Ce(OH)_4$ produced from 357g/L $NaCe(SO_4)_2$ greatly decreases from the amount produced from 238g/L in 2M NaOH.

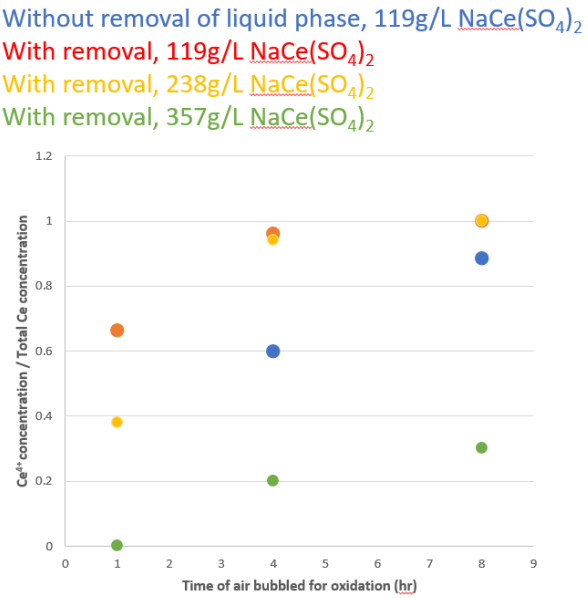

Figure 5.5: $Ce(OH)_4$ produced after wet air oxidation of $NaCe(SO_4)_2$ to $Ce(OH)_4$; control variables are the loadings of $NaCe(SO_4)_2$ and the option to replace the original NaOH liquid phase.

The main parameters that affected the oxidation rate of $Ce(OH)_3$ according to Zou et al. were air flow rate, temperature, reaction time, and pH (2014). This experiment also suggests that the presence of ions such as Na^+ and SO_4^{2-} also affect the oxidation rate - the removal of the liquid phase prior to air bubbling to convert $Ce(OH)_3$ to $Ce(OH)_4$ was observed to increase the rate of $Ce(OH)_4$ production according to Figure 5.5.

Overall, a residence time of 4 hours was required to convert over 95% of the $Ce(OH)_3$ to $Ce(OH)_4$ at room temperature. A thickener is likely necessary for the separation of the $Ce(OH)_3$ from the liquid phase prior to oxidation.

5.3.3. Chemical regeneration – Dissolution of $Ce(OH)_4$

The dissolution of CeO_2 in sulfuric acid has been documented by Um et al. to require high concentrations of acid and temperature – requiring 3 days to dissolve 4 mmol of CeO_2 completely in 12M H_2SO_4 at 90°C (Um, 2011). Although milder conditions can be used to dissolve $Ce(OH)_4$, the acid concentration and temperature were found to similarly improve the dissolution rate greatly. Figure 5.6 shows the concentrations of Ce^{4+} in the solution after the dissolution of 0.50M $Ce(OH)_4$ in 2.5M HNO_3, and 1.0M $Ce(OH)_4$ in 5.0M HNO_3, at room temperature and at 65°C.

$$Ce(OH)_4 + 4H^+ \rightarrow Ce^{4+} + 4H_2O \qquad 5.4$$

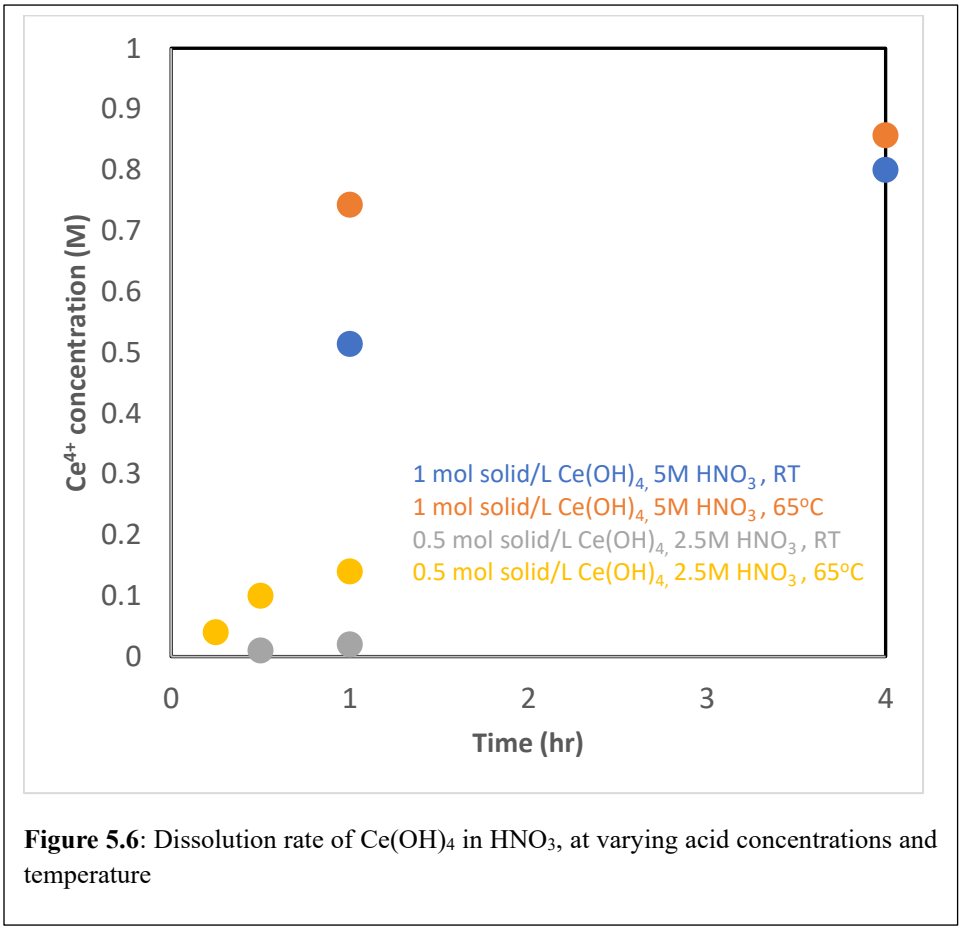

Figure 5.6: Dissolution rate of $Ce(OH)_4$ in HNO_3, at varying acid concentrations and temperature

A major concern with the dissolution of $Ce(OH)_4$ is the presence of very small undissolved solids that render the leaching less effective, and the reprecipitation of $Ce(OH)_4$ when the acid concentration is diluted. The incomplete dissolution of $Ce(OH)_4$ in dilute acids has also been observed by McNeice et al. – the oxidation of Ce^{3+} to Ce(IV) using various oxidants such as hydrogen peroxide, potassium permanganate, and sodium hypochlorite yielded a $Ce(OH)_4$ precipitate at pH of 1 (McNeice, 2019). Although the issue of reprecipitation could be mitigated by increasing the excess acid concentration or increasing the dissolution time of $Ce(OH)_4$, the leaching rate of chemically obtained Ce^{4+} remained consistently slower than the electrochemically regenerated Ce^{4+}. Table 5.3 shows the nickel leached from leaching 40g/L of 15.7wt% Ni-grade concentrates in leach solution at room temperature after 1 hour.

Table 5.3: % Copper leached from copper concentrates for chemically and electochemically generated Ce^{4+} solutions

Experiment #	$Ce(OH)_4$ or $(NH_4)_2Ce(NO_3)_6$ concentration	HNO_3 concentration	Electrochemical/ Chemical	% copper leached
1	1 mol solid/l	5M, 65°C, 1hr	Chemical	58
2	1 mol solid/l	8M, 65°C, 1hr	Chemical	61
3	1 mol solid/l	1M	Electrochemical	65

Overall, obtaining a Ce^{4+} solution utilizing air oxidation faces many issues in the dissolution step, requiring a high acid concentration, operating temperature, and reaction time. The overall process is expected to consume large amounts of unrecoverable acid and base.

5.3.4. Electrochemical Regeneration – Dissolution of $Ce(OH)_3$

Due to the slow dissolution rate of $Ce(OH)_4$, the electrochemical regeneration method was also investigated. Mixing 1M $Ce(OH)_3$ in 4M HNO_3 for 1 minute at room temperature yielded a total cerium concentration measured at 0.98M, and the Ce^{4+} concentration measured at 0.02M. Mixing 1M $Ce(OH)_3$ in 4M H_2SO_4 for 1 minute at room temperature yielded similar results, with a total cerium concentration of 0.93M and a Ce^{4+} concentration of 0.02M. The dissolution rate of $Ce(OH)_3$ over $Ce(OH)_4$ is a major advantage in favor of electrochemical regeneration over chemical regeneration.

The experiment was repeated with the liquid portion removed completely by filtration instead of decanting. With the total cerium concentration measured at 0.54M, Ce^{4+} concentration at 0.15M, with white precipitate remaining after 10 minutes of mixing in 4M HNO_3, these results show that $Ce(OH)_3$ is susceptible to air oxidation even if the filtered solids are not completely dry. In a large-scale process, this indicates a thickener would be preferred over filtration to remove the liquids.

5.3.5. Electrochemical Regeneration – Dissolution of $NaCe(SO_4)_2$ with Ca^{2+}

An alternative method of dissolving Ce^{3+} was by mixing $NaCe(SO_4)_2$ with Ca^{2+} to precipitate out $CaSO_4$, allowing the Ce^{3+} to be dissolved according to Reaction 5.5. This process would eliminate the need for acid-base swings and would condense the overall electrochemical regeneration process.

$$NaCe(SO_4)_2 + 2Ca^{2+} \rightarrow 2CaSO_4 + Na^+ + Ce^{3+} \qquad 5.5$$

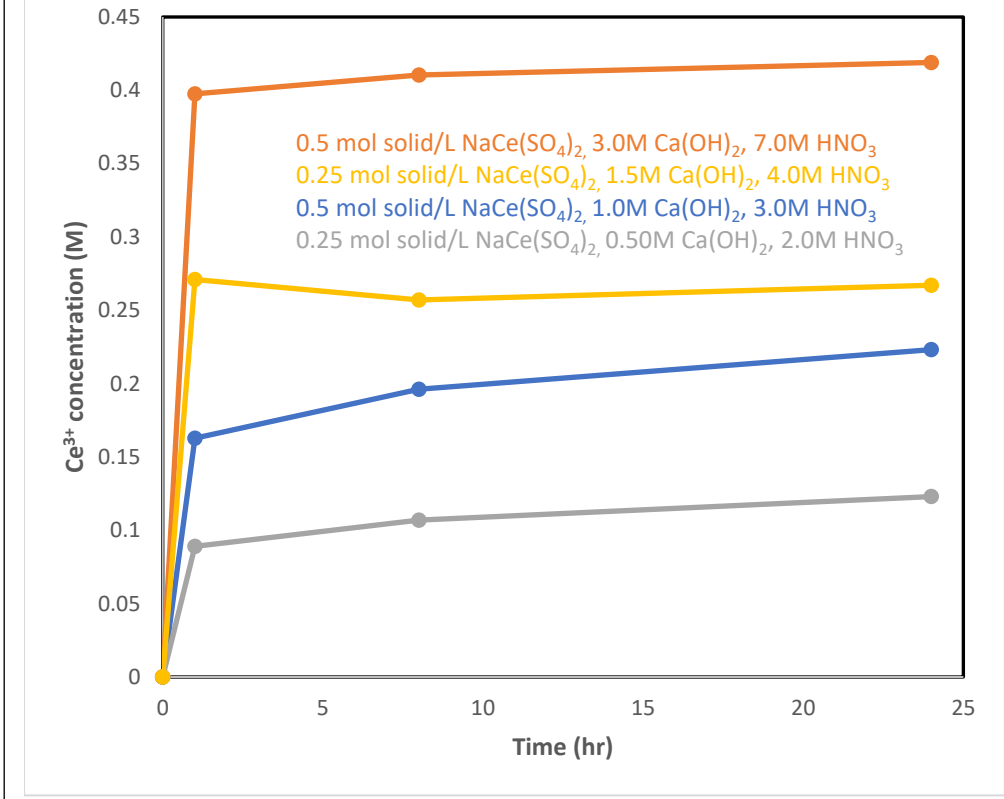

Figure 5.7. Concentration of Ce^{3+} measured after reacting $NaCe(SO_4)_2$ with $Ca(OH)_2$

Results in Figure 5.7 indicate that the reaction is near completion with 1 hour of reaction time at room temperature. The excess concentration of Ca^{2+} was crucial in dissolving Ce^{3+}, as having an excess Ca^{2+}:Ce^{3+} of 6:1 ratio yielded a higher Ce^{3+} concentration than the minimum ratio of 2:1.

Nevertheless, some cerium remains undissolved, as only 0.42M Ce^{3+} was dissolved after mixing 0.5M $NaCe(SO_4)_2$ in 3M Ca^{2+}. It is possible that a higher Ca^{2+} concentration would yield a higher Ce^{3+} concentration. More research is needed to determine whether this process is a viable alternative.

5.3.6. Electrochemical Regeneration

The main priorities of electrochemical regeneration of Ce^{3+} to Ce^{4+} was to confirm this method could be used in a large production setting. Although most incumbent cerium flow battery systems utilize methanesulfonic acid due to the higher solubilities of cerium, the overall process uses a leach solution mainly composed of sulfate anions.

Table 5.4 shows the coulombic efficiency achieved for each experimental setup utilizing the H-cell shown in Figure 5.2., applying a constant current density of $40mA/cm^2$.

Table 5.4: Conversion and coulombic efficiency for each Ce^{3+} anolyte solution, at various H_2SO_4 concentrations

Anolyte	Time	Coulombic efficiency	Ce^{4+} concentration
0.2M Ce^{3+}, 0.10M H_2SO_4	1.1 hr	15%	0.025M
0.2M Ce^{3+}, 0.25M H_2SO_4	1.5 hr	55%	0.12M
0.2M Ce^{3+}, 0.50M H_2SO_4	1.3 hr	59%	0.16M
0.2M Ce^{3+}, 1.0M H_2SO_4	1.4 hr	66%	0.18M

The general trends show an increase in efficiency with increasing sulfuric acid concentration, suggesting that the sulfuric acid concentration must be above a certain threshold during the operation of the electrolysis cell. A current density of $40mA/cm^2$ is achievable, as increasing the sulfuric acid concentration to 1.0M yielded an 88% conversion rate at reasonable efficiency. Increasing the acid concentration was observed to reduce the precipitate formed during the oxidation of Ce^{3+}, suggesting a possible formation of $Ce(OH)_4$ instead of Ce^{4+} in mildly acidic conditions, as referenced by McNeice et al (2019).

The current density can be increased further by increasing the Ce^{3+} concentration. Although the solubility of $Ce_2(SO_4)_3$ in 0.1M sulfuric acid at room temperature is reported to be

only 0.207M by Paulenova et al., the maximum Ce^{3+} concentration could be increased to 0.5M experimentally if obtained by reducing Ce^{4+} in sulfuric acid to Ce^{3+}, or by dissolving $Ce(OH)_3$ in sulfuric acid. Figure 5.8 shows the cyclic voltammetry analysis of Ce^{3+} solution obtained after reducing $Ce(SO_4)_2$, 0.1M H_2SO_4 solution with H_2O_2. The diagram suggests the current density can be increased further if Ce^{3+} is obtained by dissolution of $Ce(OH)_3$, outlined in Section 5.5.

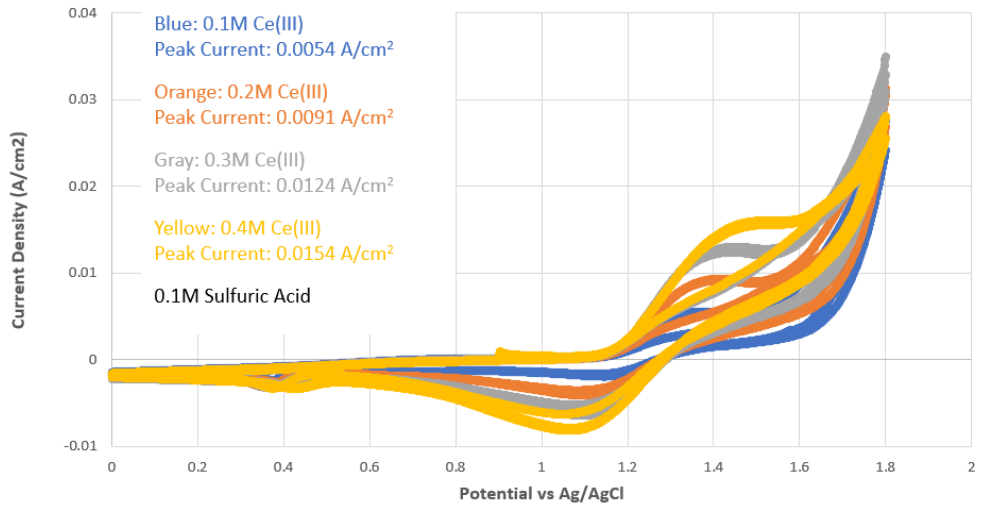

Figure 5.8: Cyclic voltammetry analysis of $Ce(SO_4)_2$, 0.1M H_2SO_4 solutions reduced with H_2O_2. Platinum anode and cathode were used, at a sweep rate of 0.02V/s.

As shown in Figure 4.2, the electrochemical regeneration reactor may also enable copper separation, with copper removed from the catholyte by electrodeposition, and the iron separated from Ce^{3+} by $NaCe(SO_4)_2$ precipitation. The electrochemical regeneration performance of Ce^{3+} solution mixed with Cu^{2+} and Fe^{3+} was confirmed by loading 100mL of 0.1M $Ce_2(SO_4)_3$, 0.4M $Fe_2(SO_4)_3$, 0.1M H_2SO_4 solution in the anolyte, and 100mL of 2M H_2SO_4 solution in the catholyte, and applying 40mA/cm^2 in the aforementioned setup. With a coulombic efficiency of

49% and 0.13M Ce^{4+} regenerated, this performance is better than the Ce^{3+} solution with no Fe^{3+} present, at 0.1M H_2SO_4. The presence of Fe^{3+} was confirmed to not hinder the regeneration.

The regeneration of Ce^{3+} to Ce^{4+} while simultaneously reducing Cu^{2+} and H^+ in the catholyte has also been confirmed in the experimental setup shown in Figure 5.9. A conversion of 85% was achieved, oxidizing 0.17M of 0.20M cerium to Ce^{4+}, with the anolyte to catholyte volume ratio of 2:1, using 0.1M $Ce_2(SO_4)_3$, 0.1M H_2SO_4, 0.06M $CuSO_4$, 0.16M $Fe_2(SO_4)_3$ for both the anolyte and the catholyte.

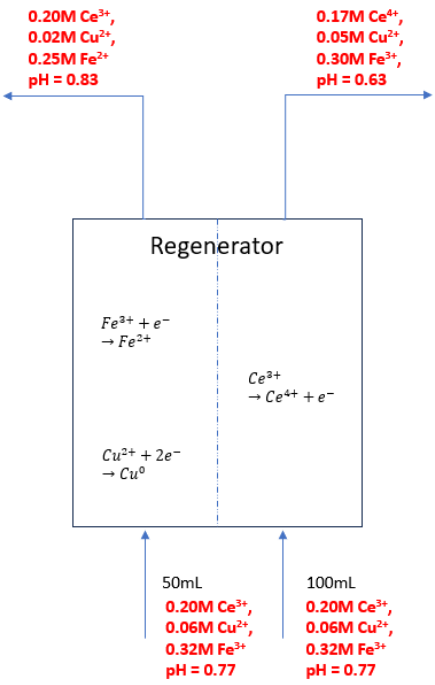

Figure 5.9: Experimental setup of regeneration of 0.1M $Ce_2(SO_4)_3$, 0.1M H_2SO_4 containing Cu^{2+}, Fe^{3+} while simultaneously utilizing the same solution in the catholyte to remove copper from the system.

This chapter shows that the electrochemical regeneration using 0.1M $Ce_2(SO_4)_3$, 1.0M H_2SO_4 solution in the anolyte and catholyte is viable, as the regeneration achieves a high coulombic efficiency of 88%. Although the solubility of cerium is a concern, the concentration of cerium is temporarily higher if achieved by dissolution of $Ce(OH)_3$ in sulfuric acid, perhaps due to the time required for sulfate ions to affect the Ce^{3+} ions. The time required for equilibration for $Ce_2(SO_4)_3$-H_2SO_4 system is suggested to be 10 days in room temperature by Paulenova et al. (2002). The DFT calculations also suggest that $Ce(H_2O)_9^{3+}$ is most stable, suggesting that the coordination of Ce^{3+} with sulfate ions is delayed (Buchanan,

2022). Overall, the electrochemical regeneration method would appear to be preferable over the chemical regeneration method.

5.4. Conclusion

In comparing the two regeneration methods for converting Ce^{3+} to Ce^{4+}, while the electrochemical process has limitations regarding its solubility and processing rate, it remains as a serviceable option. The chemical air oxidation method is hindered by its high reagent consumption and difficulty dissolving $Ce(OH)_4$ into solution. Overall, the electrochemical method is most likely better suited for scale-up into the cerium leaching process

5.5. References

Cunha, Á., Martins, J., Rodrigues, N., Brito, F.P. Vanadium redox flow batteries: a technology review. *International Journal of Energy Research* **2015**, *39*, 889–918.

Arenas, L.F., Ponce de León, C., Walsh, F.C. Electrochemical redox processes involving soluble cerium species. *Electrochimica Acta* **2016,** *205*, 226-247.

Kocyigit, N., Gencten, M., Sahin, M., Sahin, Y. A novel electrolytes for redox flow batteries: cerium and chromium couples in aqueous system. *International Journal of Energy Research* **2021**, *45*, 16176–16188.

Lokshin, E.P., Tareeva, O.A., Ivlev, K.G., Levin, B.V. A Study of the Solubility of Hydrated Orthophosphates of Yttrium, Lanthanum, Cerium, and Neodymium in Sulfuric-Phosphoric Acid Solutions at 20°C. *Russian Journal of Applied Chemistry* **2005**, *78*, 1913–1916.

Dean, J.A. Lange's handbook of chemistry, 12th ed. *McGraw-Hill* **1979.**

Paulenova, A., Creager, S.E., Navratil, J.D., Wei, Y. Redox potentials and kinetics of the Ce^{3+}/Ce^{4+} redox reaction and solubility of cerium sulfates in sulfuric acid solutions. *Journal of Power Sources* **2002**, *109*(2), 431–438.

Yu, P., Hayes, S.A., O'Keefe, T.J., O'Keefe, M.J., Stoffer, J.O. The phase stability of cerium species in aqueous systems: II. The Ce(III/IV) – H_2O – H_2O_2 / O_2 systems. Equilibrium considerations and Pourbaix diagram calculations. *Journal of Electrochemical Society* **2005**, *153*, C74.

Zou, D., Chen, J., Cui, H., Liu, Y., Li, D. Wet air oxidation and kinetics of cerium(III) of rare earth hydroxides. *Industrial & Engineering Chemistry Research* **2014**, *53*, 13790–13796.

Um, N., Miyake, M., Hirato, T. Dissolution of cerium oxide in sulfuric acid. In: Yao, T. (eds) Zero-Carbon Energy Kyoto 2010. Green Energy and Technology. Springer, Tokyo. **2011**.

McNeice, J., Kim, R., Ghahreman, A. Oxidative precipitation of cerium in acidic chloride solutions: part I – fundamentals and thermodynamics. *Hydrometallurgy* **2019**, *184*, 140-150.

Buchanan, C.A., Herrera, D., Balasubramanian, M., Goldsmith, B.R., Singh, N. Unveiling the cerium(III)/(IV) structures and charge-transfer mechanism in sulfuric acid. *JACS Au* **2022**, *2*(12), 2742-2757.

Chapter 6:

Conclusion and Future Works

As the global push toward carbon-free energy accelerates, the demand for copper in the United States is projected to rise sharply. This thesis explores room-temperature hydrometallurgical methods for processing copper concentrates that may help meet this demand more economically than conventional high-temperature oxidative processes. The research focused on two promising approaches: vanadium-based reductive leaching and cerium-based oxidative leaching.

The primary reaction for the vanadium reductive leaching method was the reduction of $CuFeS_2$-based copper concentrates to Cu_2S or Cu^0, with the release of Fe^{2+} and H_2S into the solution as V^{2+} was oxidized to V^{2+}. This process demonstrated significant advantages, such as its ability to work with moderate particle sizes (P_{80} = 75 μm), short residence time needed for high copper recovery yields (90% in 1 hour), flexibility from a variety of ore compositions, and competitive processing rates against incumbent processes, especially when implemented in a continuous flow reactor. The process proved particularly effective when enhanced with $FeSO_4$, and staged leaching further improved recoveries in low-iron concentrates.

The primary reaction for the cerium oxidative leaching method was the oxidation of $CuFeS_2$-based copper concentrates to Cu^{2+}, with the release of Fe^{3+} into the solution, and the production of S^0 or SO_4^{2-} as Ce^{4+} was reduced to Ce^{3+}. Prior to cerium oxidative leaching, pretreating the copper concentrates with ferric sulfate significantly increased leaching rates of copper (80% in 24 hours). However, the low solubility of Ce^{4+} and the high consumption of Ce^{4+} required for oxidation limited the solid loading. Compared to the vanadium reductive leaching method, cerium oxidative leaching method was less efficient in kinetics. Although cerium is overall cheaper than vanadium and the cerium oxidative leaching method is less environmentally

harmful due to the absence of H_2S, these advantages were not enough to justify the difference in processing rates.

Although operating at room temperature is a main advantage, both vanadium reductive leaching method and cerium oxidative leaching method require unique procedures that are not seen in typical leaching processes, such as the regeneration of consumed ions after leaching, and the separation of the consumed ions from the copper products. A critical evaluation of both processes is included in this thesis, including flowsheet development, reactor sizing, and energy consumption, indicating that vanadium leaching is more scalable and cost-effective despite requiring gas treatment for H_2S. Cerium leaching, in contrast, demands significantly larger reactor volumes and higher power inputs.

The regeneration of Ce^{3+} was particularly unique because although it is possible electrochemically in flow batteries, the limited solubility of Ce^{3+} in sulfate media limited the concentration of the final Ce^{4+} solution, increasing the process complexity. The chemical regeneration was also explored as an alternative. The chemical process involved the conversion of Ce^{3+} to $NaCe(SO_4)_2$, then to $Ce(OH)_3$ in base, air oxidation to $Ce(OH)_4$, then dissolution to Ce^{4+} in acid. Although possible, the chemical regeneration process faced major challenges, such as the consumption of large amounts of unrecoverable acids and bases, and the overall intense conditions required for the dissolution step, including high operating temperature, acid concentration, and residence time. Overall, the electrochemical method was found to be more feasible, with the Ce^{3+} solubility concerns alleviated by the temporary increase in solubility when dissolving $Ce(OH)_3$ in sulfuric acid.

Although this thesis concludes that vanadium reductive leaching method is more viable for copper production, it is likely different for other precious metals, such as nickel. Although

$CuFeS_2$ was reduced quickly by V^{2+} and oxidized slowly by Ce^{4+}, the potentials required and the passivation characteristics for each mineral is different, resulting in different leaching rates for each. Although hindered by the concentrate loading for copper processing, the same might not apply for the processing of other metals. A detailed analysis might be considered for the future.

In summary, this thesis provides a comprehensive assessment of two room-temperature leaching strategies. While both present unique challenges, vanadium-based leaching is the more promising candidate for commercial application due to its faster kinetics, higher yields, and lower energy demands. Future work should focus on optimizing leachant recycling systems, minimizing environmental risks, and pilot-scale testing to further validate the industrial applicability of the proposed processes.